Doctoral Dissertation

Prediction Methods for Time-dependent Corrosion Behavior of Unpainted Steel Plate Surfaces

JIANG FENG

December 2022

Department of Civil Engineering
Division of Global Architecture
Graduate School of Engineering
Osaka University

Abstract

The assessment of corrosion damage is an important part of the maintenance of steel structures. It is important to numerically analyze the characteristics of the corroded surface to accurately predict the corroded surface. In this study, four unpainted steel plates, SM400A, SM490A, SMA400AW, and SMA490AW, were used for corrosion experiments under a new accelerated corrosion test ISO16539 Method B, accelerated corrosion test CCT Method A and two atmospheric exposure environments in different regions. The corrosion depth of the steel plates was measured by a laser focus measurement system. Semivariograms were used in the geostatistical analysis to investigate the spatial autocorrelation structure of the corroded surface. By using this method and the ordinary kriging technique, a method to simulate the spatial characteristics of the corroded surface was proposed. The simulation results showed that the corrosion depth and surface morphology of the corroded surface were highly consistent with the experimental results. In addition, a deep learning model based on generative adversarial networks (GAN) was used to build a predictive model of the corroded surface. The spatial properties of the prediction model were validated using the geostatistical analysis method proposed in this study, and the results showed that the predicted results had similar spatial properties with the actual corroded surfaces. This study proposed a feasible new accelerated corrosion test through comparing several corrosion tests. A corrosion prediction model that can be used for uniform corrosion of multiple unpainted steels in different corrosion environments has been established. It has a positive significance for cost and time savings in steel structure maintenance.

Table of contents

Chapter 1 Introduction

1.1 Introductory remarks

Today, there are still many pre-1930s steel structures in use around the world for public service. And during the period of rapid economic growth in Japan between the 1950s and 1970s, many civil engineering structures, such as road and railway bridges, were also built. Many of these infrastructures have suffered varying degrees of damage and deterioration more than 50 years after they were built [1.1]. According to 2020 statistics, there are approximately 730,000 road bridges in Japan. More than 23% of these bridges have been in service for more than 50 years, and by 2030 this percentage will exceed 50% [1.2]. In the past years, more and more cases about steel structure deterioration and damage have occurred [1.3].

A major cause of deterioration and damage to steel structures is corrosion [1.4]. Steel corrosion is an electrochemical reaction, i.e., a redox reaction, that occurs on the surface of the steel. Anodes and cathodes are produced on the surface of steel. This chemical reaction produces iron oxide through iron ions and iron hydroxide, which turns into rust. Corrosion causes material loss from the surface of steel members [1.5], which thins the cross-sectional area of the steel structure and reduces the stiffness and load-bearing capacity of the structure [1.6]. Therefore, this can become a major public safety issue. On the other hand, corrosion on the surface of steel members can also hinder safety and efficiency in industry, causing significant damage and economic losses. According to estimates, the economic losses due to the corrosion on the surface of steel structures represent approximately 4% of the gross national product of industrialized countries [1.7] [1.8]. Therefore, it is important to treat steel structures against corrosion. Currently, anti-

corrosion coatings are widely used as anti-corrosion methods such as painting, galvanizing or thermal spraying to prevent corrosion. The use of weathering steel depends on the environmental conditions to which the steel structure is subjected. Weathering steels are made by adding alloying elements such as copper, chromium, and nickel to form a dense and stable protective film of rust on the surface in the air to improve the corrosion resistance of the steel. These steels are more resistant to corrosion and can be used for longer periods of time than ordinary steels. Nevertheless, these anti-corrosion methods only delay the time of steel corrosion, and monitoring and controlling corrosion on a long-time scale is a difficult task. Therefore, more and more researchers are working on more accurate monitoring and prediction of corrosion to guarantee the timely maintenance of steel structures. This has become an important task for infrastructure maintenance.

1.2 Corrosion tests

1.2.1 Atmospheric exposure test

In any case, the sustainability of the steel material or coating shall be properly assessed to determine its life expectancy. Then, a series of corrosion experiments need to be performed. The most dependable is the direct atmospheric exposure test, by which steel materials are exposed to a particular test site and tested using an actual corrosion environment.

The atmospheric exposure test is a test in which specimens are exposed to atmospheric conditions to study their chemical and physical properties and changes. Atmospheric exposure test methods include direct exposure test methods, under glass exposure test methods, and shielding exposure test methods. The direct exposure test method is one of

the most widely used methods to expose the specimen to the atmospheric environment that directly affects the corrosion durability of the material to observe the progress of corrosion of the specimen. The atmospheric exposure test is affected by environmental factors at the exposure test site, such as temperature, humidity, precipitation, and the amount of salt in the air, so the results of corrosion durability vary depending on the geographical location of the exposure test site across Japan. When a compliant test method is performed at a designated exposure test site, data such as start time, installation angle, and environmental factors should be recorded [1.9].

Because atmospheric exposure tests are conducted under real atmospheric conditions, the actual corrosion durability of steel products can be accurately assessed. Also, the durability results of steel from atmospheric exposure tests can provide criteria for assessing the corrosion durability of steel based on the outcomes of various accelerated corrosion tests. However, the disadvantages are that real corrosion is a long-term process, atmospheric exposure tests take a long time, and the assessment is carried out under the limited conditions of exposure test sites in different regions of Japan, making them less generalizable.

1.2.2 Accelerated corrosion test

To address the drawbacks of atmospheric exposure tests, accelerated corrosion tests can be performed using corrosion gas pedals, which accelerate corrosion under conditions that are more severe than the actual corrosion environment [1.10]. Standardized test methods, such as the salt spray test (SST) authorized by ISO 9227 [1.11], the cyclic corrosion test (CCT) authorized by ISO 14993, and other standards [1.12], [1.13] are widely used to assess the corrosion resistance of surface-treated steel plates. These

accelerated corrosion tests impose severe corrosion environments on the steel materials, such as brine spraying, continuous wet/dry cycles, etc. Compared to the actual corrosion environment, the corrosion of the steel material or the deterioration of the coating is accelerated during the required test cycle.

The salt spray test specified in JIS Z 2371 is a method to evaluate corrosion resistance by spraying a 5% concentration of sodium chloride (NaCl) solution in a salt spray test chamber to accelerate the corrosion of metallic materials or parts with electroplated or painted coatings. The combined cycle test accelerates the degradation state of metallic materials, plating, coatings, and paints by repeating salt spray, drying, and wetting cycles in an environmental test apparatus. The combination of drying and wetting cycles enables corrosion evaluation closer to the actual environment than the salt spray test. In recent years, it has been used to evaluate the durability and estimate the service life of products and materials, particularly in the automotive industry [1.14].

Advantages of accelerated corrosion tests include the ability to evaluate corrosion resistance relatively earlier than atmospheric exposure testing, the ease of quantifying the relative relationship to comparative materials and standards, and the potential for reproducible experiments that simulate real environments. Several previous studies have been conducted to examine the connection between accelerated corrosion tests and atmospheric exposure tests for various steel materials. Despite the limited test requirements and materials, the tendency of results of the two tests was similar [1.15], [1.16]. However, although accelerated corrosion tests are effective in assessing the sustainability of metals or coated materials under certain situations in the short term, the correlation between actual corrosion environments and accelerated corrosion tests is not clearly defined. Researchers have recognized the difficulty of complete consistency

between accelerated corrosion tests and the actual corrosion environments [1.17]. Several previous studies have pointed out that the correlation between CCT and corrosion in the actual environment is not clear regarding the evaluation of corrosion resistance of surface-treated steel plates for household appliances, and the superiority of corrosion resistance between materials may be reversed between CCT and the actual environment [1.18]. These two cases may not reflect the real corrosion environment in terms of the corrosion resistance order and corrosion pattern of the steel. Some accelerated tests on steels for automotive products and galvanized steels have also shown different trends [1.14]. This suggests that some accelerated corrosion tests are not reflective of the actual corrosion environments of the vehicle. The different accelerated corrosion tests do not consistently rank the durability of the materials. Therefore, it is also important to investigate the relationship between accelerated corrosion tests and atmospheric exposure tests when applying any accelerated corrosion test to assess the sustainability of metals and coated materials.

1.3 Spatial analysis of corrosion

Corrosion of deteriorating steel structures can be a serious danger to safety if not maintained in a timely manner. Consequently, the estimation and prediction of corrosion conditions are of great importance during the maintenance of steel structures. Nevertheless, in general environments, corrosion behavior usually takes a long time. Traditional monitoring methods based on visual inspection and experience to determine the extent of corrosion are both time-consuming and inaccurate. Therefore, it would be of great interest for practical maintenance if a fast and accurate corrosion simulation and prediction model could be established mathematically. For example, it is possible to

assess whether the corrosion conditions observed during periodic steel bridge inspections are likely to lead to serious damage before the next inspection. It makes sense to be able to predict when the damage will become severe even with a short cycle of repeated inspections, so that maintenance can be performed from a long-term perspective. In addition, it is difficult to obtain detailed information about the distribution of corroded surface profiles during normal inspections, but through specific numerical analysis, the spatial characteristics of corroded surface profiles can be predicted, allowing more accurate information to be obtained using finite element analysis and other methods to assess the load-bearing capacity of the structure. A quantitative standard for the progression of corrosion is also provided, rather than relying only on rough experience. Therefore, with the development of numerical simulation techniques, more effective prediction of corrosion has become of increasing interest. These new techniques allow the numerical analysis of the spatial properties of steel structures, modeling of corroded surfaces, and prediction of the corroded surface of steel structures to save monitoring time and offer an early warning for facility maintenance.

In previous studies, numerical analysis of corroded surfaces was important for modeling corrosion damage and determining the corrosion state [1.19]. Fractal and spatial autocorrelation have already been applied to assess the surface characteristics of corroded parts obtained from actual structural members [1.20]. Furthermore, Monte Carlo modeling methods have been applied to evaluate the progress of the corrosion process with the use of the probability distributions of the corrosion growth rates [1.21], [1.22]. And a predictive model was developed to consider the variation of corrosion rate by Bayesian inference [1.23]. However, since the objective materials in every approach are limited, the relationship between corrosion damage and deterioration is still a difficult

task. A widely applicable approach is needed to effectively predict corrosion behavior over time.

Semivariogram is one of the spatial statistical methods that elucidate the spatial autocorrelation structure of corroded surfaces and their time-dependent features [1.24]. Semivariogram is a method for quantitatively evaluating the spatial correlation of distances and variances of every data, which was evolved from mining to detect the spatial distribution pattern of deposits [1.25]. This analytical approach has been used in numerous areas such as mining, meteorology, economics, and geography [1.26].

1.4 Prediction of corrosion

Thompson et al. noted that the cost of maintenance for aging such as corrosion may be more than two to ten times the cost of the material used [1.27]. Such indirect costs could be greatly minimized by improving the administration of infrastructure maintenance. Therefore, either conducting corrosion tests or numerical analysis of corroded surfaces, and ultimately developing an efficient corrosion prediction model would be of practical engineering significance.

Abbas et al. outlined recent advances and future trends in the management of asset maintenance strategies for corroded steel structures in extreme marine environments. They provided an extensive review and analysis of corrosion prediction models and industry best practices. The application of state-of-the-art technologies including computerized maintenance management systems (CMMS), artificial intelligence (AI), and Bayesian networks (BN) were as well discussed [1.28]. Kiefner and Kolovich developed an approach to derive plausible corrosion rates and to build integrity reassessment intervals for metallic losses due to pipeline corrosion [1.21]. The corrosion

pit depth at a point in time was used in this method, and it could be determined in a variety of ways, which include directly measured, indirect extrapolation from inspection data, and a combination of both. Through Monte Carlo modeling, the approach allowed the determination of corrosion rate with an 80% confidence.

Kainuma et al. used regression tree analysis to delineate corrosion areas based on surface characteristics of corrosion. They then used semivariograms to create a prediction model and used a general kriging model to predict the corrosion depth at arbitrary locations [1.24]. This approach attained reliable prediction accuracy for the evaluated corroded surfaces. In a different study [1.29], a frame was developed to build a prediction model for corrosion damage. It modeled the corrosion growth rate according to time using a generalized extreme value distribution that varies with time. Bayesian extrapolation was applied to evaluate the network parameters and to build a reliable prediction model. The model has been demonstrated to be dependable and robust in different environments. The variation of the corroded surface is considered to be stochastic because of the lack of information on the factors influencing the corrosion progress and their changes over time [1.30],[1.31],[1.32]. The probability distribution of corrosion rates is associated with the properties of the corroded surface, which is the base for simulation and prediction models [1.33].

Nevertheless, each of the mentioned approaches has been limited to the objective material and is not sufficiently generalizable to corrosion environments. In recent years, deep learning methods for image synthesis have been extensively used. Deep generation methods, in particular generative adversarial networks (GAN), have shown advanced capabilities. Ganz et al. [1.34] presented an improved image synthesis on the basis of observation generators as a representative of the synthesis procedure of convolutional

sparse coding (CSC) and its multilayer version (ML-CSC). Also on the basis of GAN, Chen et al. [1.35] developed a generator-based series strategy to address the challenge of converting high-resolution remote sensing images into maps for cartography. The series strategy resulted in higher quality multi-scale map generation. Saseendran et al. [1.36] proposed a conditional generative adversarial network (CGAN) to generate images with a specific number of objects defined from a given class. Yu et al. [1.37] worked on various improvements to improve the performance of GAN in image generation, including proposing a novel double contrast loss to improve the performance of the discriminator, revisiting the attention in the generator, and proposing a reference attention mechanism in the discriminator. Combining the above improvements, the model achieves significant improvements in Fréchet Inception Distance (FID) on several benchmark datasets. Several studies have been conducted to use SVM (Support Vector Machine) for the quantitative evaluation of pipeline corrosion [1.38] [1.39]. The corrosion of weathering steel bridges, which often undergo serious surface corrosion damage resulting in structural performance degradation, was studied. Conventional manual monitoring and categorization approaches are time-consuming and very subjective, and do not offer quantitative assessments. Yan et al [1.40] developed an innovative image-based approach to quantitatively assess the corrosion of weathering steel bridges. With the advancement of deep learning techniques, they have been extensively applied to modeling and prediction missions. However, applications in corrosion prediction are rare. In addition, unsupervised learning for corrosion prediction requires further study.

1.5 Objective of this study

In this study, a series of experiments were conducted on uncoated steel plates under

different corrosive environments, and the experimental data were numerically analyzed using geostatistical analysis and deep learning-based analysis methods. The main objectives of this study are as follows: 1) To investigate the relationship between corrosion progress and corrosion time for different types of steel under different corrosion environments through experiments on unpainted steel plates in different corrosion environments. 2) To quantify the spatial characteristics of the corroded surface of steel plates using the method of geostatistical analysis and to investigate how the spatial characteristics of the corroded surfaces change over time. 3) To propose a deep learning-based approach to a corrosion prediction model that can make accurate predictions of corroded surfaces.

Therefore, this study goes from experiments to data analysis to building a corrosion prediction model that can be practically applied. The achievements of this study can eventually be applied to the actual maintenance of steel structures. For example, it is possible to evaluate whether the corrosion condition observed during a five-yearly periodic inspection of a steel bridge is likely to lead to serious damage before the next inspection. Even if inspections are repeated on a five-year cycle, it is useful to be able to predict when damage will become serious to perform maintenance from a long-term perspective. In addition, it is difficult to obtain detailed information on the distribution of corroded surface properties during normal inspections, but with the spatial numerical analysis, it can predict the spatial characteristics of corroded surface properties, making it possible to evaluate the load-bearing capacity of structures using finite element analysis and other methods, obtaining more precise information. This study contributes a corrosion prediction method that can greatly save the cost and time of corrosion maintenance and is more accurate in its corrosion status judgment.

1.6 Contents of the dissertation

Considering the observation and analysis of the basic corrosion behavior of steel, this study mainly takes weathering steel as the object of study and compares it with normal carbon steel, without considering the case of having a coating on the steel plate surface. The corrosion depth data of the corroded surface of the steel plate was obtained from several corrosion tests, from the basic numerical analysis to the analysis of the spatial properties of the corroded surface, and then to the establishment of an effective corrosion prediction model. A complete comparative experiment was conducted and a model with good generalizability for corrosion assessment was developed.

This dissertation consists of six chapters including an introduction, in Chapter 1 and conclusions, in Chapter 6. In Chapter 2, four steels were subjected to atmospheric exposure corrosion tests and accelerated corrosion tests, including a newly developed accelerated corrosion test authorized by ISO16539 Method B. This test condition is characterized by the integration of a procedure of uniform spraying of artificial seawater on the surface of the specimen surface and the process of repeated drying/wetting cycles at a constant absolute humidity. The relationship between this kind of experimental conditions and the actual environment of metal-coated steel supplied with electricity has been verified by the developers of this experimental method in local and limited conditions [1.41]. By accumulating experimental data, the test method is expected to be extended to other industrial areas, such as automotive and infrastructure. Corroded surface observation, corrosion depth measurement, and basic statistical analysis were performed on the specimens. In Chapter 3, to further investigate the spatial statistical properties of the corroded surface, a spatial statistical analysis was performed using a

semivariogram. This method can capture the spatial nature of the corroded surface, making a uniform evaluation criterion for steel subjected to corrosion in different corrosion environments. The spatial properties of corrosion of different steels in different environments were compared to investigate the simulation of accelerated corrosion tests on the real corrosive environment. In Chapter 4, in order to build an efficient corrosion model that can be practically applied, adversarial learning was used to create the generation of corroded surfaces in the future. A generative adversarial network (GAN) was used as the training model because the aim of this chapter was to predict the next stage of corrosion based on the current stage of corrosion and to determine the experimental time of the present corrosion state. The input to the GAN model shall be the present data rather than a traditional random vector. To expand the diversity of the dataset, Gaussian noise and GAN were used to enrich the dataset, which could increase the accuracy of the prediction model. Combined with UNet [1.42] and MobileNetV2 [1.43], the model could be used to predict the next stage of corrosion (output) based on the current corrosion state (input). The prediction model could as well be used to recognize the corrosion stage and the number of days of corrosion. According to the experimental outcomes, the prediction model achieved a high accuracy in predicting the corroded surface of steel plates. This proposed method enables quicker and more accurate prediction of corrosion behavior than conventional approaches, which typically rely on personal experience. The method can result in significant cost savings in the evaluation and maintenance of steel structures. In Chapter 5, the accuracy of the prediction model was validated in conjunction with Chapters 3 and 4. As one of the drawbacks of deep learning methods, some parameters in neural networks often do not make practical sense. Therefore, the spatial statistical analysis method in Chapter 3 was used to verify whether

the prediction model can accurately predict the spatial properties of corroded surfaces.

References

1.1 Fujino, Y. and Siringoringo, D.M., 2008, July. Structural health monitoring of bridges in Japan: An overview of the current trend. In *Fourth international conference on FRP Composites in Civil Engineering (CICE2008)* (pp. 22-24).

1.2 Al Deen Taher, S.S. and Dang, J., 2023. Autonomous multiple damage detection and segmentation in structures using mask R-CNN. In *Experimental Vibration Analysis for Civil Engineering Structures* (pp. 545-556). Springer, Cham.

1.3 Farhey, D.N., Thakur, A.M., Buchanan, R.C., Aktan, A.E. and Jayaraman, N., 1997. Structural deterioration assessment for steel bridges. *Journal of Bridge Engineering*, *2(3)*, pp.116-124.

1.4 Pidaparti, R.M., Fang, L. and Palakal, M.J., 2008. Computational simulation of multi-pit corrosion process in materials. *Computational Materials Science*, *41(3)*, pp.255-265.

1.5 Secer, M. and Uzun, E.T., 2017. Corrosion damage analysis of steel frames considering lateral torsional buckling. *Procedia engineering*, *171*, pp.1234-1241.

1.6 Bonopera, M., Chang, K.C., Chen, C.C., Lin, T.K. and Tullini, N., 2018. Compressive column load identification in steel space frames using second-order deflection-based methods. *International Journal of Structural Stability and Dynamics*, *18(07),* p.1850092.

1.7 Popoola, L.T., Grema, A.S., Latinwo, G.K., Gutti, B. and Balogun, A.S., 2013. Corrosion problems during oil and gas production and its mitigation. *International Journal of Industrial Chemistry*, *4*(1), pp.1-15.

1.8 Awad, M.K., Mustafa, M.R. and Elnga, M.M.A., 2010. Computational simulation of the molecular structure of some triazoles as inhibitors for the corrosion of metal surface. *Journal of molecular structure: theochem*, *959*(1-3), pp.66-74.

1.9 Morcillo, M., Chico, B., Díaz, I., Cano, H. and De la Fuente, D., 2013. Atmospheric corrosion data of weathering steels. A review. *Corrosion Science*, *77*, pp.6-24.

1.10 Suzumura, K. and Nakamura, S.I., 2004. Environmental factors affecting corrosion of galvanized steel wires. *Journal of materials in civil engineering*, *16*(1), pp.1-7.

1.11 ISO9227:2017. Corrosion tests in artificial atmospheres – salt spray tests.

1.12 ISO14993:2018. Corrosion of metals and alloys – accelerated testing involving cyclic exposure to salt mist, dry and wet conditions.

1.13 SAE J 2334. 2016. Laboratory cyclic corrosion test.

1.14 LeBozec, N., Blandin, N. and Thierry, D., 2008. Accelerated corrosion tests in the automotive industry: a comparison of the performance towards cosmetic corrosion. *Materials and corrosion*, *59*(11), pp.889-894.

1.15 Draẑić, D.M. and Vaŝĉiẑ, V., 1989. The correlation between accelerated laboratory corrosion tests and atmospheric corrosion station tests on steels. *Corrosion science*, *29*(10), pp.1197-1204.

1.16 Lin, C.C. and Wang, C.X., 2005. Correlation between accelerated corrosion tests and atmospheric corrosion tests on steel. *Journal of applied electrochemistry*, *35*(9), pp.837-843.

1.17 Fujita, S. and Mizuno, D., 2007. Corrosion and corrosion test methods of zinc coated steel sheets on automobiles. *Corrosion science*, *49*(1), pp.211-219.

1.18 Fujii, K., Ohashi, K. and Kajiyama, H., 2006. Corrosion aspect of electrical appliances–development of new accelerated corrosion Test simulating appliances environment (1). *Zairyo-to-Kankyo*, *55*, pp.349-355.

1.19 Xue, L., 2007. Damage accumulation and fracture initiation in uncracked ductile solids subject to triaxial loading. *International journal of solids and structures*, *44*(16), pp.5163-5181.

1.20 Fujii, K., Kaita, T., Hirai, K. and Okumura, M., 2002. Applicability of spatial auto-correlation model for corroded surface modeling in corroded steel plate. *J. Struct. Eng*, *48*, pp.1031-1038.

1.21 Kiefner, J.F. and Kolovich, K.M., 2007, March. Calculation of a corrosion rate using Monte Carlo simulation. In *CORROSION 2007*. OnePetro.

1.22 Caleyo, F., Velázquez, J.C., Valor, A. and Hallen, J.M., 2009. Probability distribution of pitting corrosion depth and rate in underground pipelines: A Monte Carlo study. *Corrosion Science*, *51*(9), pp.1925-1934.

1.23 Vereecken, E., Botte, W., Lombaert, G. and Caspeele, R., 2021. A Bayesian inference approach for the updating of spatially distributed corrosion model parameters based on heterogeneous measurement data. *Structure and Infrastructure Engineering*, *18*(1), pp.30-46.

1.24 Kainuma, S., Yang, M., Xie, J. and Jeong, Y.S., 2021. Time-dependent prediction on the localized corrosion of steel structure using spatial statistical simulation. *International Journal of Steel Structures*, *21*(3), pp.987-1003.

1.25 Wang, S., Si, G., Wang, C., Cai, W., Li, B., Oh, J. and Canbulat, I., 2022. Quantitative assessment of the spatio-temporal correlations of seismic events induced by longwall coal mining. *Journal of Rock Mechanics and Geotechnical Engineering*.

1.26 Arbia, G., Ghiringhelli, C. and Nardelli, V., 2022. Effects of Confidentiality-Preserving Geo-Masking on the Estimation of Semivariogram and of the Kriging Variance. *Geographical Analysis*.

1.27 Thompson, N.G., Yunovich, M. and Dunmire, D., 2007. Cost of corrosion and corrosion maintenance strategies. *Corrosion Reviews*, *25*(3-4), pp.247-262.

1.28 Abbas, M. and Shafiee, M., 2020. An overview of maintenance management strategies for corroded steel structures in extreme marine environments. *Marine Structures*, *71*, p.102718.

1.29 Kim, K., Lee, G., Park, K., Park, S. and Lee, W.B., 2021. Adaptive approach for estimation of pipeline corrosion defects via Bayesian inference. *Reliability Engineering & System Safety*, *216*, p.107998.

1.30 Melchers, R.E., 2005. The effect of corrosion on the structural reliability of steel offshore structures. *Corrosion science*, *47*(10), pp.2391-2410.

1.31 Shibata, T., 1996. 1996 WR Whitney Award lecture: Statistical and stochastic approaches to localized corrosion. *Corrosion*, *52*(11).

1.32 Alamilla, J.L., Oliveros, J. and García-Vargas, J., 2009. Probabilistic modelling of a corroded pressurized pipeline at inspection time. *Structure and infrastructure engineering*, *5*(2), pp.91-104.

1.33 Caleyo, F., Velázquez, J.C., Valor, A. and Hallen, J.M., 2009. Probability distribution of pitting corrosion depth and rate in underground pipelines: A Monte Carlo study. *Corrosion Science*, *51*(9), pp.1925-1934.

1.34 Ganz, R. and Elad, M., 2021. Improved Image Generation via Sparse Modeling. *arXiv preprint arXiv:2104.00464*.

1.35 Chen, X., Yin, B., Chen, S., Li, H. and Xu, T., 2021. Generating Multi-scale Maps from Remote Sensing Images via Series Generative Adversarial Networks. *arXiv preprint arXiv:2103.16909*.

1.36 Saseendran, A., Skubch, K. and Keuper, M., 2021. Multi-Class Multi-Instance Count Conditioned Adversarial Image Generation. In *Proceedings of the IEEE/CVF International Conference on Computer Vision* (pp. 6762-6771).

1.37 Yu, N., Liu, G., Dundar, A., Tao, A., Catanzaro, B., Davis, L.S. and Fritz, M., 2021. Dual contrastive loss and attention for gans. In *Proceedings of the IEEE/CVF International Conference on Computer Vision* (pp. 6731-6742).

1.38 Luo, Z., Hu, X. and Gao, Y., 2013. Corrosion research of wet natural gathering and transportation pipeline based on SVM. In *ICPTT 2013: Trenchless Technology* (pp. 964-972).

1.39 Zhao, H., Zhang, X., Ji, L., Hu, H. and Li, Q., 2014. Quantitative structure–activity relationship model for amino acids as corrosion inhibitors based on the support vector machine and molecular design. *Corrosion Science*, *83*, pp.261-271.

1.40 Yan, B., Goto, S., Miyamoto, A. and Zhao, H., 2014. Imaging-based rating for corrosion states of weathering steel using wavelet transform and PSO-SVM techniques. *Journal of Computing in Civil Engineering*, *28*(3), p.04014008.

1.41 Kajiyama, H., Fujita, S., Fujii, K. and Sakai, M., 2006. Problem of Conventional Accelerated Corrosion Tests and Development of New Accelerated Corrosion Test: Development of New Accelerated Corrosion Test Simulating Electrical Appliance. *Corrosion Engineering*, *55*(8), pp.475-490.

1.42 Ronneberger, O., Fischer, P. and Brox, T., 2015, October. U-net: Convolutional networks for biomedical image segmentation. In *International Conference on Medical image computing and computer-assisted intervention* (pp. 234-241). Springer, Cham.

1.43 Sandler, M., Howard, A., Zhu, M., Zhmoginov, A. and Chen, L.C., 2018. Mobilenetv2: Inverted residuals and linear bottlenecks. In *Proceedings of the IEEE conference on computer vision and pattern recognition* (pp. 4510-4520).

Chapter 2 Accelerated corrosion tests and atmospheric exposure tests on unpainted steel

2.1 Introduction

In this chapter, corrosion tests were carried out on specimens of four types of steel in four corrosion environments. The four types of steel include two normal carbon steels and two weathering steels. Weathering steel can be used in the construction of steel bridges and is a high strength, low alloy steel with good resistance to atmospheric corrosion. In the suitable environment, it will form an adherent protective rust to prevent further corrosion. Normal carbon steel is rarely used without anti-corrosion coatings in the construction of steel structures. This study, it was used for comparison with weathering steels and to analyze the basic corrosion behavior of steel plate surfaces. The four corrosion environments included two accelerated corrosion tests and two atmospheric corrosion tests in different regions, and the applicability of the accelerated corrosion tests was verified by comparing these tests.

In the experiments of this chapter, three stages were set for the corrosion duration of the accelerated corrosion tests to investigate the progress of corrosion, and three specimens were used for each stage in order to enrich the sample size, a total of 96 specimens were subjected to corrosion tests. The appearance of the rust layer on the corroded surface of the steel plates at each stage was recorded. After removing the rust, the corroded surface of each stage of the specimen was measured. Basic data statistics and comparative analysis were performed using the average corrosion depth. In this chapter, a comparative analysis of the corrosion progress of different steel types under different corrosion environments was carried out to investigate the relationship between corrosion progress

and corrosion time of weathering steel and normal carbon steel under different corrosion environments. At the same time, the accelerated corrosion test and the atmospheric exposure test in the real environment were compared, and the degree of simulation of the accelerated corrosion test on the atmospheric exposure test was confirmed.

2.2 Material and specimen

2.2.1 Material

Table 2-1. Chemical compositions and mechanical properties of material.

	Chemical compositions (wt%)								Mechanical properties		
	C	Si	Mn	P	S	Cu	Ni	Cr	Yield stress (N/mm^2)	Tensile strength (N/mm^2)	Elongation (%)
SM400A	0.18	0.17	0.5	0.015	0.006	-	-	-	279	442	29
SM490A	0.16	0.02	1.04	0.011	0.005	-	-	-	426	542	20
SMA400AW	0.12	0.2	0.67	0.015	0.004	0.31	0.09	0.49	305	445	33
SMA490AW	0.12	0.22	1.14	0.015	0.002	0.31	0.09	0.49	391	514	30

In this study, four materials of steel, SM400A, SM490A, SMA400AW, and SMA490AW, were used for the experiments. Normally, it is necessary to paint steel materials in steel structures to avoid and minimize corrosion. In this study, in order to research the fundamental corrosion behavior of the ordinary steel materials after coating degradation, as well as weathering steel materials generally used without painting, the experimental specimens were unpainted. The chemical compositions and the mechanical properties of the materials used as the experimental specimens are listed in Table 2-1. SM400A and SM490A are carbon steel specified by JIS G 3106. SMA400AW and SMA490AW are weathering steel specified by JIS G 3114.

2.2.2 Specimen

Figure 2-1 illustrates the shape and size of the specimen. The materials were incised into rectangular steel plates, 150 mm long, 70 mm wide and 9 mm thick. The surface of each specimen was blasting treated to remove the mill scale. The side surfaces and bottom surfaces of the steel plates were coated with anti-corrosive tape to confirm the corrosion progress of the top surface only during the corrosion tests. All edges of the top surface of each specimen were also wrapped with 5 mm anti-corrosion tape so that the non-corroded portion of the edge served as a reference for corrosion depth measurements. A rectangular area of 50 mm * 60 mm at the center of the specimen surface was selected as the corrosion depth measurement area for this study, considering the possible influence of the anti-corrosion tape on the junction of the corroded surface and the anti-corrosion tape.

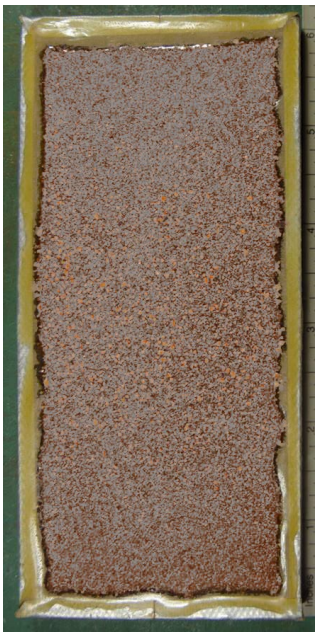

(a) Photograph of the specimen

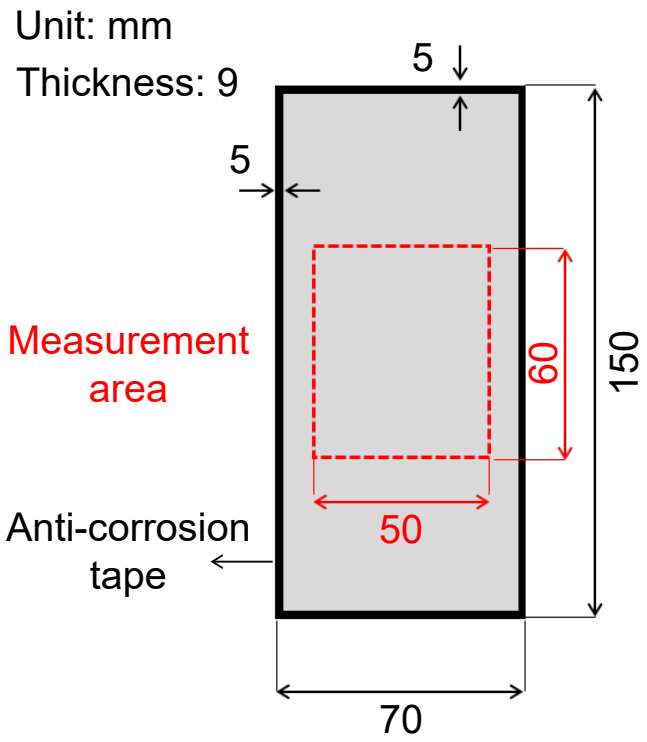

(b) Detailed parameters of the specimen

Figure 2-1. The shape and size of the specimen.

2.3 Conditions of corrosion tests and experimental setups

2.3.1 Direct atmospheric exposure corrosion test

The atmospheric exposure corrosion tests were carried out at the fields of the Japan Weathering Testing Center. In consideration of the climatic characteristics of Japan, there

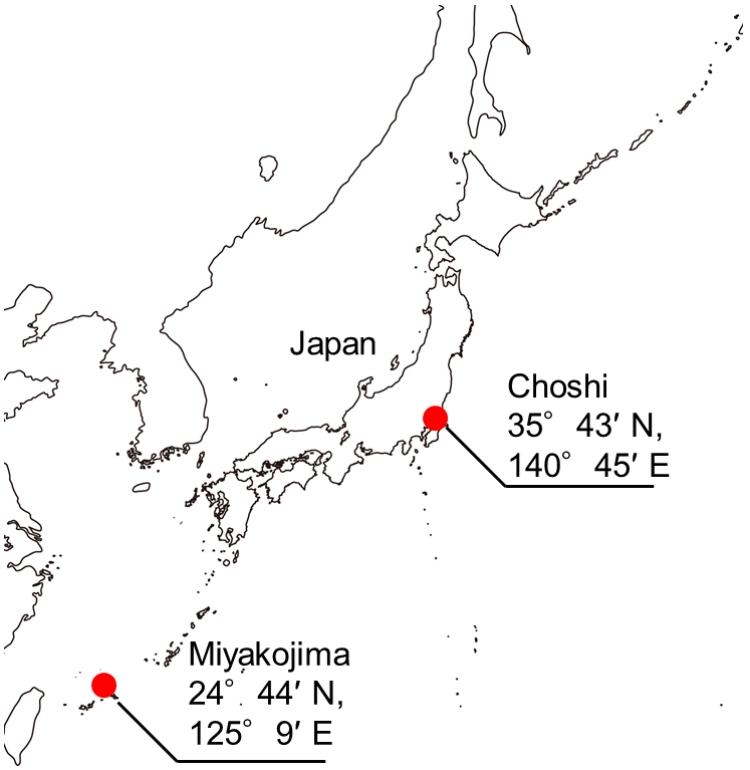

Figure 2-2. The locations of the atmospheric exposure test fields.

Figure 2-3. The appearance of the atmospheric exposure test.

are different atmospheric corrosion environments. Therefore, a location for a severe corrosion environment and a location for a general corrosion environment were selected to facilitate comparison. One of the sites was the Miyakojima exposure test and research center, located at 24°44′ N, 125°9′ E, 2 km from the nearest coastal area and 50.0 m from sea level. This site is a harsh environment with a maritime subtropical climate and degradation factors such as high temperature and humidity, abundant solar radiation, and large amounts of sea salt particles. The other site was the Choshi exposure test and research center, located at 35°43′ N, 140°45′ E, 4 km from the nearest coastal area and 53.6 m from sea level. This site has a general corrosion environment [2.1]. Figure 2-2 illustrates the locations of the experiment sites.

Figure 2-3 illustrates the appearance of the atmospheric exposure test. The steel plates were arranged in a horizontal position on the experiment stand according to JIS Z 2381 [2.2]. The specimens were directly exposed without any rooftops and eaves. The corrosion depths of the surfaces of the specimens facing skyward were estimated.

The direct atmospheric exposure tests were performed on three specimens for each type of steel for 6 months from April 2021 at Miyakojima and three specimens for each type of steel for 12 months from September 2020 at Choshi. A total of 24 specimens were subjected to atmospheric exposure tests. The basic environmental conditions for each test site during the experiment period are presented in Table 2-2.

Table 2-2. Environment conditions at exposure test sites.

Site	Period	Average temperature (℃)	Average relative humidity (%)	Average precipitation (mm)	Airborne salt (mdd)
Miyakojima	2021.04	22.5	79	0.8	0.28
	2021.05	26.7	92	5.4	0.14
	2021.06	28.0	93	11.9	0.36
	2021.07	28.8	87	4.4	0.17
	2021.08	27.9	92	9.0	0.27
	2021.09	28.0	89	6.7	0.17
Choshi	2020.09	23.7	89	6.9	0.14
	2020.10	17.2	82	9.0	0.12
	2020.11	13.7	79	8.4	0.07
	2020.12	7.2	71	1.1	0.13
	2021.01	5.1	68	2.5	0.14
	2021.02	7.5	59	1.7	0.36
	2021.03	12.0	74	5.0	0.13
	2021.04	13.8	68	3.9	0.30
	2021.05	18.0	82	3.8	0.07
	2021.06	20.8	86	4.6	0.08
	2021.07	24.1	92	15.0	0.07
	2021.08	25.9	90	12.4	0.05

2.3.2 Accelerated corrosion test ISO16539 Method B

Figure 2-4 illustrates the test procedure of ISO16539 Method B. Figure 2-5 illustrates the experimental setup for this test. The device for synthetic ocean water spraying and the test chamber for applying uniform temperature and humidity (SH-642, ESPEC Corp.) were separated. Synthetic ocean water with a salinity of 3.5% was sprayed on the surface of the steel plate. The target salt deposition of 28.0 ± 2.8 g/m^2 per specimen was achieved

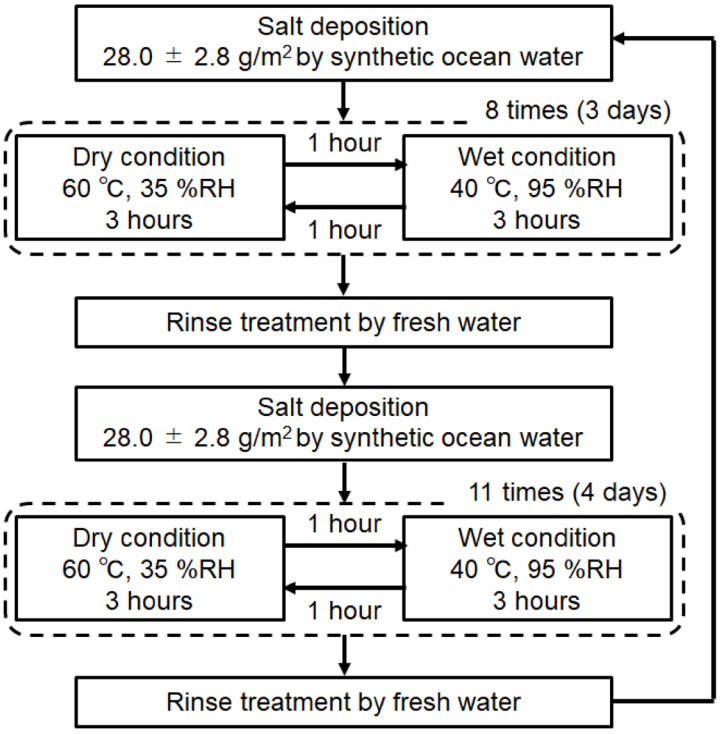

Figure 2-4. The procedure of accelerated corrosion test ISO16539 Method B.

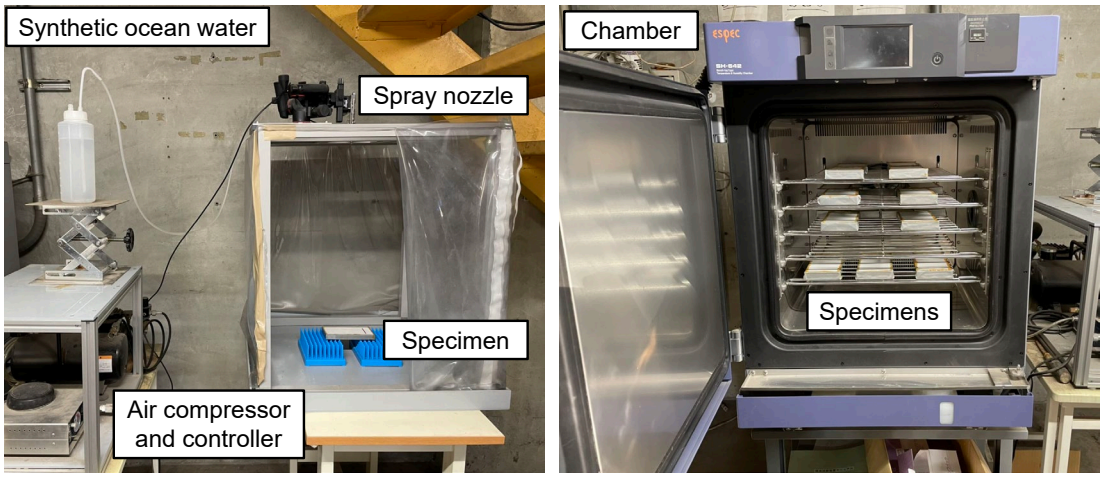

Figure 2-5. Experimental system for accelerated corrosion test ISO16539 Method B.

by the measurement of weight increase just after spraying. The processes of drying (60 ℃, 35 %RH) and wetting (40 ℃, 95 %RH) were repeated by every 3 hours with the transition

process of 1 hour. The one cycle consisting of the drying, the transition, the wetting, and the transition was 8 hours. This cycle continued for 8 runs, then, the surface of the specimen was rinsed with fresh water. After that, the synthetic ocean water was sprayed on the surface of the specimen, then, the drying and wetting procedures were continued for 11 runs. These test cycles took 7 days.

This test condition was based on the corrosion behavior of the metallic coated steels for the electric supplies in a couple of actual corrosion environments [2.3]. The developers of this test emphasized the importance of the control of the amount of salt deposition over a wide range and the relationship between the amount of salt deposition and the corrosion rate. The results of corrosion environment monitoring showed that the dry/wet cycle could be controlled by changing the temperature/humidity under the condition of constant absolute humidity. It was preferable to set the wetting rate to less than 50% in the dry/wet cycle. The developer of this test mentioned that the amount of salt deposition and the dry/wet conditions of 60 ℃, 35%RH and 40 ℃, 95%RH of this test were set closer to the actual environments compared to the other Salt Spray Test (SST) and Cyclic Corrosion Test (CCT) conditions [2.4]. In addition, ISO16539 mentions that this test condition can better reproduce the corrosion phenomenon in the atmospheric environments containing large amounts of sea salt than other accelerated corrosion tests such as the neutral salt spray test (NSS) by ISO9227 and the wet (salt/fog)/dry/humidity test by ISO14993 [2.5]. The accelerated corrosion test under this condition was performed on three specimens for each type of steel for 1 month (28 days), 3 months (84 days), and 6 months (168 days), respectively. A total of 36 specimens were subjected to the accelerated corrosion test ISO16539 Method B.

2.3.3 Accelerated corrosion test CCT Method A

This is an accelerated corrosion test named Cyclic Corrosion Test (CCT) Method A developed by Public Works Research Institute (PWRI), which is a developed accelerated corrosion test widely used in Japan. CCT has been proven to be effective in accelerated corrosion tests in steel structures, the automotive industry, and coating protection [2.6] [2.7] [2.8]. Figure 2-6 shows the test condition of CCT Method A. Figure 2-7 shows the experimental system for this test. One complete cycle required 24 h. It included 1 hour of wetting (30 ℃, 95%RH), 2 hours of surface spraying with saltwater (30 ℃, 5%NaClaq), 6 repetitions of one and half hours of wetting (50 ℃, 95%RH), 1.5 hours of drying (50 ℃, 20%RH), and another 1.5 hours of drying (30 ℃, 20%RH).

Same as the accelerated corrosion test ISO16539 Method B. The accelerated corrosion test by this condition was performed on three specimens for each type of steel for 1 month (28 days), 3 months (84 days), and 6 months (168 days), respectively. A total of 36 specimens were subjected to the accelerated corrosion test by Cyclic Corrosion Test Method A.

Therefore, in this study, a total of 96 (24 + 36 + 36) specimens were subjected to corrosion tests.

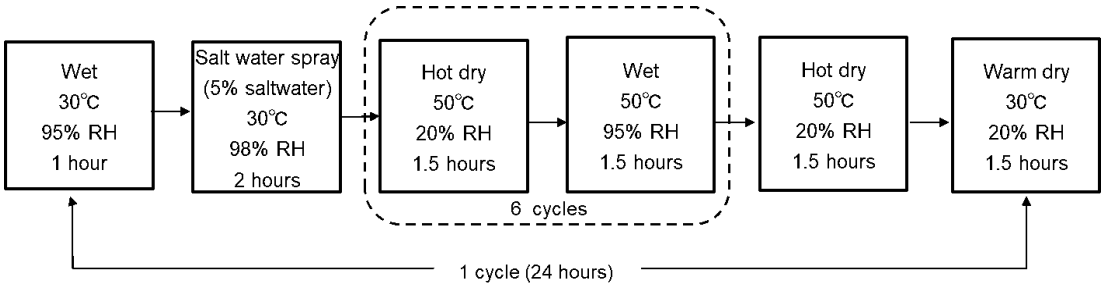

Figure 2-6. The procedure of accelerated corrosion test CCT Method A.

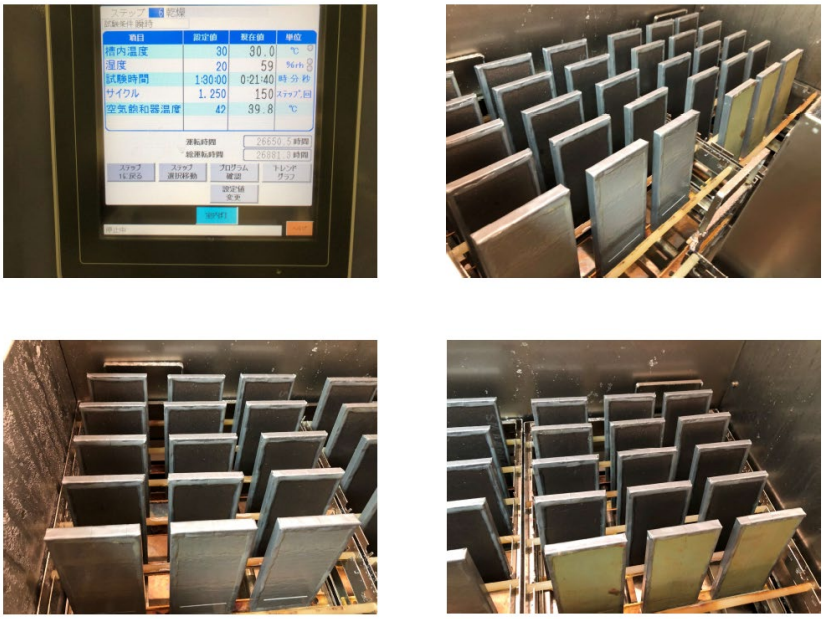

Figure 2-7. Experimental system for accelerated corrosion test CCT Method A.

2.4 Experimental results

2.4.1 Corroded surface observation

As the rust of the corroded surface needs to be removed when measuring its corrosion depth, the rust generated on the surface of the specimen after each corrosion test was observed prior to the corrosion depth measurement. Figure 2-8 shows the results of the specimen surface observations of 4 kinds of steel in 3 corrosion tests. The appearance of the corroded surface of the specimen prior to the removal of the rust produced by each corrosion test is shown.

In Miyakojima and Choshi atmospheric exposure tests, the surfaces of the steel plates were covered with a relatively adherent rust layer that could not be easily removed by hand. The color of the rust layer appears to be brown or orange. Visually, there was no

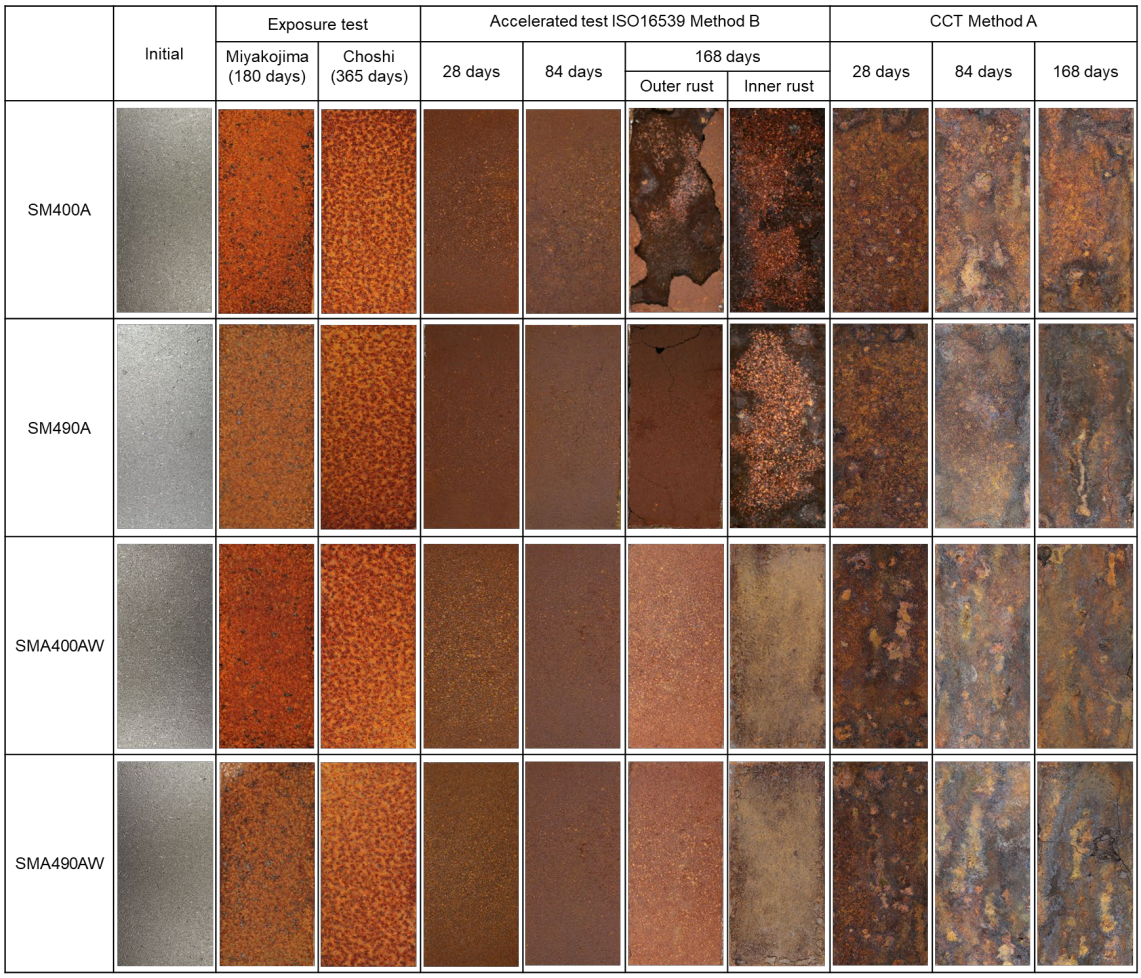

Figure 2-8. Rust observations of 4 kinds of steel in each corrosion test.

obvious difference between the rust of weathering steel and normal carbon steel.

In the accelerated corrosion test by ISO16539 Method B, the outer surfaces of the specimens were covered with a reddish-brown rust layer for the 28-day test period. The same rust layers were observed for the 84-day and 168-day test periods. These rust layers were very brittle and could be easily removed by hand. For the 28-day and 84-day test periods, there was no significant difference between the rust layers of weathering steel and normal carbon steel. However, for the 168-day test period, the rust layers of normal carbon steel were darker than that of weathering steel and the rust layers flaked off more

easily. The yellowish-brown rust layers on the surfaces of the specimens appear inside the outer reddish-brown rust layers. These yellowish-brown rust layers were not easily scraped off. After brushing the relatively adherent rust off the surfaces of the specimens with a wire brush, the normal carbon steel specimens reveal dark red rust layers, while the weathering steel specimens reveal reddish-grey rust layers.

In the accelerated corrosion test, CCT Method A developed by PWRI, all types of steel showed an uneven rust layer. For the 28-day test period, the corroded surfaces were covered by a reddish-brown rust layer. For the 28-day and 84-day test periods, the specimens had a reddish-grey rust layer. Visually, there was no significant difference between the rust layer of weathering steel and normal carbon steel. Compared to the accelerated corrosion test by ISO16539 Method B, the accelerated corrosion test CCT Method A seems to progress corrosion more quickly for the same experimental time.

2.4.2 Corrosion depth measurement and results

The rust on corroded surfaces was removed by blasting. After scraping off the rust on the corroded surfaces of the specimens, the corrosion depth data were measured by a laser focus measuring system, which resolution was 0.2 μm, and the measurement interval was 0.3 mm. Figure 2-9 shows the setup of the laser focus measuring system and the measurement area, a rectangular region of 50 mm * 60 mm in the center of the specimen. As shown in Figure 2-1, the reference spots were arranged at the edges of the surface of the specimen where the corrosion did not happen for being covered by the anti-corrosion tape. The baseline surface was set by three reference spots in the not corroded section. The difference in displacement between the baseline surface and the measured point was determined as the corrosion depth of the measured point. The mean corrosion depths for

every specimen were calculated from the measurements. In addition, the measured data was used for the spatial statistical analysis of the corrosion distribution of the corroded surfaces.

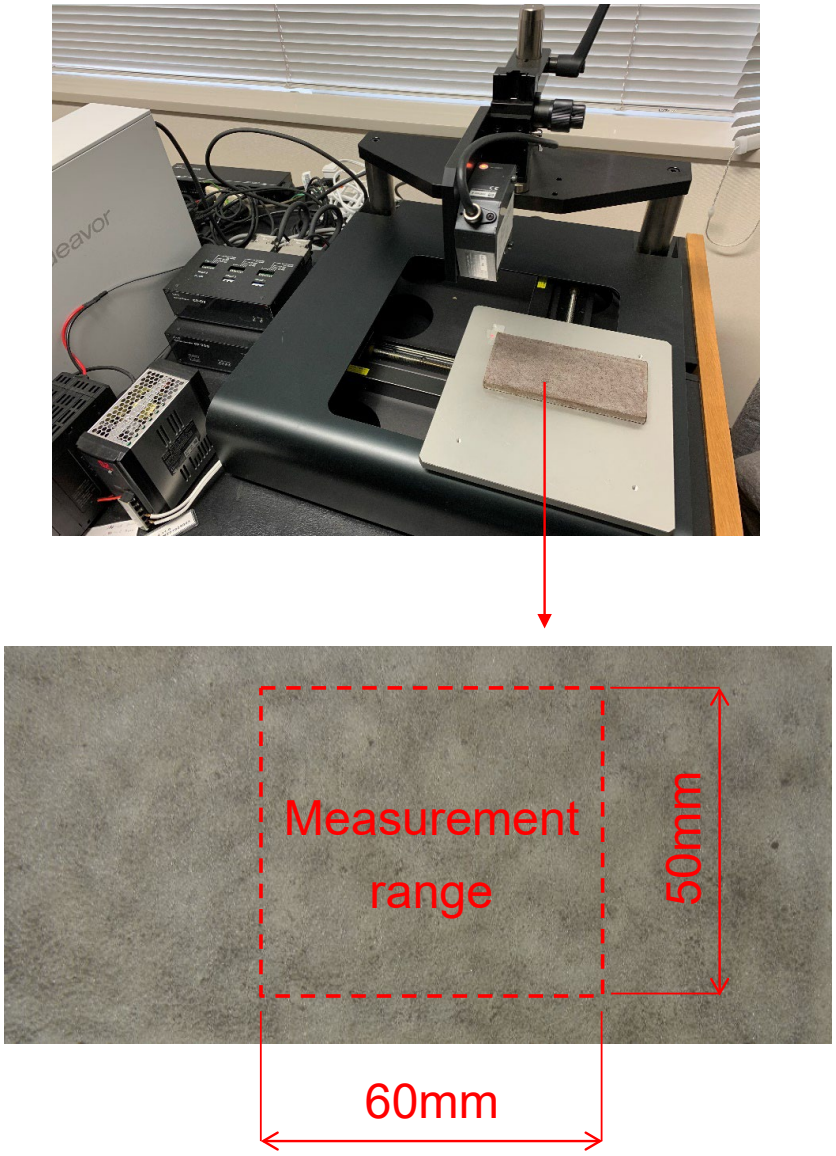

Figure 2-9. Rust observations of 4 kinds of steel in each corrosion test.

Figure 2-10 illustrates the mean corrosion depths of the specimens for the four kinds of steel in the atmospheric exposure tests. The magnitudes of the corrosion depths by the short terms of the exposure tests were small. Therefore, the standard deviations were relatively large in comparison with the mean values. From the figure, it could be observed that the mean corrosion depth of the weathering steel surface was lower than the mean corrosion depth of the normal carbon steel surface. Figure 2-11 and Figure 2-12 show the

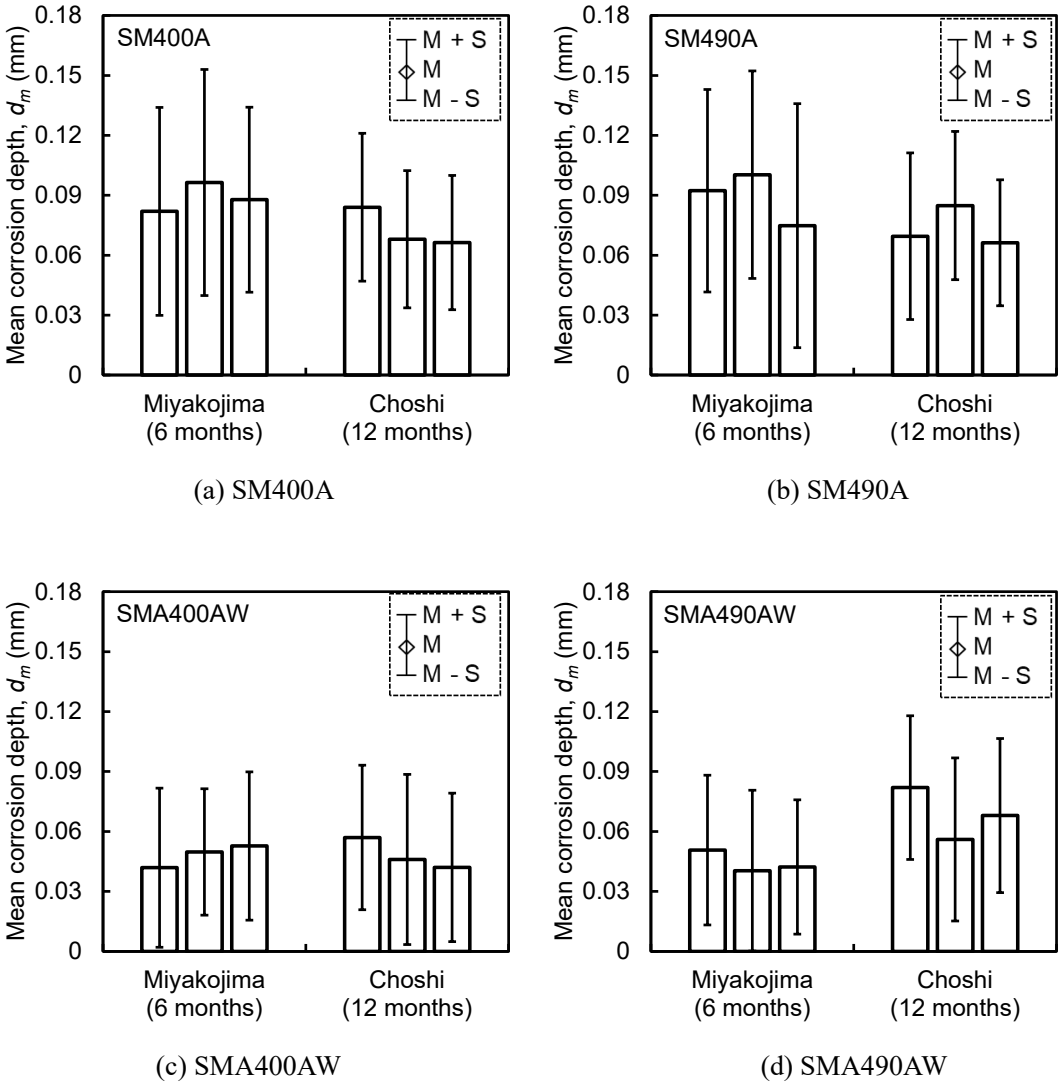

(a) SM400A (b) SM490A

(c) SMA400AW (d) SMA490AW

Figure 2-10. Mean corrosion depths of the specimens for the four kinds of steel (SM400A, SM490A, SMA400AW, and SMA490AW) in the two atmospheric exposure tests.

relationship between the mean corrosion depth and the period of the accelerated corrosion test by synthetic ocean water salt-deposition process, and the relationship between the mean corrosion depth and the period of the accelerated corrosion test CCT Method A for four kinds of steel on each specimen. According to previous research, the power approximation curve was used to fit the mean corrosion depth [2.9]. The coefficients of determination of the fitted curves for all four steels, R^2, were high. The mean corrosion depths of the accelerated corrosion tests increased with the test periods. From the figures, it could be observed that in the two accelerated corrosion tests, the corrosion depth of weathering steel was significantly smaller than that of normal carbon steel at the early stage of the tests (28 days), but with the increase of the experiment time, the corrosion depth of weathering steel was gradually similar to that of normal carbon steel. On the other hand, comparing these two accelerated corrosion tests, the corrosion progress of the four kinds of steel in the accelerated corrosion test CCT Method A was slightly faster than that in the accelerated corrosion test by ISO16539 Method B, especially in the late test time (84 days, 168 days).

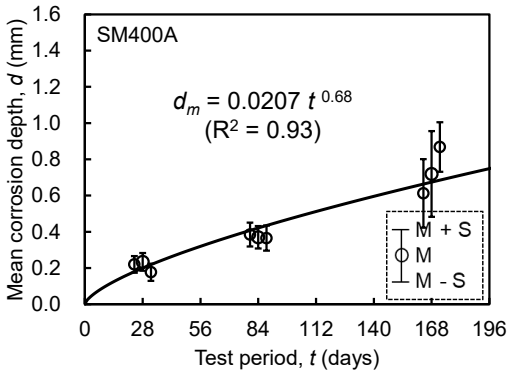

(a) SM400A

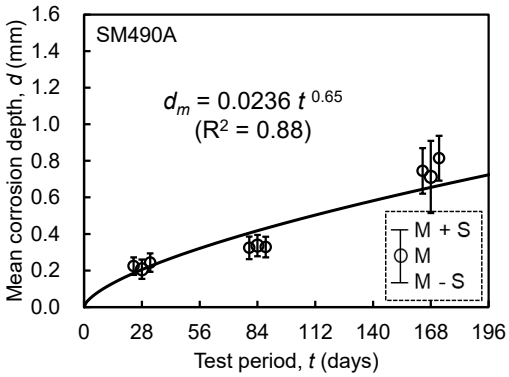

(b) SM490A

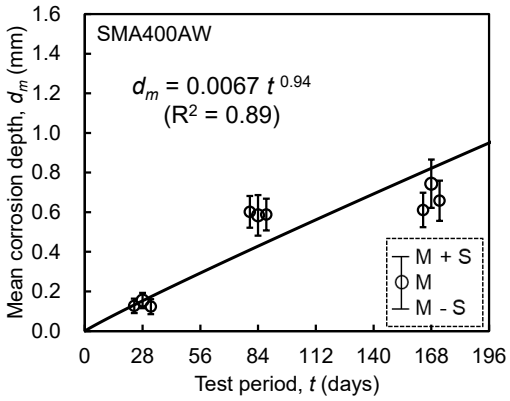

(c) SMA400AW

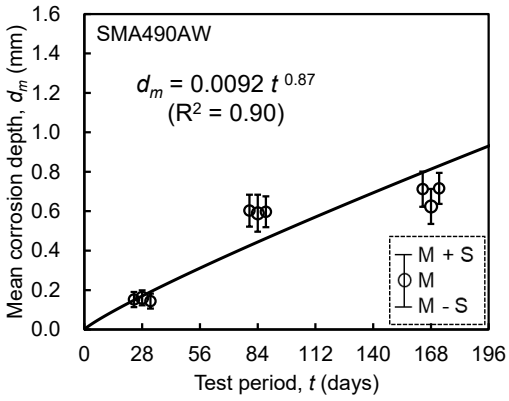

(d) SMA490AW

Figure 2-11. The relationship between the mean corrosion depth and the period of the accelerated corrosion test ISO16539 Method B for four kinds of steel (SM400A, SM490A, SMA400AW, and SMA490AW) on each specimen.

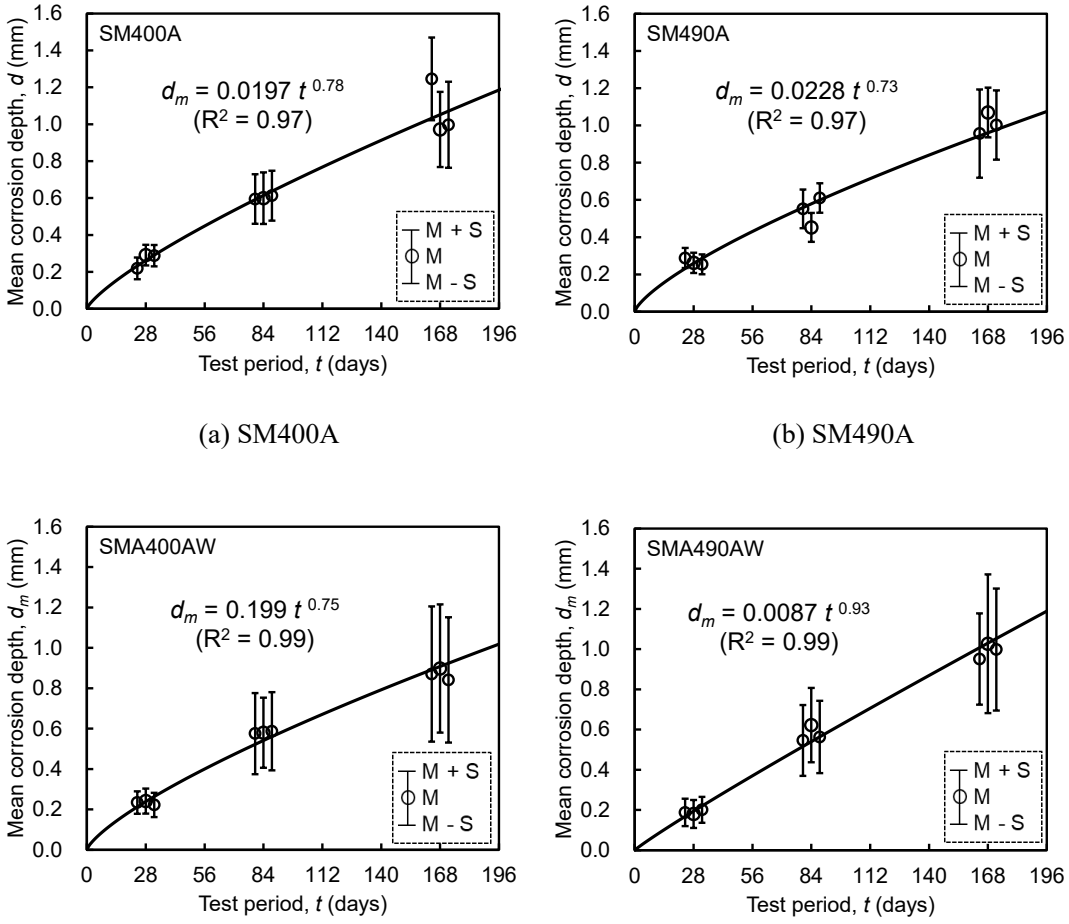

(a) SM400A

(b) SM490A

(c) SMA400AW

(d) SMA490AW

Figure 2-12. The relationship between the mean corrosion depth and the period of the accelerated corrosion test CCT Method A for four kinds of steel (SM400A, SM490A, SMA400AW, and SMA490AW) on each specimen.

Table 2-3. Averages of the mean corrosion depths of each kind of steel (mm).

	Miyakojima	Choshi	ISO16539			CCT Method A		
days	180	365	28	84	168	28	84	168
SM400A	0.089	0.073	0.210	0.373	0.733	0.266	0.602	1.072
SM490A	0.089	0.074	0.225	0.329	0.757	0.268	0.538	1.009
Average	0.089	0.073	0.218	0.351	0.745	0.267	0.570	1.040
SM400AW	0.048	0.048	0.135	0.591	0.671	0.232	0.581	0.870
SMA490AW	0.044	0.069	0.152	0.597	0.684	0.190	0.577	0.992
Average	0.046	0.059	0.143	0.594	0.677	0.211	0.579	0.931

Table 2-3 shows the averages of the mean corrosion depths of four kinds of steel in different corrosion environments. The averages of the mean corrosion depths of normal carbon steel and weathering steel specimens were 0.089 mm & 0.044 mm at Miyakojima for 6 months, and 0.073 mm & 0.059 mm at Choshi for 12 months. The averages of the mean corrosion depths of normal carbon steel and weathering steel specimens in ISO16539 Method B and CCT Method A were 0.218 mm & 0.143 mm and 0.267 mm & 0.211 mm at 28 days. The accelerated test gave greater corrosion depths than the exposure tests. The average mean corrosion depth by the accelerated corrosion test ISO16539 Method B of 28 days for normal carbon steel was 2.4 to 3.0 times larger than those by the atmospheric exposure tests of 6 months at Miyakojima and 12 months at Choshi. And the average mean corrosion depth by the accelerated test ISO16539 Method B of 28 days for weathering steel was 2.4 to 3.1 times larger than those by the exposure tests of 6 months at Miyakojima and 12 months at Choshi. The average mean corrosion depth by the accelerated test CCT Method A of 28 days for normal carbon steel was 3.0 to 3.7 times larger than those by the exposure tests of 6 months at Miyakojima and 12 months at

Choshi. And the average mean corrosion depth by the accelerated test CCT Method A of 28 days for weathering steel was 3.6 to 4.6 times larger than those by the exposure tests of 6 months at Miyakojima and 12 months at Choshi.

2.5 Summary

In this chapter, the corrosion progress of two normal carbon steels and two weathering steels under different corrosion environments were compared. The basic data analysis and comparison of the corrosion progress of the steels in different corrosion environments were also carried out. And these basic analyses will be used for the spatial statistical analysis in Chapter 3.

References

2.1 Kamimura, T., Hara, S., Miyuki, H., Yamashita, M. and Uchida, H., 2006. Composition and protective ability of rust layer formed on weathering steel exposed to various environments. *Corrosion Science*, *48*(9), pp.2799-2812.

2.2 JIS, Z 2381:2017. General requirements for atmospheric exposure testing.

2.3 Fujii, K., Ohashi, K. and Kajiyama, H., 2006. Corrosion aspect of electrical appliances–development of new accelerated corrosion Test simulating appliances environment (1). *Zairyo-to-Kankyo*, *55*, pp.349-355.

2.4 Kajiyama, H., Fujita, S., Fujii, K. and Sakai, M., 2006. Problem of Conventional Accelerated Corrosion Tests and Development of New Accelerated Corrosion Test: Development of New Accelerated Corrosion Test Simulating Electrical Appliance. *Corrosion Engineering*, *55*(8), pp.475-490.

2.5 ISO16539:2013. Corrosion of metals and alloys – accelerated cyclic corrosion tests with exposure to synthetic ocean water salt-deposition process – 'Dry' and 'wet' conditions at constant absolute humidity.

2.6 Prosek, T., Larché, N., Vlot, M., Goodwin, F. and Thierry, D., 2010. Corrosion performance of Zn–Al–Mg coatings in open and confined zones in conditions simulating automotive applications. *Materials and Corrosion*, *61*(5), pp.412-420.

2.7 Liu, M., Guo, Y., Wang, J. and Yergin, M., 2018. Corrosion avoidance in lightweight materials for automotive applications. *NPJ Materials Degradation*, *2*(1), pp.1-4.

2.8 Hosking, N.C., Ström, M.A., Shipway, P.H. and Rudd, C.D., 2007. Corrosion resistance of zinc–magnesium coated steel. *Corrosion science*, *49*(9), pp.3669-3695.

2.9 Jiang, F., Hirohata, M., Liu, J. and Ojima, K., 2022. Application of accelerated cyclic test with synthetic ocean water salt-deposition process to the evaluation on corrosion characteristics of weathering steel. *Corrosion Engineering, Science and Technology*, *57*(3), pp.280-289.

Chapter 3 Spatial statistical analysis of corroded surface

3.1 Introduction

In Chapter 2, the corrosion depth data of the corroded surfaces were obtained for different cases by four kinds of steel in four corrosion environments. Although the basic statistical analysis was carried out by methods such as surface observation and average corrosion depth, there was no in-depth analysis of the spatial properties of the corroded surfaces. Quantification of the corrosion situation is an important topic. In this chapter, the spatial properties of the corroded surfaces of the steel plates were analyzed using the semivariogram function as a method of spatial statistical analysis. The spatial properties of the corroded surfaces of different steel materials under accelerated corrosion tests and atmospheric exposure tests were compared by means of range and sill, which represent the spatial statistical information of the corroded surfaces and are mentioned later in this chapter, to verify whether the two accelerated corrosion tests performed in this study can simulate the real atmospheric corrosion environment.

3.2 Semivariogram

In statistics, the kriging variogram model is a method of interpolation based on the gaussian process governed by prior covariances [3.1]. To make a prediction with the kriging interpolation method, two tasks are necessary. The first step is to reveal the rules of dependency. The variograms and covariance functions are generated to estimate the statistical dependence values that depend on the autocorrelation model. The second step is to predict the unknown values. In this step, semivariogram is used to fit the prediction model.

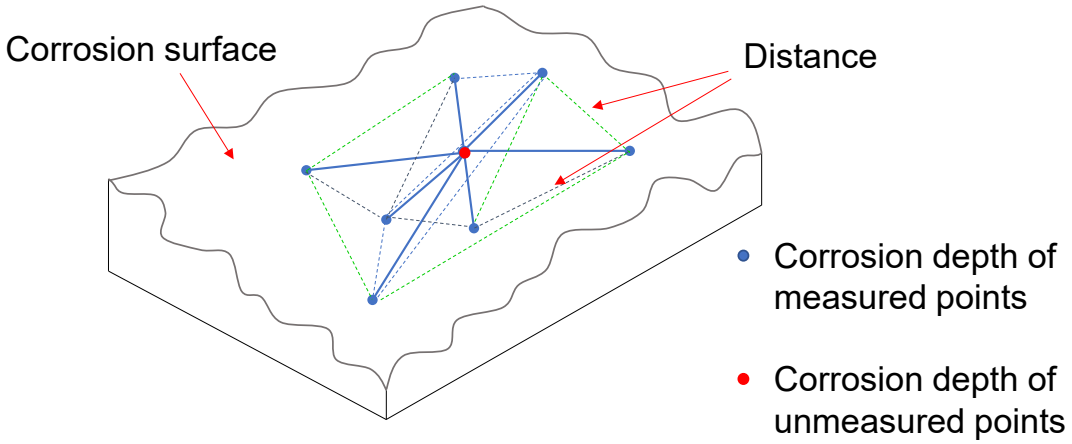

Figure 3-1. Spatial modeling of measured points for semivariogram analysis.

Kriging weights the surrounding measured values to originate a prediction for an unmeasured location. The general formula is formed as a weighted sum of the data described by equation (3.1).

$$\hat{Z}(s_0) = \sum_{i=1}^{N} \lambda_i Z(s_i) \tag{3.1}$$

Where $Z(s_i)$ is the measured value at the i-th location; λ_i is an unknown weight for the measured value at the i-th location; s_0 is the prediction location; $\hat{Z}(s_0)$ is the predicted value at the location of s_0; N is the number of measured values.

λ_i depends on a fitted model to the measured points, the distance to the prediction location, and the spatial relationships among the measured values around the prediction location. For clarifying the spatial autocorrelation structure on the corroded surface of the corroded specimens, a semivariogram has been used to extract the spatial statistics of range, and sill representing the properties of the corroded surface [3.2] [3.3] [3.4].

The semivariogram is an indicator of the spatial correlation between the corrosion depth at an arbitrary location and the corrosion depth at a distance from the arbitrary location

on the corroded surface. In the spatial modeling of measured points on the corroded surface using semivariogram, all pairs of locations separated by a distance, h, is calculated with the difference squared between the corrosion depths of the paired locations. Figure 3-1 shows the image of the corrosion depth and the distance of a pair of measured points. This process repeats for each measured point.

The range and sill, which are representing the autocorrelation structure of the corroded surface, were calculated from the semivariogram by determining, $\gamma(h)$, shown in equation (3.2).

$$\gamma(h) = \frac{1}{2|N(h)|}\sum_{i=1}^{N(h)}\left(z_j - z_k\right)^2 \tag{3.2}$$

Where $\gamma(h)$ is the range; $N(h)$ is the set of all pairwise Euclidean distances j - k = h; $|N(h)|$ is the number of distinct pairs in $N(h)$; z_j, z_k are the corrosion depths at spatial

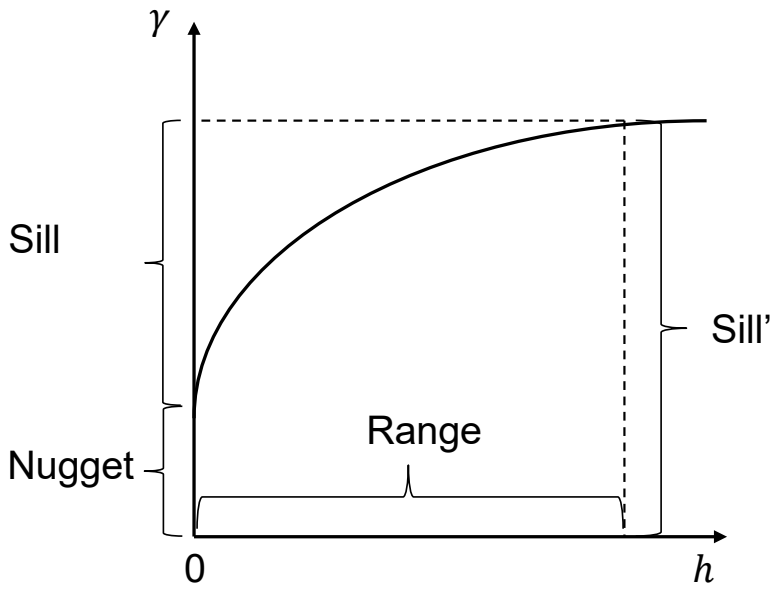

Figure 3-2. The structure of a semivariogram.

locations j and k, respectively.

If two locations, j and k, are close to each other in terms of the distance measure of $d(j,k)$, they are expected to be similar, so the difference in their values, $z_j - z_k$, will be small. As j and k get farther apart, they become less similar, so the difference in their values, $z_j - z_k$, will become larger. This can be seen in the following Figure 3-2, which shows the anatomy of a typical semivariogram.

Spatial autocorrelation quantifies a basic principle of geography: things that are closer are more alike than things farther apart. Thus, pairs of locations that are closer (far left on the *x*-axis of the semivariogram cloud) should have more similar values (low on the *y*-axis of the semivariogram cloud). As pairs of locations become farther apart (moving to the right on the *x*-axis of the semivariogram cloud), they should become more dissimilar and have a higher squared difference (moving up on the *y*-axis of the semivariogram cloud).

The variance of the difference increases with distance, so the semivariogram can be thought of as a dissimilarity function. Several terms are often associated with this function, and they are also used in Geostatistical analysis. The height that the semivariogram reaches when it levels off is sill'. It is often composed of two parts: a discontinuity at the origin, called the nugget effect, and the sill; added together, these give the sill'. The nugget effect can be further divided into measurement error and microscale variation. Theoretically, at zero separation distance, the semivariogram value is 0. However, at an infinitely small separation distance, the semivariogram often exhibits a nugget effect, which is a value greater than 0. The nugget effect is simply the sum of measurement error and microscale variation, since either component can be zero, the nugget effect can be composed wholly of one or the other. The distance at which the semivariogram levels off to the sill' is the range.

In this study, the semivariogram analysis was carried out for all directions assuming isotropy because the corroded surface properties did not have spatial variation in specific directions. Consequently, the semivariogram calculated from this analysis can only be treated as a function of distance. There are deviations of the points on the empirical semivariogram from the model; some points are above the model curve, and some points are below. However, if add the distance each point is above the line and add the distance each point is below the line, the two values should be similar. To fit a model to the points forming the empirical semivariogram, several types of semivariogram models are available. The most frequently applied variogram functions are the spherical, exponential, and Gaussian models. The spherical and exponential functions have essentially a similar shape, but their effective ranges are different. The low-range spherical variogram describes observables with spatial dependencies over short distances. Exponential variograms describe correlation lengths over longer distances. A Gaussian model is of a fundamentally different shape describing a different spatial dependency. Therefore, in this study, the spherical model is the most suitable semivariogram model. The previous studies also show that the spherical model could fit the semivariogram of the corroded surfaces of the steel plates [3.5] [3.6] [3.7]. Its features are that it has a linear growth when the distance between 2 points is short (closer to the point of origin); however, when it passes the range value, it will be a line parallel to the horizontal axis. In other words, this model shows a progressive decrease of spatial autocorrelation until some distance, beyond which autocorrelation is zero. The formula of the spherical model is described by equation (3.3).

$$\gamma = \begin{cases} 0, & h = 0 \\ C_0 + C\left(\frac{3}{2}\frac{h}{a} - \frac{1}{2}\frac{h^3}{a^3}\right), & 0 < h \leq a \\ C_0 + C, & h > a \end{cases} \tag{3.3}$$

Where C_0 is the nugget constant; C is the sill; a is the effective range.

From the above, the spatial autocorrelation structure of the whole corroded surface in this study can be quantitatively evaluated by the spatial statistics (sill and range) calculated from the theoretical semivariogram by the spherical model.

3.3 Sill and range results of each specimen

Using an SM400A specimen from the exposure test at Miyakojima as an example, Figure 3-3 shows how to calculate the sill and range of the corroded surface of this specimen. The spherical model presented in equation (3.3) is consistent with the experimentally measured values. Tables 3-1 and Table 3-2 show the specific sill and range values for every specimen, respectively.

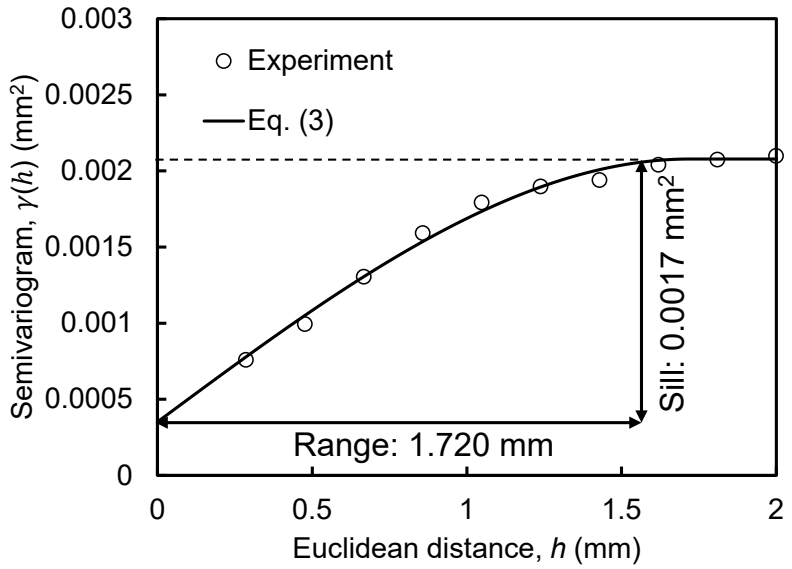

Figure 3-3. The calculation of the sill and range of the corroded surface.

Table 3-1. Results of sill (mm^2).

	Miyakojima	Choshi	ISO16539			CCT Method A		
days	180	365	28	84	168	28	84	168
SM400A	0.00173	0.00058	0.00123	0.00203	0.01000	0.00214	0.01685	0.02468
	0.00214	0.00068	0.00094	0.00220	0.01395	0.00197	0.01559	0.02133
	0.00189	0.00071	0.00116	0.00261	0.01489	0.00216	0.01346	0.02077
SM490A	0.00227	0.00044	0.00128	0.00267	0.01083	0.00148	0.00538	0.02319
	0.00270	0.00091	0.00064	0.00202	0.01462	0.00154	0.00308	0.02011
	0.00208	0.00057	0.00058	0.00213	0.01315	0.00140	0.00316	0.01673
SMA400AW	0.00094	0.00059	0.00084	0.00390	0.00681	0.00142	0.02404	0.02843
	0.00049	0.00078	0.00098	0.00436	0.01129	0.00231	0.03015	0.03213
	0.00083	0.00098	0.00120	0.00415	0.00896	0.00211	0.02712	0.02977
SMA490AW	0.00089	0.00089	0.00096	0.00426	0.00560	0.00290	0.02196	0.02731
	0.00094	0.00071	0.00113	0.00369	0.00632	0.00434	0.02543	0.02974
	0.00057	0.00051	0.00087	0.00333	0.00460	0.00288	0.02144	0.02916

Table 3-2. Results of range (mm).

	Miyakojima	Choshi	ISO16539			CCT Method A		
days	180	365	28	84	168	28	84	168
SM400A	1.720	1.028	0.581	6.442	20.495	5.477	7.641	20.144
	1.796	1.158	0.579	7.986	17.678	5.828	6.096	22.434
	1.654	1.232	0.552	8.658	10.773	5.976	8.143	19.883
SM490A	1.693	1.260	5.515	7.425	10.687	4.382	3.664	17.002
	1.842	0.885	1.108	7.816	17.393	2.939	4.755	16.838
	1.708	1.046	1.589	6.651	8.482	3.112	6.881	19.354
SMA400AW	1.924	1.499	2.660	5.658	6.692	5.251	7.253	7.899
	1.880	1.040	2.778	5.687	7.080	6.805	5.179	7.931
	1.795	0.552	2.237	6.712	7.208	5.112	6.873	8.181
SMA490AW	1.997	1.092	1.963	6.085	6.392	6.534	12.159	16.184
	2.091	1.303	1.682	6.721	6.324	5.768	6.979	7.881
	1.083	1.501	3.368	5.827	5.854	5.469	7.295	9.322

3.4 Relationship between mean corrosion depth and spatial statistical values

The previous research has verified that the spatial statistical values of the corroded steel surfaces demonstrated the dependency on the mean corrosion depth [3.7]. The research on the relationship between the spatial statistical values and the mean corrosion depth of corroded surfaces makes it possible to compare the spatial properties of steels in different corrosive environments. In this section, the relationship between the spatial statistical values and the mean corrosion depth of the four kinds of steel in different corrosive environments was examined. According to previous studies, their relationship can be approximated by some functions [3.3]. The spatial statistics values and average corrosion depths from the long-time accelerated test (168 days) may be too large to be compared with atmospheric data of one year or less, and using any model that fits the range or sill will give similar results. However, when using an approximate curve fit, consideration needs to be given to whether it is realistic. When the mean corrosion depth is zero, it means that corrosion has not yet started, and at this point, the spatial properties representing sill and range should also be zero. Therefore, the fitted curve should pass through the zero point. Then, as the corrosion becomes more severe, the corrosion depth at any point on the corroded surface will be increasingly affected by the surrounding point corrosion. This means that the fitted curve should be an increasing function. As corrosion proceeds, the range of corrosion depths affecting any point cannot be infinite. Therefore the power function is the appropriate fitting method.

In this study, the relationship between spatial statistics values (sill and range) and mean corrosion depth of four kinds of steel under the accelerated corrosion test by ISO16539 Method B and CCT Method A were investigated, and they were compared with the spatial statistics values and mean corrosion depth under atmospheric exposure environment to

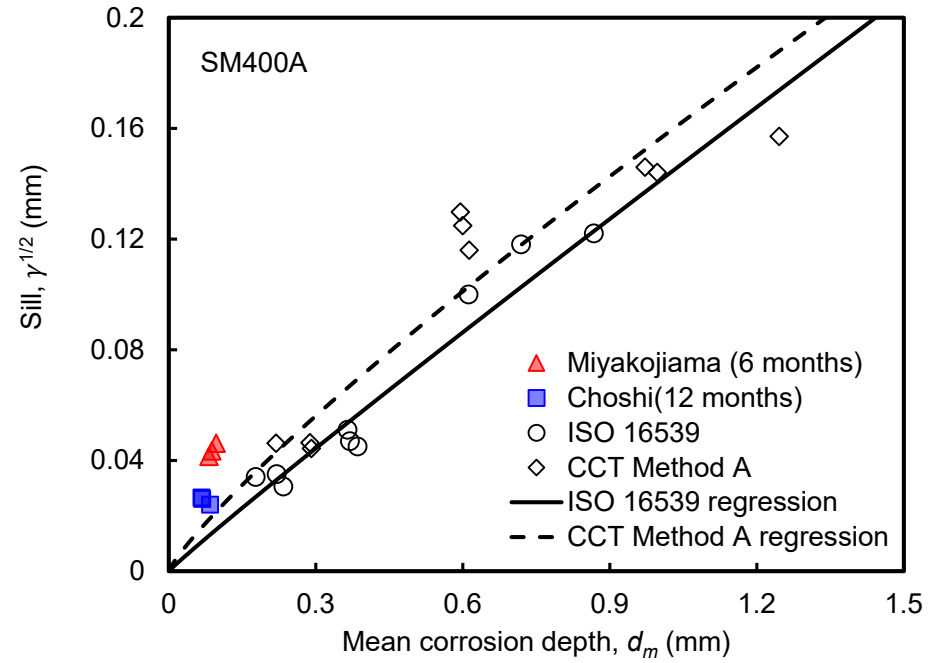

(a) SM400A in four kinds of corrosion environments

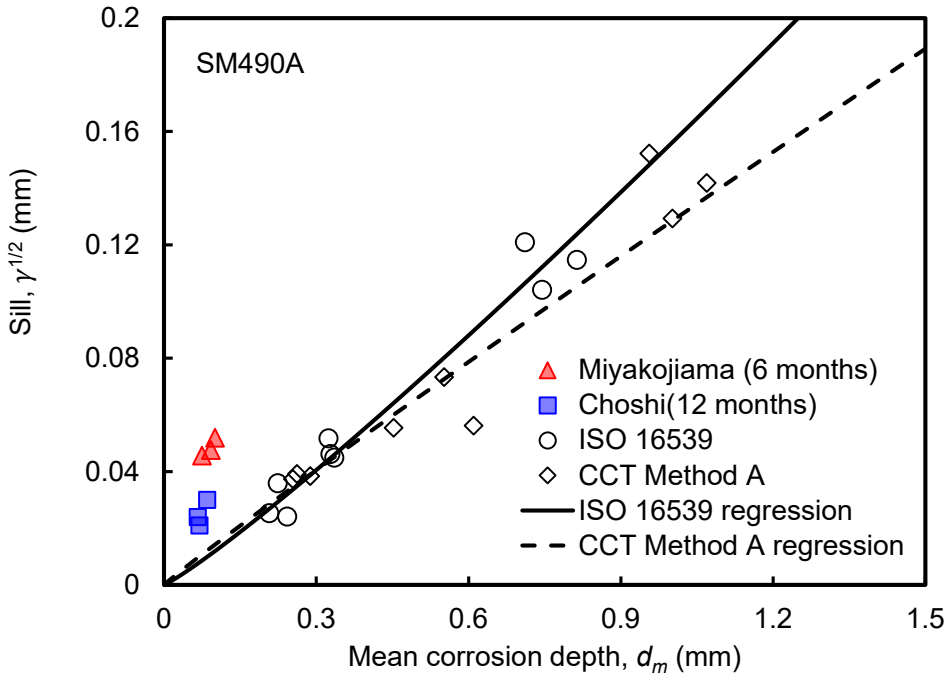

(b) SM490A in four kinds of corrosion environments

Figure 3-4. The relationships between the sill and the mean corrosion depth.

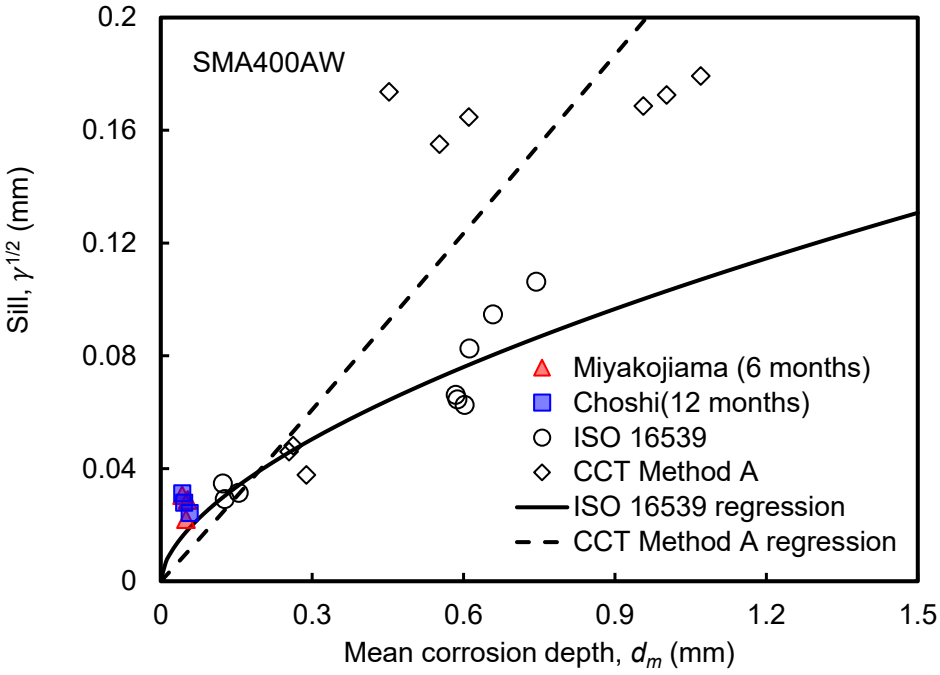

(c) SMA400AW in four kinds of corrosion environments

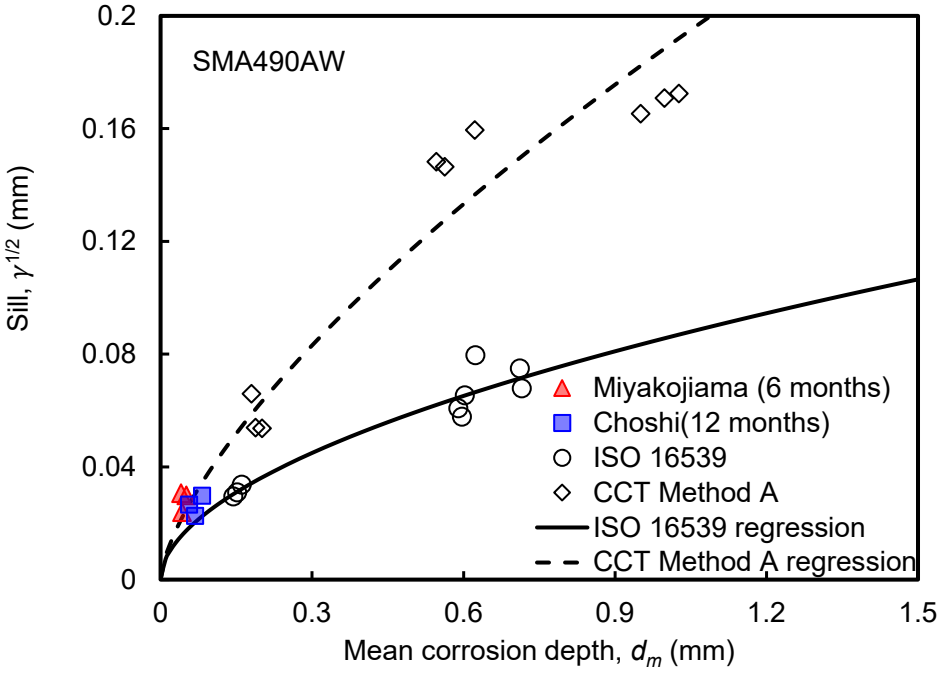

(d) SMA490AW in four kinds of corrosion environments

Figure 3-4. The relationships between the sill and the mean corrosion depth.

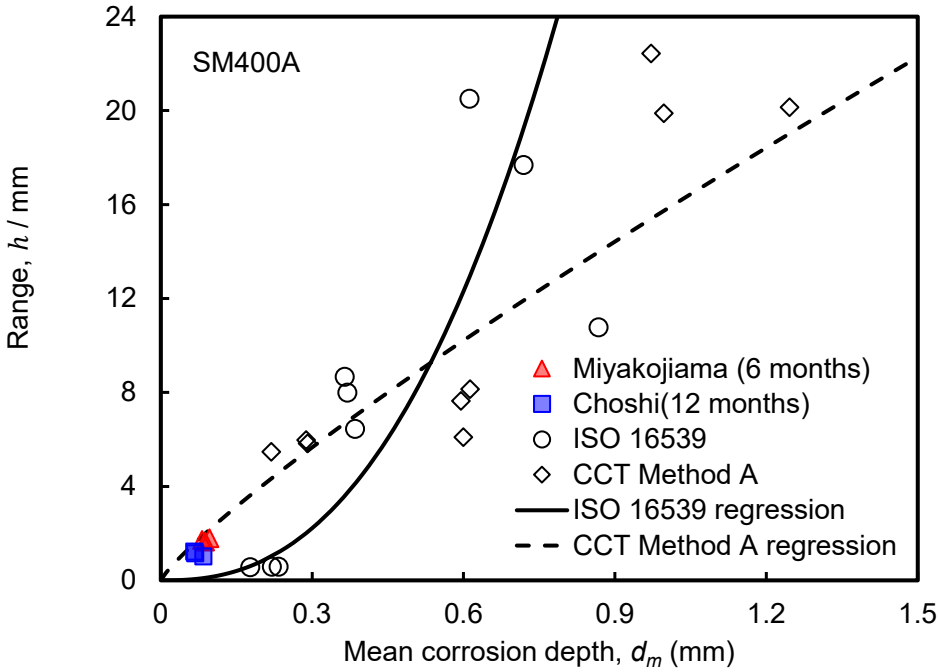

(a) SM400A in four kinds of corrosion environments

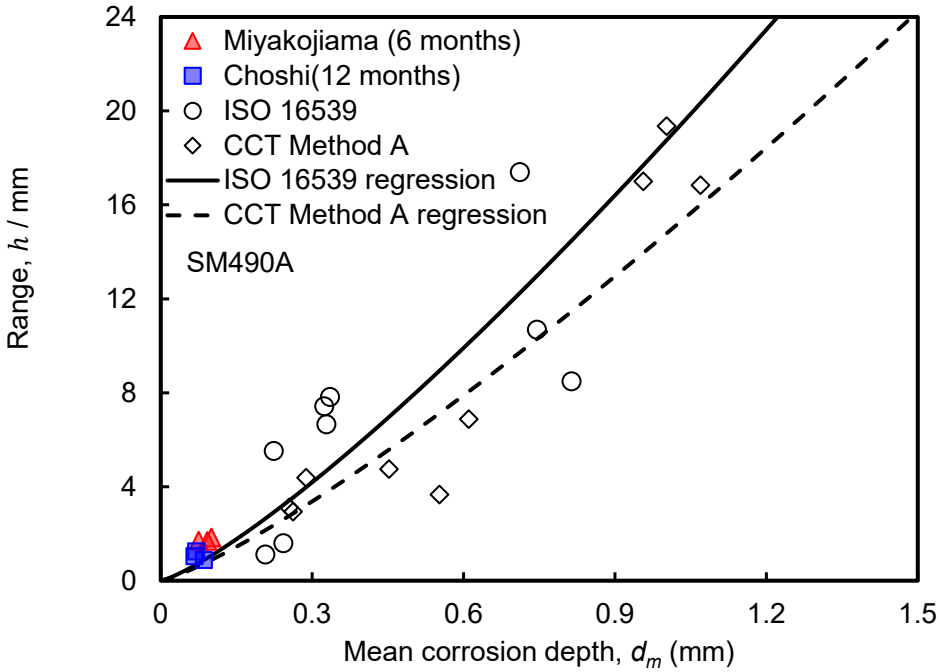

(b) SM490A in four kinds of corrosion environments

Figure 3-5. The relationships between the range and the mean corrosion depth.

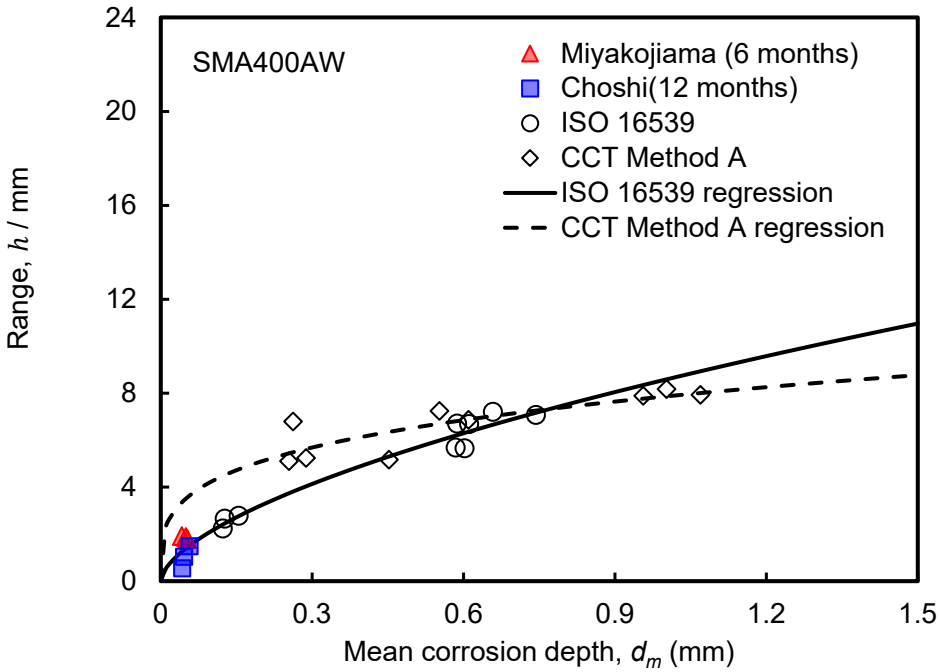

(c) SMA400AW in four kinds of corrosion environments

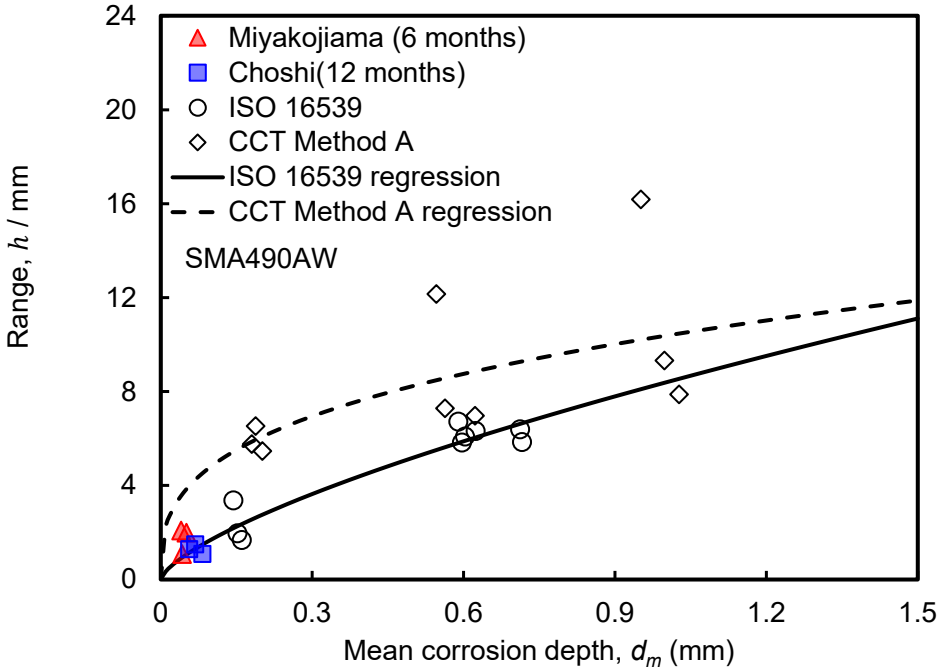

(d) SMA490AW in four kinds of corrosion environments

Figure 3-5. The relationships between the range and the mean corrosion depth.

verify the simulation effect of two accelerated corrosion tests on the actual corrosion environment. Figure 3-4 shows the relationships between the sill and the mean corrosion depth. Figure 3-5 shows the relationships between the range and the mean corrosion depth. Because of the short test time of the atmospheric exposure test, it is equivalent to the early stage of the accelerated corrosion tests. From the figure can be observed, weathering steel and normal carbon steel have different spatial properties of corrosion, and different standards of the same type of steel (SM400A & SM490A, SMA400AW & SMA490AW) have similar spatial properties. The early stages of both accelerated corrosion tests can fit the atmospheric exposure test, but their spatial statistics of corrosion are not similar. Root Mean Square Error (RMSE) is calculated for discussing the accuracy of the fitted curve. The RMSE is the standard deviation of the residuals (prediction error), which indicates the degree of concentration of the data near the best-fit line. It is often used in regression analysis to verify experimental results. Equation (3.4) explains the calculation of RMSE. The smaller the value of RMSE, the more the accelerated corrosion test can simulate the actual exposure test.

$$\mathrm{RMSE} = \sqrt{\frac{1}{N}\sum_{i=1}^{N}(Y_i - f(x_i))^2} \tag{3.4}$$

Where N is the number of specimens of a certain type of steel in Miyakojima and Choshi; Y_i is the spatial statistics values in Miyakojima and Choshi; $f(x_i)$ is the predicted values based on fitting curves of two accelerated corrosion tests.

The RMSE results of the sill and range by the power function models of two accelerated corrosion tests are shown in Table 3-3. Basically, when the steel is normal carbon steel, the RMSE value of accelerated corrosion test CCT Method A is smaller, which means that for normal carbon steel, the corroded surface properties of steel under accelerated

Table 3-3. RMSE of sill and range.

	Sill (mm^2)		Range (mm)	
	ISO16539	CCT Method A	ISO16539	CCT Method A
SM400A	0.024	0.018	1.371	0.478
SM490A	0.029	0.027	0.653	0.785
SMA400AW	0.011	0.019	0.481	2.084
SMA490AW	0.010	0.006	0.649	2.528

corrosion test by ISO16539 Method B are not as similar as those of accelerated corrosion test CCT Method A to atmospheric exposure test. When the steel is weathering steel, the RMSE value of the accelerated corrosion test by ISO16539 Method B is smaller, which means that for weathering steel, the corroded surface properties of the steel under ISO16539 Method B are closer to the atmospheric exposure test.

3.5 Summary

In this chapter, the applicability of the accelerated corrosion test ISO16539 Method B for assessing the corroded surface properties of the unpainted steel was investigated by comparing it with the atmospheric exposure tests and the accelerated corrosion test CCT Method A. Spatial statistical analysis was performed on the corroded surfaces of specimens that were subjected to the atmospheric exposure tests and two accelerated corrosion tests. The results showed that the corrosion properties of unpainted steels in actual atmospheric environments could be predicted in a relatively short period of time by accelerated tests ISO16539 Method B and CCT Method A. The semivariogram representing the geometric properties of the corroded surface profile showed a similar trend in the same type of steel. However, the values of the spatial properties of the corroded surface showed differences in different types of steel. Under accelerated test

CCT Method A, the spatial properties of corroded surfaces of normal carbon steels were closer to those of exposure tests. And under accelerated test ISO16539 Method B, the spatial properties of corroded surfaces of weathering steels were closer to those of exposure tests. Therefore, different accelerated corrosion tests can be selected according to the actual situation to simulate the real corrosion situation.

References

3.1 Gottschalk, H. and Kahl, K., 2020. Coarsening in Algebraic Multigrid using Gaussian Processes. *arXiv preprint arXiv:2004.11427*.

3.2 Sadawy, M.M., Ismael, A.F. and Gouda, M.A., 2015. Geostatistical analysis for corrosion in oil steel tank. *Am J Sci Technol*, *2*, pp.38-42.

3.3 Shigenobu, K., Young, S.J., Kazuhiro, U. and Jin, H.A., 2012. Numerical simulations for time-dependent corrosion surfaces of unpainted carbon steel plates in atmospheric corrosive environments using spatial statistical techniques. *Corrosion Engineering*, *61*(7), pp.203-203.

3.4 Kainuma, S., Yang, M., Xie, J. and Jeong, Y.S., 2021. Time-dependent prediction on the localized corrosion of steel structure using spatial statistical simulation. *International Journal of Steel Structures*, *21*(3), pp.987-1003.

3.5 Merino, G.G., Jones, D., Stooksbury, D.E. and Hubbard, K.G., 2001. Determination of semivariogram models to krige hourly and daily solar irradiance in western Nebraska. *Journal of Applied Meteorology*, *40*(6), pp.1085-1094.

3.6 Ly, S., Charles, C. and Degre, A., 2011. Geostatistical interpolation of daily rainfall at catchment scale: the use of several variogram models in the Ourthe and Ambleve catchments, Belgium. *Hydrology and Earth System Sciences*, *15*(7), pp.2259-2274.

3.7 Jiang, F., Hirohata, M., Liu, J. and Ojima, K., 2022. Application of accelerated cyclic test with synthetic ocean water salt-deposition process to the evaluation on corrosion characteristics of weathering steel. *Corrosion Engineering, Science and Technology*, *57*(3), pp.280-289.

Chapter 4 A corrosion prediction model using generative adversarial network (GAN)

4.1 Introduction

In recent years, artificial intelligence has been developing rapidly, and neural networks have been developed from simple artificial neural networks to various kinds of deep neural networks, which have been applied in various fields [4.1].

Generative adversarial network (GAN) is a product of the development of neural networks and a more active field of deep learning in recent years. It uses the idea of the game to optimize the generator, and then reuses the generator to generate data after completing training. In 2014, Ian Goodfellow et al. proposed GAN, and GAN started a revolution in the field of deep learning [4.2]. This revolution has produced some major technological breakthroughs. The rise of GAN was inevitable, and both academia and industry began to embrace and welcome it. First, the best thing about GAN is that its learning nature is unsupervised. GAN also does not require labeled data, which makes GAN powerful because the job of labeling data is very tedious. Secondly, the application potential of GAN makes it tremendous in many fields. It can generate high quality images, image enhancement, generate images from text, convert images from one domain to another, etc. GAN has two networks, the generator network, and the discriminator network. These two networks can be neural networks, ranging from convolutional neural networks, and recurrent neural networks to autoencoders. In this configuration, the two networks participate in a competitive game and try to outperform each other while helping them to complete their own tasks. After thousands of iterations, if all goes well, the generator network can perfectly generate realistic false images, and the discriminator

network can determine well whether the image is real or false. In other words, the generator network transforms random noise vectors from the potential space (not all GAN samples from the potential space) into samples from the real dataset. Training in GAN is a very intuitive process.

Today, GAN has a large number of practical use cases in a variety of industries. For example, in the field of image processing, face photo generation is possible, Tero Karras et al. conducted a study to generate face photos that are very realistic [4.3]. The photos were generated with the faces of famous people as input, resulting in the generation of cases with the facial features of famous people. Realistic photos can also be generated. Andrew Brock et al. used the BigGAN technique to generate synthetic photos [4.4]. The case photos are almost indistinguishable from real photos. Image transformation is also possible. Phillip Isola et al. in 2017 proposed a method for image-to-image transformation based on conditional generative adversarial networks [4.5]. The network not only learns the mapping relationship from the input image to the output image but is also able to learn the loss function used to train the mapping relationship. In addition, it can improve image quality, image stylization or coloring artwork generation, and video generation, among other more interesting tasks. Due to the excellent performance of GAN in the field of image processing, the technique has been applied to many other fields where image processing is required. Such as autonomous driving, medical care, geostatistical analysis, etc. Likewise, in the traditional construction industry, especially in the maintenance of infrastructure, the use of new technologies can greatly improve efficiency. The establishment of a GAN-based corrosion prediction method is expected.

4.2 Methodology

4.2.1 Generative adversarial network (GAN)

Synthetic data is a machine learning algorithm that learns the random statistical patterns implied in real-world data to generate "fake" corresponding data. Generative adversarial network (GAN) is widely used in various fields for its useful performance. GAN is not a simple way to copy and imitate from training samples, nor to combine and average multiple training data, but to deeply learn the statistical laws inherent in training data. Generative adversarial network models based on neural networks provide different ideas for generating synthetic data. There are usually two modules in the GAN model framework: the generative model and the discriminative model. The generative model is responsible for processing random noise to simulate fake data similar to the real training samples. The discriminative model is responsible for identifying the fake data generated by the generator in the training samples. The two models play and learn from each other, and eventually, the fake data produced by the generator will be enough to pass off as real. Although there are generators and discriminators in the GAN model, it is generally expected to generate data that is comparable to reality. Therefore, the focus of GAN is on the generators. Before introducing specific GAN models, the concept of "generation" needs to be explained. Generation is the process by which a model learns some data and then generates similar data. For example, the model is asked to look at some images of steel corrosion and then generate the corrosion images themselves. Many techniques could be used for the generation before GAN was proposed. For example, Auto-encoder (AE), proposed by Rumelhart et al, can be used to process high-dimensional complex data, and it facilitated the development of neural networks [4.6]. The structure of the auto-

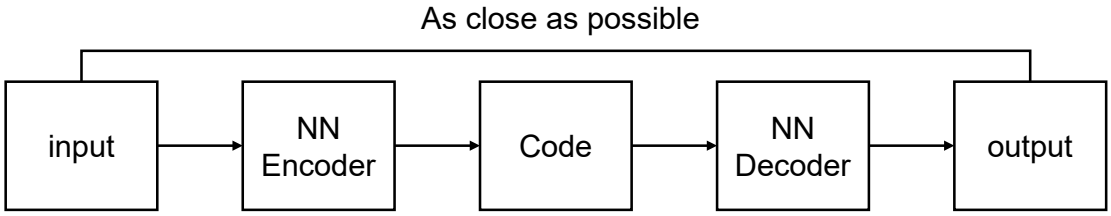

Figure 4-1. The structure of auto-encoder.

encoder is shown in Figure 4-1. Usually, the input image is fed to NN Encoder to obtain a latent code, which is usually much smaller than the dimension of the input object, and it is a compact representation of the input object. Next, this latent code is fed to the NN Decoder for decoding, and the reconstructed original object is output. The auto-encoder neural network is an unsupervised learning algorithm (training example not labeled) that uses a back-propagation algorithm that works to make the output as close to the input as possible. However, both the Encoder and Decoder of AE use DNN, which is a nonlinear transformation process, so there is often no regularity in transforming between points on latent space. One way to solve this problem is to introduce noise to expand the coding area of the image so that it can cover the distorted blank coding area. The robustness of the output is enhanced by increasing the diversity of the input. Therefore, Variational Auto-Encoder (VAE) was proposed by DP Kingma et al, which is to add suitable noise to the encoding in the structure of AE [4.7]. VAE is an unsupervised generative model whose theoretical basis is based on the Gaussian mixture model. Although VAE is much better than the AE model training, the images it generates will be blurred compared to GAN using adversarial learning directly. This is because it is by directly calculating the mean square error between the generated image and the original image, so the obtained loss may be very different in the goodness of the generated image even if it is the same.

VAE uses KL-divergence and encoder-decoder to approximate the real distribution. However, GAN has gained popularity over the years for its "end-to-end" flexibility and implicit objective function. VAE training relies entirely on a hypothetical loss function and KL divergence to approximate the real distribution. Instead of assuming a single loss function, GAN allows a zero-sum game between discriminator ***D*** and generator ***G***. On the one hand, generator ***G*** aims to generate fake samples (loss evaluation) to fool discriminator ***D*** into believing that they are real samples. On the other hand, the discriminator ***D*** has to distinguish the real sample *x* from the fake sample *G(z)* as the final goal (loss evaluation). In general, discriminator ***D*** is a stronger network than generator ***G*** in GAN training, because network ***G*** has to learn from the discriminative process of ***D*** in

order to pass off fake as true.

Figure 4-2 illustrates the basic structure of a GAN model. Where *z* is random noise; ***G*** is the generator; *G(z)* is generated data; *x* is the training set; ***D*** is the discriminator. A rudimentary GAN model takes a random variable (either a Gaussian distribution, or a uniform distribution between 0 and 1) and inverse samples the probability distribution through a parameterized probability generating model (usually parameterized with a neural network model), resulting in a generated probability distribution. The principle of GAN is that the generator network generates faked images based on random noise *z*, and the discriminator network judges the images as real or fake. The goal of the discriminator is to try to judge the real image as real and judge the discriminator faked picture as fake

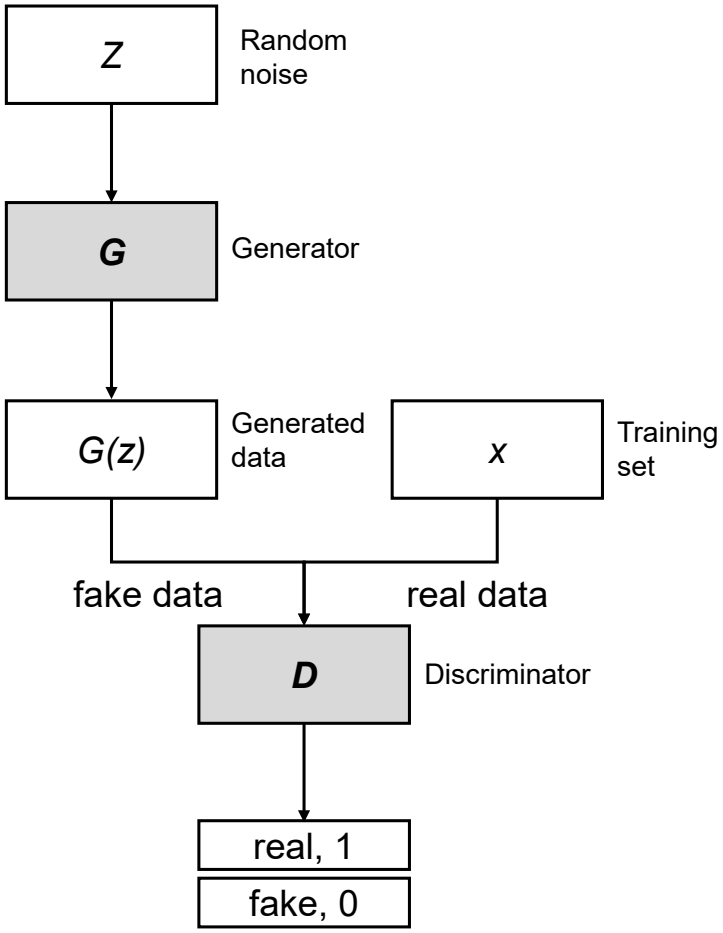

Figure 4-2. The basic structure of a GAN model.

to improve the accuracy of judging real and fake. The goal of the generator is to try to make the faked images look real and reduce the accuracy of the discriminator. Therefore, based on this adversarial principle, Equation (4.1) shows the formula for discriminator ***D***. It is a binary classification problem that uses a cross entropy loss function as the optimization objective of the discriminator. Let *D(x)* be the probability that the image is real, then the objective function is:

$$max_D V(D) = E_{x\sim P_r}\big[log\big(D(x)\big)\big] + E_{z\sim P_z}\big[log\big(1 - D(G(z))\big)\big] \tag{4.1}$$

Equation (4.2) shows the formula of the generator ***G***. The objective of ***G*** is to fight against the discriminator ***D***, its objective function wants the model to generate images with the highest possible value of *D(x)* to fool the discriminator:

$$min_G V(G) = E_{z\sim P_z}\big[log\big(1 - D(G(z))\big)\big] \tag{4.2}$$

Thus, combining Equation (4.1) and Equation (4.2) gives Equation (4.3), which is the standard formula for the original GAN. It is a minimax game in which ***G*** wants to minimize *V* while ***D*** wants to maximize it.

$$min_G max_D V(D,G) = E_{x\sim P_r}\big[log\big(D(x)\big)\big] + E_{z\sim P_z}\big[log\big(1 - D(G(z))\big)\big] \tag{4.3}$$

Where P_r is real data distribution; P_z is Gaussian random noise distribution; ***G*** is a generative network, whose input is a random noise that captures the distribution of the real data during training, thus generating the most realistic data possible and making ***D*** wrong; ***D*** is a discriminative network that determines whether the generated data is real or not. Its input parameter is *x*, and the output *D(x)* represents the probability that *x* is real data, where a value of 1 means 100% real data, and a value of 0 means that it cannot be real data.

Combining Figure 4-2 and Equation (4.3), the training steps for the GAN model are as

follows.

The first step generates the fake image, then fixes the generator so that it does not update the parameters and makes the loss smaller by updating the parameters of the discriminator. The label of the real image is 1, and the generated fake image is 0. The loss is the measure of whether the discriminator labels the real image. The loss is a measure of the accuracy of the discriminator in labeling the real image as 1 and the fake image as 0. The smaller the loss value of the model, the better. Therefore, the discriminator can distinguish the real image and the fake image. The second step is to fix the discriminator and the training set, update the parameters of the generator, and make the loss of the discriminator bigger and bigger, so that the discriminator cannot distinguish them at all. This time, the parameter update repeats the first step, fixing the generator, and iterating continuously. Eventually, the generated image will be indistinguishable from the real image.

GAN has many advantages over traditional models. There are two different networks instead of a single network, and the training method is adversarial. The gradient update information of ***G*** in GAN comes from discriminator ***D***, not from the data samples. GAN can generate clearer and more realistic samples than all other models. Compared to VAE, GAN has no variational lower bound, and if the discriminator is well trained, the generator can learn the distribution of the training samples perfectly.

4.2.2 Conditional generative adversarial network (CGAN)

In some classical GAN models (WGAN, LSGAN, DCGAN, etc.), the input noise is often obtained by random sampling from the sample space, and the generated image belongs to a random class. These models are unable to generate data of a specified class. Combined with the characteristics of this study, because there are a variety of steel and a variety of

corrosion environments, it is expected that the model can generate the data of the specified category as required. Therefore, the conditional generative adversarial network (CGAN) proposed by Mehdi Mirza et al. is used to produce data with specified patterns, and also to solve to some extent the drawback that the original GAN training is so free that it is unstable on some complex datasets [4.8].

The CGAN model is supervised, and it utilizes the label information in the dataset. In the traditional GAN, Discriminator's scoring is very simple and brutal, generating images with higher scores for more realistic ones and lower scores for more blurred ones. However, when label information is introduced, the scoring rules need to become stricter. That is, a blurred image is still scored low, but in a clear and realistic generated image, if the image does not match its label, it is also required to be scored low. In the conventional discriminator of the original GAN, it only needs to check whether the image is real or not, it does not need to pay attention to the content of the image. Therefore, in CGAN, the discriminator also has an additional input c, which represents the content of the image. The discriminator at this time does not only check if the image is real, but also if c and the input image x are matched. The structure of CGAN is very similar to the original GAN,

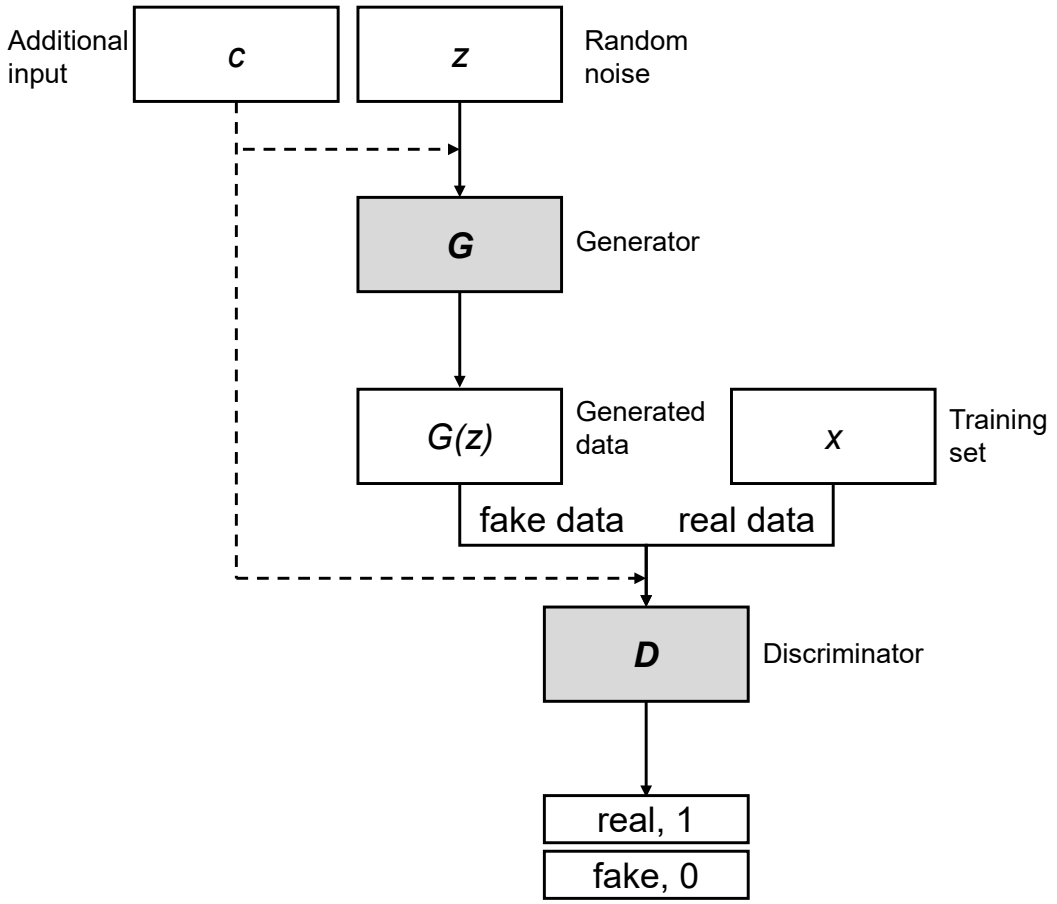

Figure 4-3. The structure of a conditional generative adversarial network (CGAN) model.

and its model is shown in Figure 4-3. The way CGAN introduces the label c is very straightforward, which is to add a one-hot vector, which is the label information of the image, to the input layer of the generator and discriminator. The whole optimization objective becomes Equation (4.4).

$$min_G max_D V(D,G) = E_{x\sim P_r}\left[log\left(D(x|c)\right)\right] + E_{z\sim P_z}\left[log\left(1 - D(G(z|c))\right)\right] \quad (4.4)$$

According to the formula, both the generator and discriminator are transformed into the form of conditional probabilities, which are computed given a label vector c. Thus, each category c corresponds to an objective function subordinate to itself. With this constraint,

if an image is generated that is clear but the categories do not match the labels, it will also be scored as a fake. Therefore, the category of the generated data can be changed by adjusting the value of the labels.

4.2.3 Information maximizing generative adversarial network (InfoGAN)

In contrast to CGAN, the information maximizing generative adversarial network (InfoGAN) uses unsupervised learning to obtain some potential feature representations, which include the categories of the data. If there is a dataset with no label information, but there are still potential category differences, InfoGAN provides an unsupervised

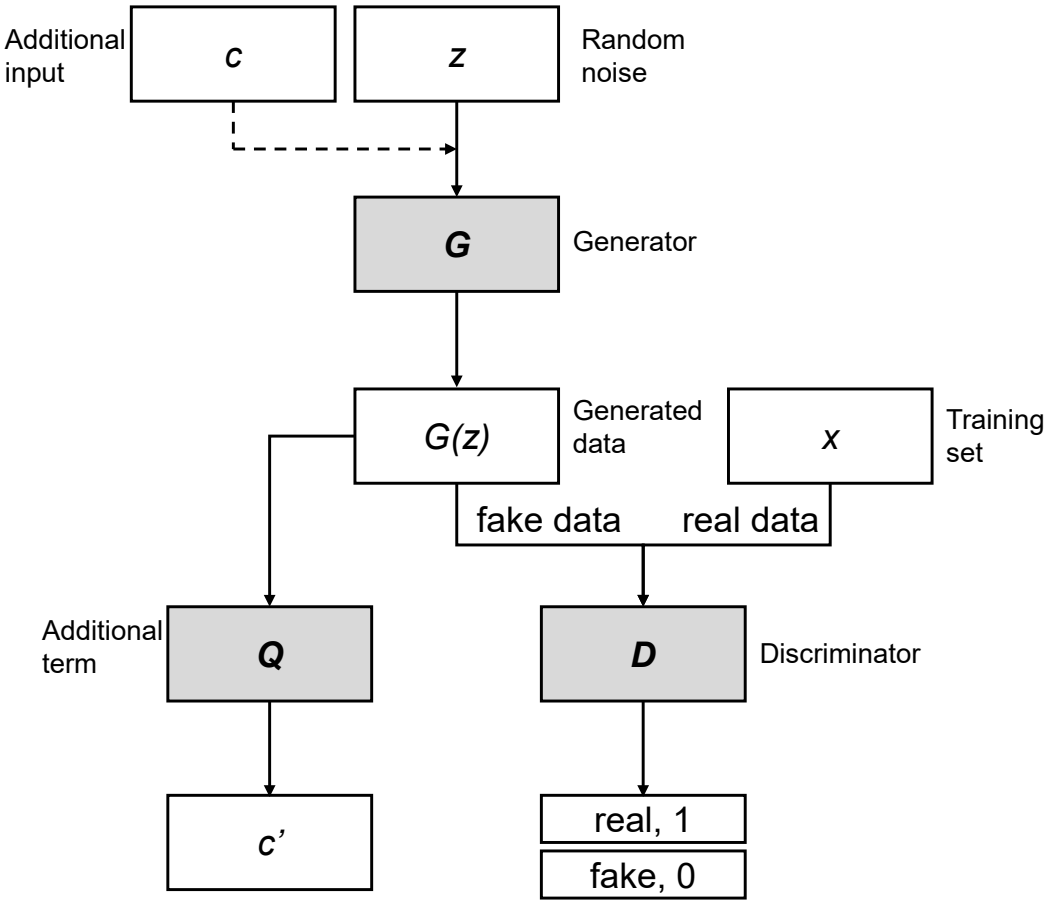

Figure 4-4. The structure of an information maximizing generative adversarial network (InfoGAN) model.

method to identify potential category differences in the data, and can generate data of a given category by controlling the latent code.

The structure of InfoGAN is shown in Figure 4-4. InfoGAN splits the input to the Generator into two parts, a latent code, denoted as c, and a noise vector z, as in the traditional GAN. Where c typically consists of two parts, one discrete and one continuous. To introduce c, Xi Chen et al. constrain c by means of mutual information, which can also be understood as a process of self-coding [4.9]. The specific operation is that the output of the generator, passes through a classifier to see if it yields c. This can be seen as the inverse process of the anto-encoder. The rest of the discriminator is the same as the original GAN. From a loss function perspective, the loss function of InfoGAN becomes Equation (4.5)

$$min_G max_D V_I(D,G) = V(D,G) - \lambda I(c; G(z,c)) \tag{4.5}$$

Compared to the original GAN, there is an additional term $\lambda I(c; G(z,c))$,which represents the mutual information between c and generator's output. The larger this term is, the more relevant c is to the output.

4.3 Model architecture

In this study, Gaussian noise and GAN were employed to increase the dataset. As a type of deep learning framework, a generative adversarial network (GAN) studies from a dataset and generates new data with similar statistics. According to the characteristics of this study, using two models to do adversarial learning not only predicts the time of corroded surface and steel type, but also enables the simulation of corrosion, so the use of GAN the model is very suitable for this research. GAN is usually applied for data augmentation, particularly when the dataset is limited. In this study, since only a limited

amount of data was available as the initial dataset. GAN generated new training samples according to the data collected from corrosion tests. Even if not the same, the distribution of the newly generated data is quite similar to the initial dataset. In this study, GAN and its two variants InfoGAN and CGAN were chosen as the experimental model. This study takes reference from the characteristics of InfoGAN, and uses Gaussian noise to simulate the random template as used in InfoGAN, and achieves higher efficiency than InfoGAN. For CGAN, the input data of the generator is the category and random vector. However, the dataset in this research involves not only categories of steel plates but also categories of corrosion. A single classification code can hardly meet the needs of this research. Meanwhile, the goal of this research is to predict the next stage of corrosion data based on the current corrosive status, which cannot be achieved using CGAN.

UNet was the generator and MobileNetV2 was the discriminator for the GAN model. The UNet was initially designed for the segmentation task of Biomedical images, which have a great characteristic that they are single channel (black and white images) [4.10]. And corrosion in this research can also be seen as single channel data, so UNet was used as the generator of GAN. There are two paths in the architecture. One is the contraction path (or the encoder), a traditional stack of convolutional and max-pooling layers, which captures the context in the image. The other path is the symmetric expanding path (or decoder) which enables precise localization using transposed convolutions. It can handle images of any size and it is a fully convolutional network (FCN). Figure 4-5 explains the details of UNet. Here the input data is the real corrosion data and Gaussian noise, and the output is the simulated corrosion situation of the next phase [4.10].

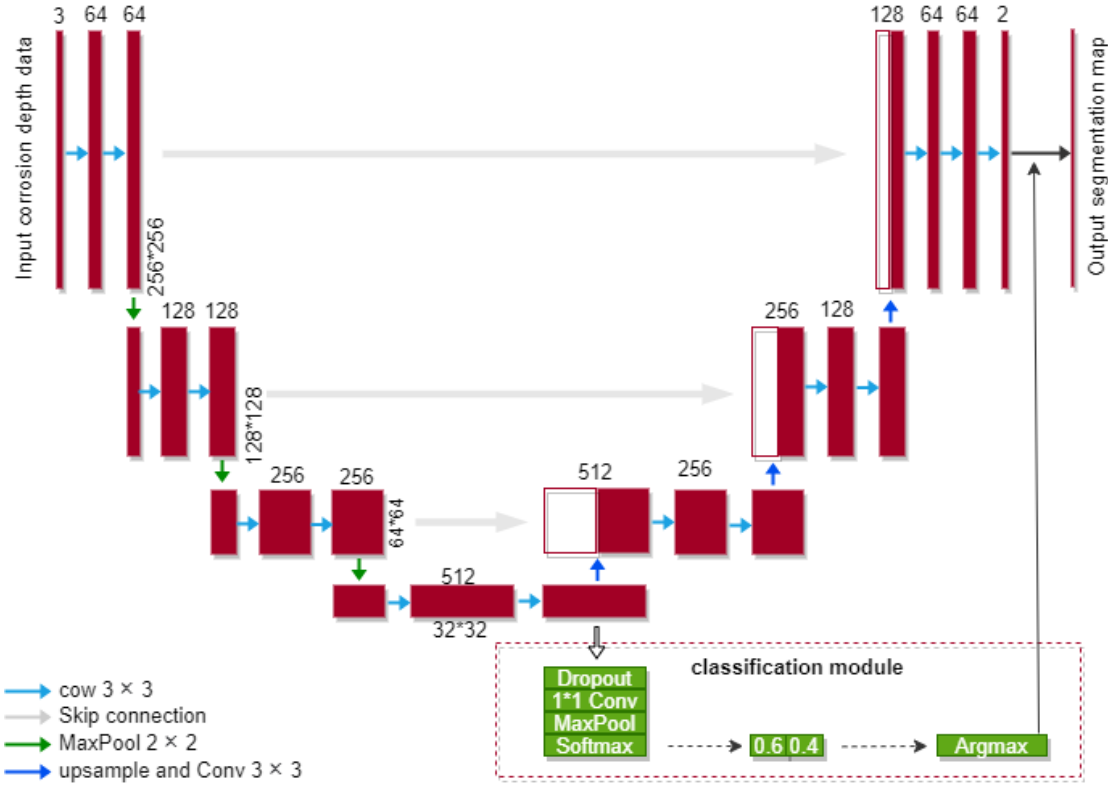

Figure 4-5. The structure of UNet.

MobileNetV2 is considered as an effective model to be used for feature extraction, object detection, and segmentation. It is a mobile architecture based on an inverted residual structure, using depthwise separable convolution as efficient building blocks. The model allows the decoupling of the input/output domains from the expressiveness of the transformation, which provides a convenient framework for further analysis. Its capabilities have been validated in many applications. The structure difference between it and UNet is large, and the number of parameters of MobileNetV2 is smaller and lighter than other classification models, which makes it more suitable as a discriminator for GAN. To better fit the discriminator, an additional Sigmoid activation function was added at the end of MobileNetV2, 0 as Fake, and 1 as Real. The generator is primarily used to simulate

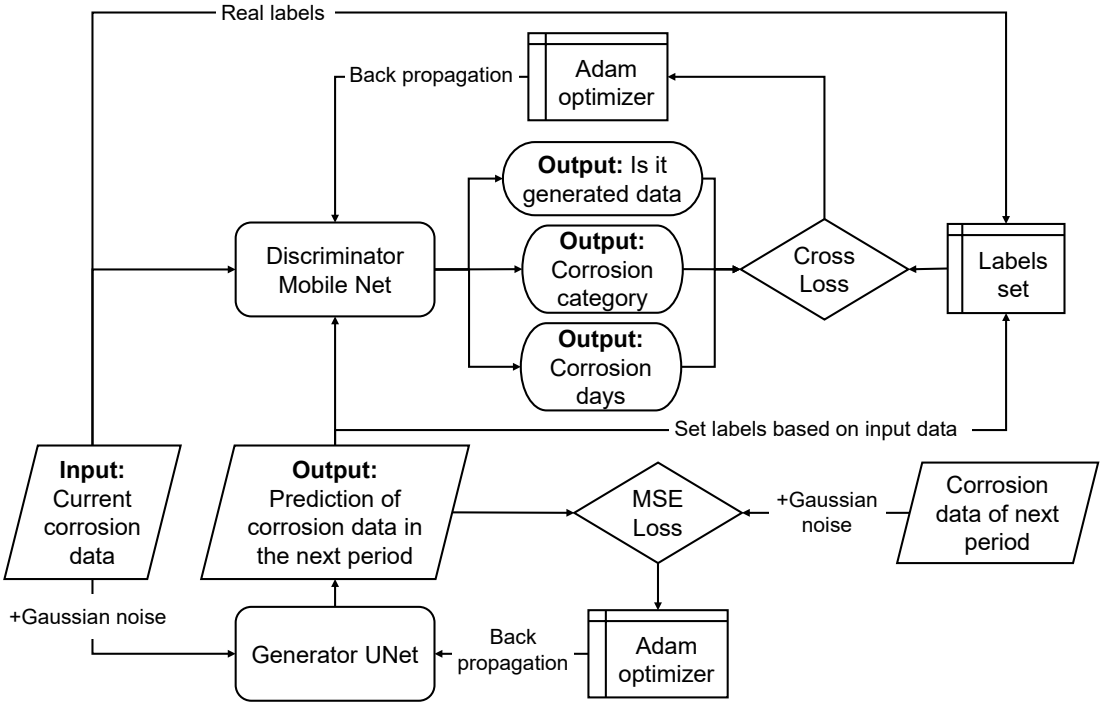

Figure 4-6. The structure of the GAN model.

the next phase of regression of the input corrosion data, the discriminator is used to determine whether the input data is the data generated by the generator. In addition, the discriminator that was used in this study could be used to predict the kind of steel and the phase of corrosion. The Adam optimizer was used in the model. Figure 4-6 illustrates the model architecture and procedure [4.11]. The input corroded surface data was 2-dimensional data. Since the corrosion depth measurement of the corroded surface was a rectangular area of 50 mm * 60 mm with a measurement interval of 0.3 mm, the size of the original input image was 167 * 200. However, MobileNetV2 requires a specific size to be specified and due to the nature of MobileNetV2 and UNet convolution, they are better at handling square images. Therefore, the input corroded surface image was resized to a size of 200 * 200. The *MSE Loss* was used in the model. *MSE* derivative is not too

computationally intensive and is commonly used. The formula of *MSE* is shown in Equation (4.6):

$$MSE = \frac{1}{n}\sum_{i=1}^{n}(y_i - \bar{y}_i)^2 \tag{4.6}$$

Where y_i is the predicted value; $\bar{y}_i$ is the labeled value.

Since this study is a multi-classification task, the *Cross Loss* of a single image is shown in Equation (4.7).

$$Cross\ Loss = -\sum_{i=1}^{n}(ylog(\tilde{y}) + (1-y)log(1-\tilde{y}) \tag{4.7}$$

Where n is the number of categories; y is the labeled value; $\tilde{y}$ is the predicted value.

4.4 Dataset settings

In this chapter, the corrosion depth data of the specimen corroded surfaces obtained in Chapter 2 was used as training sets and testing sets. In the experimental design of this section, the data set was used in six cases, which are six configurations of the training and testing sets. As shown in Table 4-1, “S1”, “S2”, “S3”, and “S4” correspond to the corroded surface data of the specimens in the four corrosion tests mentioned in Chapter 2: Accelerated corrosion test ISO16539 Method B; Accelerated corrosion test CCT Method A developed by PWRI; Direct atmospheric exposure test Atmospheric exposure I conducted at Miyakojima; And direct atmospheric exposure test Atmospheric exposure II conducted at Choshi. In Scenario 1, the corrosion data "S1" of ISO16539 Method B is the training set, and the corrosion data "S3" of Atmospheric exposure I is the testing set.

Table 4-1. Training set and testing set.

	Scenario1	Scenario2	Scenario3	Scenario4	Scenario5	Scenario6
Training set	S1	S1	S2	S2	S1+S2	S1+S2
Testing set	S3	S4	S3	S4	S3	S4

In Scenario 2, the corrosion data "S1" of ISO16539 Method B is the training set, and the corrosion data "S4" of Atmospheric exposure II is the testing set. In Scenario 3, the corrosion data "S2" of CCT Method A is the training set, and the corrosion data "S3" of Atmospheric exposure I is the testing set. In Scenario 4, the corrosion data "S2" of CCT Method A is the training set, and the corrosion data "S4" of Atmospheric exposure II is the testing set. In Scenario 5, the corrosion data "S1" and "S2" of ISO16539 Method B and CCT Method A are the training set, and the corrosion data "S3" of Atmospheric exposure I is the testing set. In Scenario 6, the corrosion data "S1" and "S2" of ISO16539 Method B and CCT Method A are the training set, and the corrosion data "S4" of Atmospheric exposure II is the testing set.

4.5 Model training

The input corroded surface data was 2-dimensional data. Since the corrosion depth measurement of the corroded surface was a rectangular area of 50 mm * 60 mm with a measurement interval of 0.3 mm, the size of the original input image was 167 * 200. And the input corroded surface image was resized to a size of 200 * 200. The learning rate was 0.0001, Adam optimizer was used, and the batch size of the generator and the discriminator was 4. The sigma activation function was chosen to be $sigma = variance^2$. The leaky rate was 0.2. The Adam beta value was [0.5, 0.99]. The training steps of the

model were: Gaussian noise and the data from the former phase were used as inputs to UNet, and the data from the next phase were the targets. MobileNetV2 was used to determine whether the input was generated by UNet or the real corrosion, and each step was trained according to the GAN model. At the end of each epoch, only the UNet was trained and the gap between the generated data and the real data was fine-tuned.

4.6 Comparative results

In this section, the root mean square error (RMSE) was used as the primary assessment indicator. RMSE is the standard deviation of the residuals, it shows how well the data are concentrated around the best-fit curve. It is often used in prediction and regression analyses to validate experimental results. The aim of this RMSE is to observe the difference between the corroded surface simulated by GAN and the real corroded surface. A model is expected to have an RMSE value that is as small as possible. the calculation of RMSE is performed by Equation (4.8), which is the same as Equation (3.4) mentioned in Chapter 3.

$$\mathrm{RMSE} = \sqrt{\frac{1}{N}\sum_{i=1}^{N}(Y_i - f(x_i))^2} \tag{4.8}$$

Where N is the number of corrosion depths that need to be predicted; Y_i is the actual measured corrosion depth data; $f(x_i)$ is the corrosion depth data predicted by the trained model.

Comparative experiments were performed on four distinct models. The baseline model XceptionNet and the three GAN-based augmentation models: GAN, CGAN, and InfoGAN.

XceptionNet is a conversational neural network architecture that relies entirely on deeply

separable convolutional layers. It outperforms Inception V3 on several datasets, achieving state-of-the-art performance on different problems [4.12]. The history of convolutional neural network design began with LeNet-style models [4.13], which were simple stacks of convolution (for feature extraction) and pooling (for spatial subsampling). In 2012, these ideas were rewritten into the AlexNet architecture [4.14], where convolution operations are repeated multiple times between maximum pooling operations, allowing the network to learn richer features at each spatial scale. The ensuing trend was to make this network style deeper, such as the VGG architecture in 2014 [4.15].

A new type of network emerged at this time, the Inception architecture introduced by Szegedy et al. in 2014 [4.16] as GoogleNet (Inception V1), which was later changed to Inception V2 [4.17], Inception V3 [4.18], and more recently Inception-ResNet [4.19]. The initial phase itself was inspired by the earlier NetworkIn-Network architecture [4.20]. Since its first introduction, Inception has been one of the best performing series on ImageNet datasets [4.21], as well as on internal datasets used by Google, in particular JFT [4.22]. Inspired by the inception module, and arguably an improvement to inception V3, mainly the depthwise separable convolution is used to replace the inception module in the original Inception V3. The inception structure is somewhere between the regular convolution and the depthwise separable convolution. Figure 4-6 shows the structure of Inception V3. It can be seen that the core idea of Inception is to concatenate the feature maps generated by various feature extraction methods such as 1 * 1 convolution, 3 * 3 convolution, 5 * 5 convolution, pooling, etc. to achieve the effect of fusing multiple features.

Xception is a modification of the inception V3 structure, which uses depthwise separable

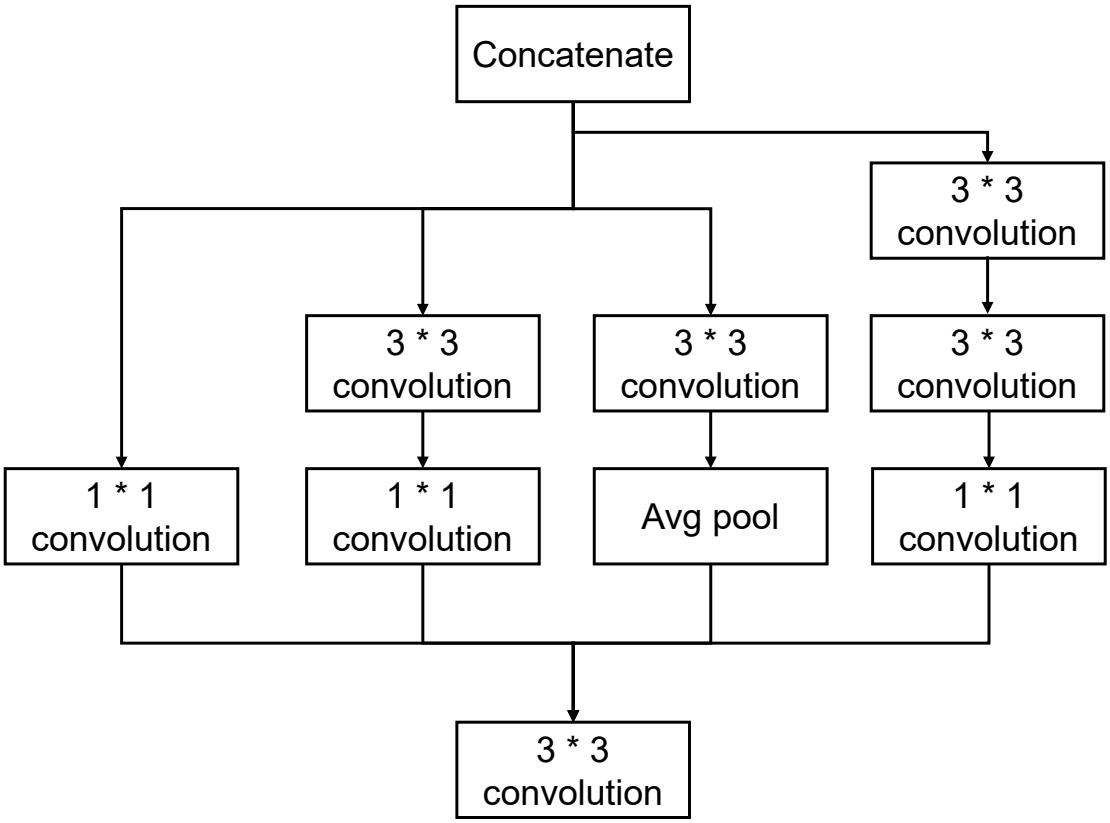

Figure 4-7. The structure of inception V3.

convolution to replace the inception module in inception V3. Xception is based on the assumption that the mapping of channel correlation and spatial correlation in the convolutional neural network feature mapping can be completely decoupled. Because this assumption is a stronger version of the assumption under the inception architecture, the architecture is named Xception. In short, the Xception architecture is a linear stack of deeply separable convolutional layers with residual connections. This makes the architecture very easy to define and modify, only 30 to 40 lines of code are needed to use high-level libraries like TensorFlow-Slim, unlike architectures like VGG-16 [4.23], but much more complex to define with Inception V2 or V3.

Table 4-2 shows the results of the comparative experiments. From the results, all the

Table 4-2. Comparative Results.

	Train: S1 Test: S3	Train: S1 Test: S4	Train: S2 Test: S3	Train: S2 Test: S4	Train: S1+S2 Test: S3	Train: S1+S2 Test: S4
GAN	0.392	0.423	0.462	0.337	0.198	0.244
InfoGAN	0.368	0.455	0.433	0.363	0.233	0.347
CGAN	0.467	0.470	0.439	0.452	0.313	0.299
XceptionNet	0.952	1.492	0.882	0.587	0.902	0.884

models with the GAN-based model have better performance than the baseline model XceptionNet. Since both InfoGAN and CGAN require a huge amount of data for training, they don't demonstrate advantages over GAN in this study. Using GAN for augmentation outperforms all other models in four scenarios (Scenario 2, Scenario 4, Scenario 5, and Scenario 6,). Therefore, using the GAN model as the prediction model is better in this study. Since both atmospheric exposure tests at Miyakojima and Choshi had only one stage of corrosion depth data, it was difficult to validate the corrosion prediction results of the prediction model. Therefore, a comparison of the corroded surface condition of the actual steel plate in stage three (168 days) under ISO16549 Method B corrosion environment and the corroded surface condition obtained by the corrosion prediction model was used as an example to demonstrate the performance of the corrosion prediction model. In this example, the predicted corroded surface condition was obtained by inputting the actual corroded surface data of the first stage (28 days).

Figure 4-8, Figure 4-9, Figure 4-10, and Figure 4-11 illustrate the comparison of the corrosion on steel plates in stage three (168 days) from the accelerated corrosion test ISO16539 Method B and corresponding simulated corrosion generated by the prediction model. Figure 4-8, Figure 4-9, Figure 4-10, and Figure 4-11 are corresponding to four

types of steel plates involved in this study. Taking Figure 4-8 as an example, it shows the corrosion of steel plate type SM400A in stage three. Figure 4-8 (a) shows the real steel plate and Figure 4-8 (b) is the simulated steel plate. The colors demonstrate the status of the corrosion. The yellow color means it is slightly corrosive. The red (and dark) color means the corrosion is worse. Figure 4-8 (a) and (b) demonstrate a similar pattern of the distribution of corrosion, which means this corrosion prediction model can accurately simulate the corrosion on the measured area. Similarly, Figure 4-9, Figure 4-10, and Figure 4-11 demonstrate the excellent performance of this corrosion prediction model in simulating or predicting the corrosion on the other three types of steel plates (SM490A, SMA400AW, and SMA490AW).

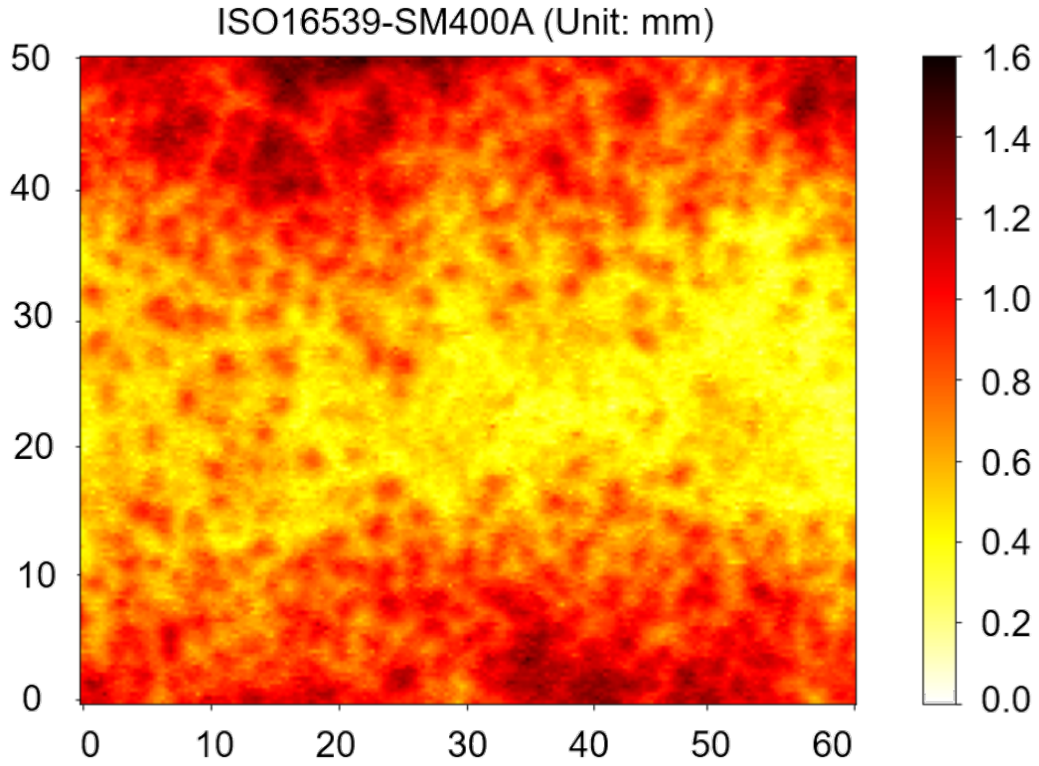

(a) The corrosion on ISO16539 type SM400A steel plate stage three

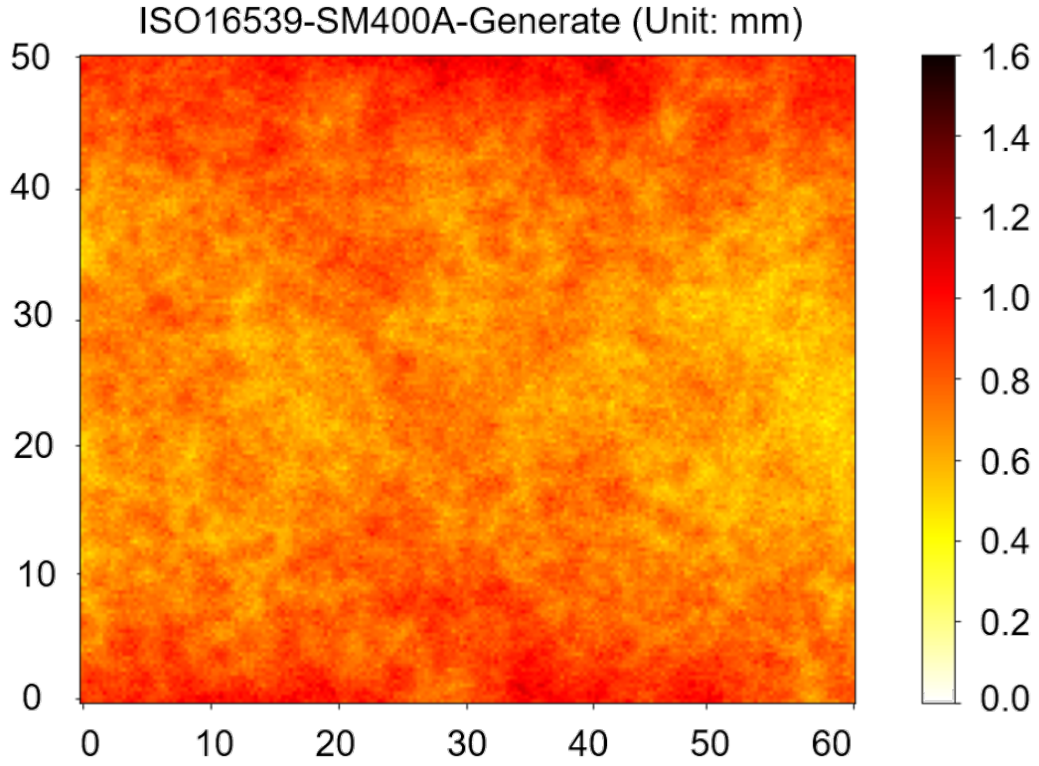

(b) The corrosion on simulated type SM400A steel plate stage three

Figure 4-8. The corrosion on ISO16539 type SM490A steel slate stage three and corresponding simulated corrosion.

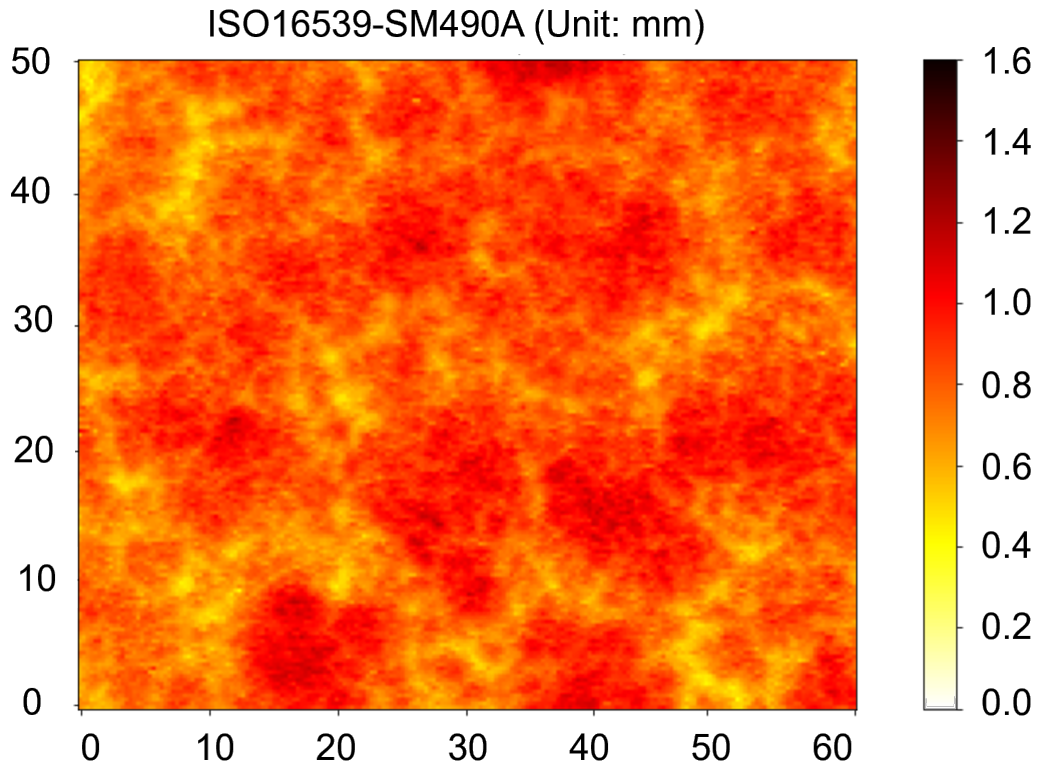

(a) The corrosion on ISO16539 type SM490A steel plate stage three

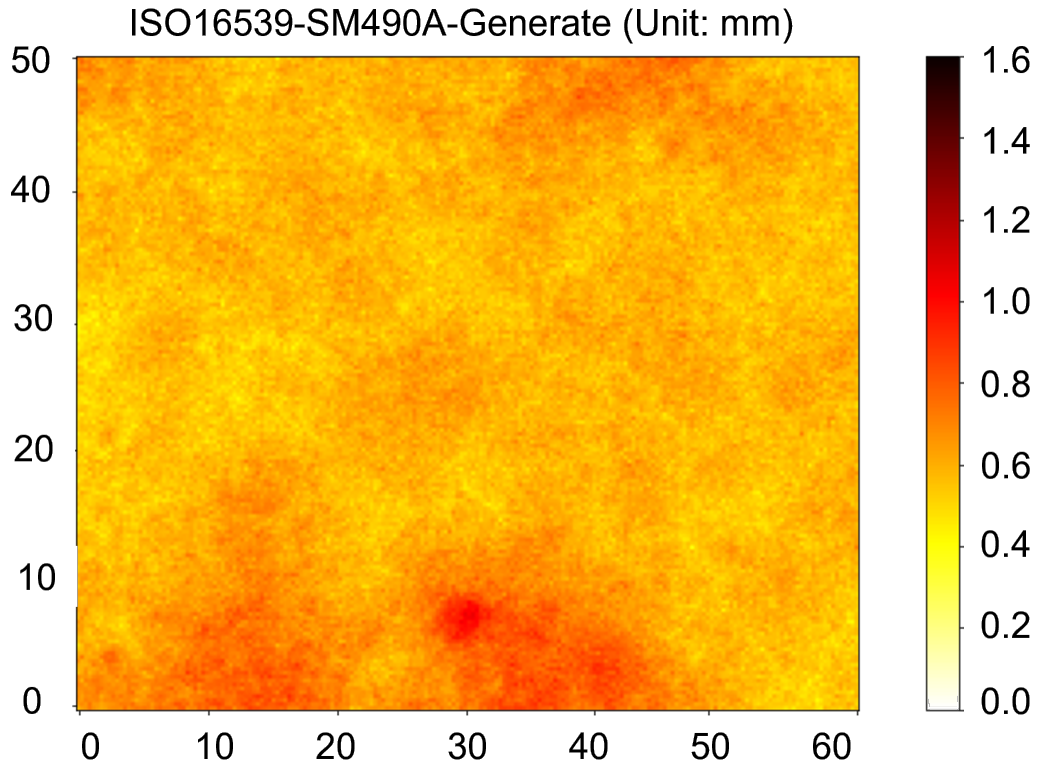

(b) The corrosion on simulated type SM490A steel plate stage three

Figure 4-9. The corrosion on ISO16539 type SM490A steel slate stage three and corresponding simulated corrosion.

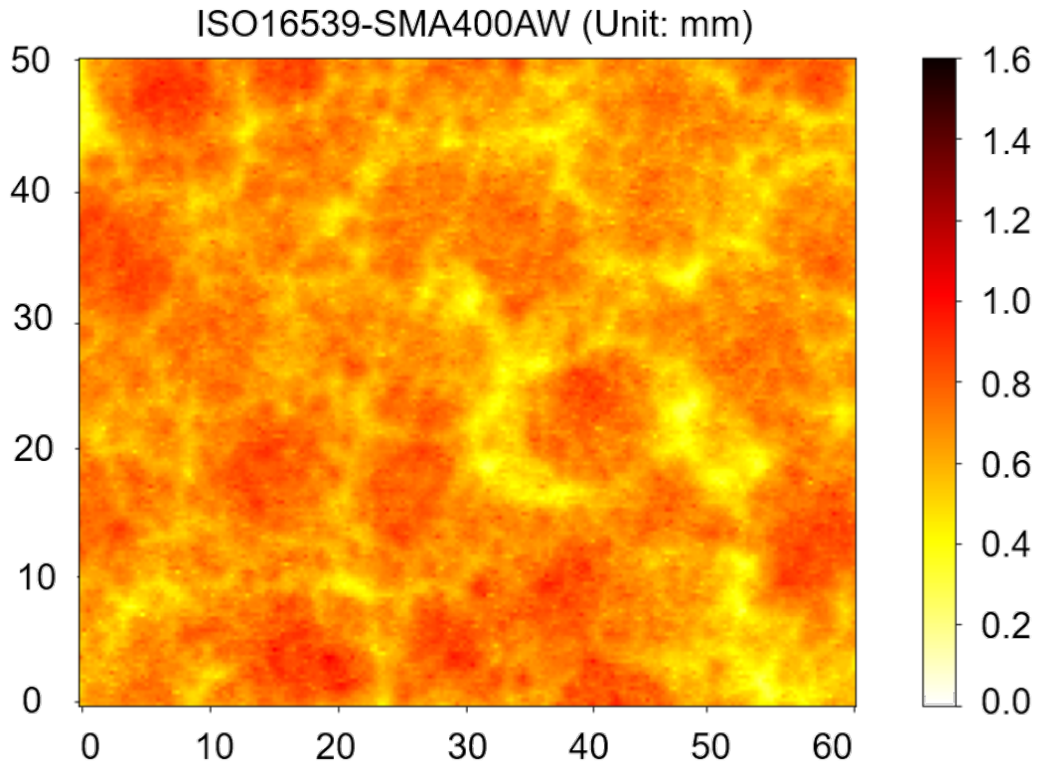

(a) The corrosion on ISO16539 type SMA400AW steel plate stage three

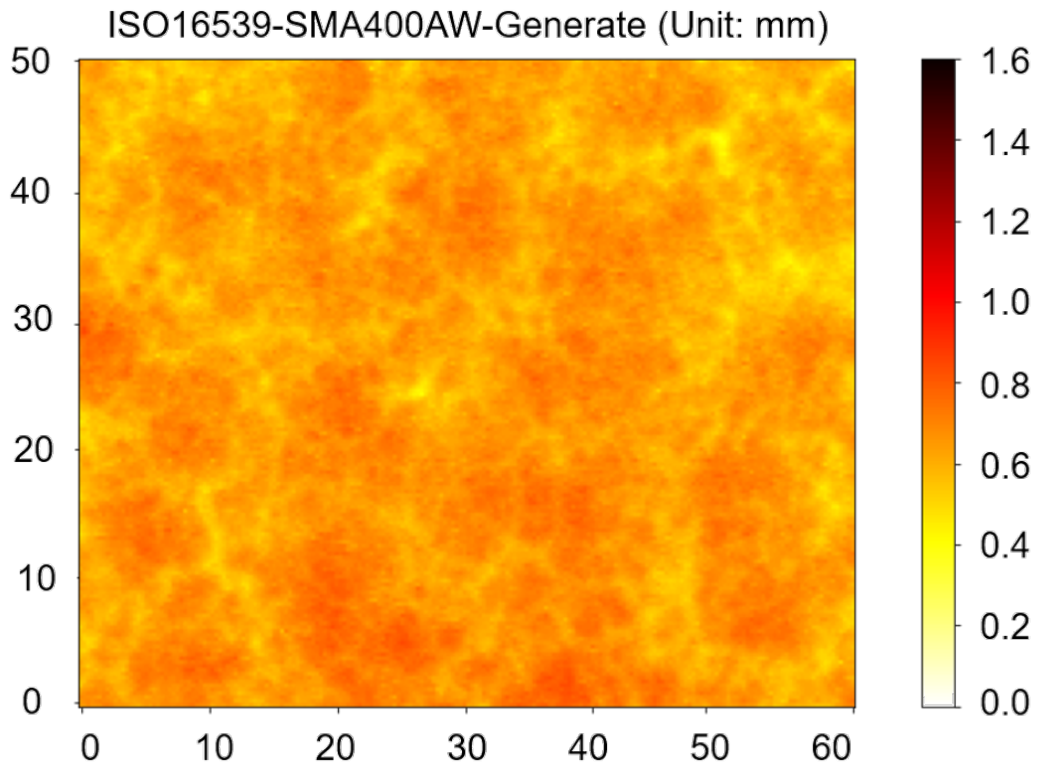

(b) The corrosion on simulated type SMA400AW steel plate stage three

Figure 4-10. The corrosion on ISO16539 type SM400AW steel slate stage three and corresponding simulated corrosion.

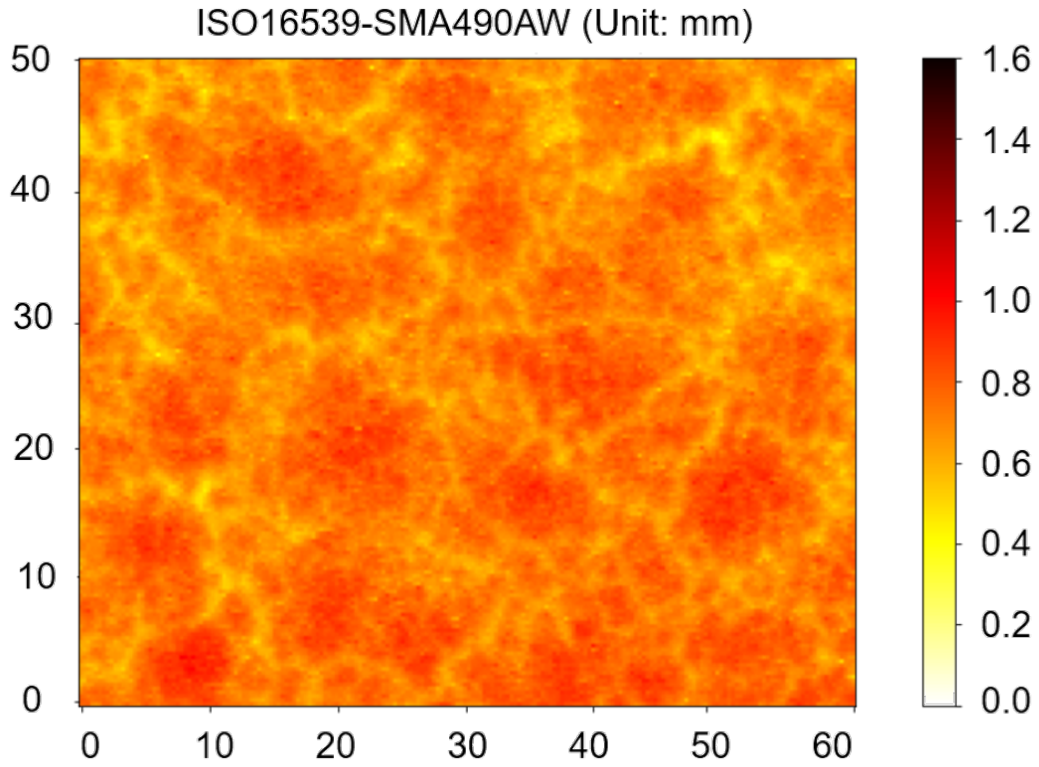

(a) The Corrosion on ISO16539 type SMA490AW steel plate stage three

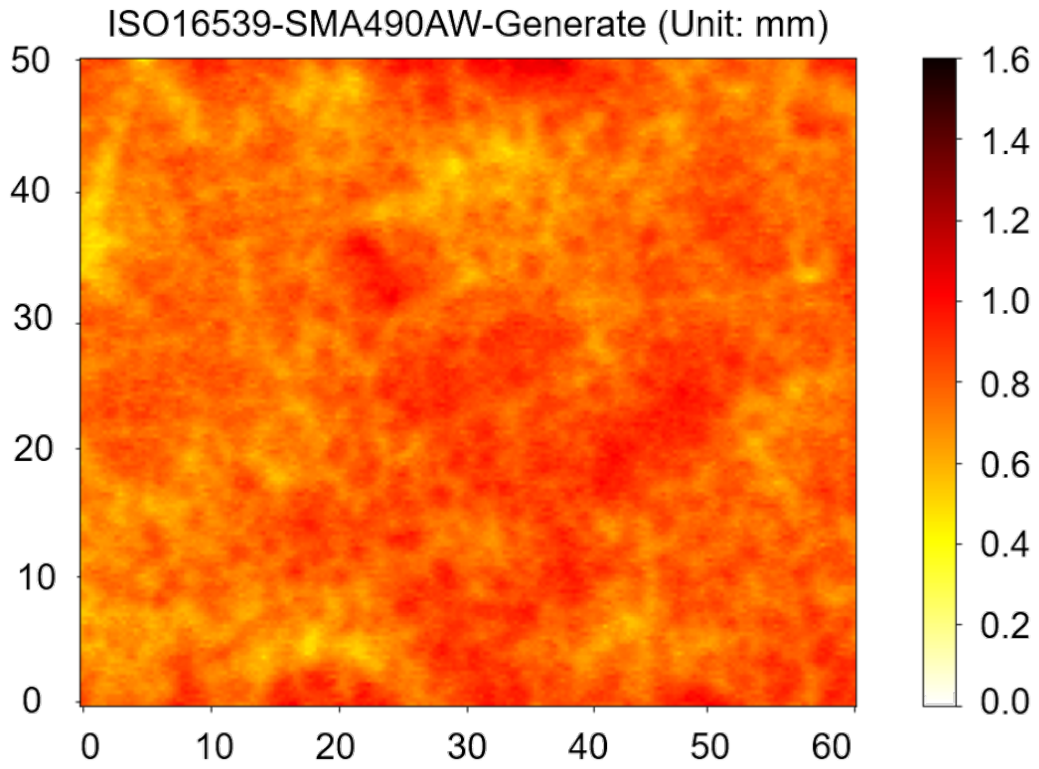

(b) The corrosion on simulated type SMA490AW steel plate stage three

Figure 4-11. The corrosion on ISO16539 type SMA490AW steel slate stage three and corresponding simulated corrosion.

4.7 Summary

The deterioration and damage of aging steel structures have led to huge economic losses and safety hazards. A big reason for the damage is the corrosion of steel members, which can cause the loss of material from the surface of steel members and reduce the thickness, stiffness, and load-bearing capacity of the steel structure. It is worth a thorough investigation to simulate and predict the corrosion on steel structures and to further achieve more effective and efficient maintenance management. Traditional corrosion assessment takes a long time and lacks clear criteria. However, the studies in this field have limitations on the target material or environment, and lack of generality. In this chapter, a GAN-based machine learning model was proposed to augment the dataset and simulate and predict the corrosion of SM400A, SM490A carbon steel, and SMA400AW, SMA490AW weathering steel in four environments: ISO16539 Method B, CCT Method A, Atmospheric exposure I at Choshi, Atmospheric exposure II at Miyakojima. The proposed method could effectively predict the corrosion behavior of uncoated steel structures over time and under different circumstances. It could achieve faster and more accurate predictions of corrosion. UNet was used to simulate the corroded surface. The structure of UNet determines that the distribution of the generated data was very close to the original data. MobileNet-V2 required a small number of parameters and had a relatively high score among other image classification algorithms. Meanwhile, the GAN structure was better controlled compared to CGAN and InfoGAN. The GAN structure composed of UNet and MobileNet-V2 provided outstanding performance to address the research problems in this study. Through comparative experiments, the corrosion prediction model achieved high prediction accuracy and was verified to be reliable and generally applicable.

However, while using RMSE as the accuracy evaluation method was a good way to determine which model had better results, it did not determine whether the model actually accurately predicts changes in the spatial properties of the corroded surface. Therefore, in the next chapter, a validation method of the prediction model combined with the spatial properties of the corroded surface is proposed.

References

4.1 Huang, C.J. and Kuo, P.H., 2019. Multiple-input deep convolutional neural network model for short-term photovoltaic power forecasting. *IEEE access*, *7*, pp.74822-74834.

4.2 Goodfellow, I., Pouget-Abadie, J., Mirza, M., Xu, B., Warde-Farley, D., Ozair, S., Courville, A. and Bengio, Y., 2014. Generative adversarial networks. In *Advances in Neural Information Processing Systems*, pp. 2672–2680.

4.3 Karras, T., Laine, S. and Aila, T., 2019. A style-based generator architecture for generative adversarial networks. In *Proceedings of the IEEE/CVF conference on computer vision and pattern recognition* (pp. 4401-4410).

4.4 Brock, A., Donahue, J. and Simonyan, K., 2018. Large scale GAN training for high fidelity natural image synthesis. *arXiv preprint arXiv:1809.11096*.

4.5 Isola, P., Zhu, J.Y., Zhou, T. and Efros, A.A., 2017. Image-to-image translation with conditional adversarial networks. In *Proceedings of the IEEE conference on computer vision and pattern recognition* (pp. 1125-1134).

4.6 Rumelhart, D.E., Hinton, G.E. and Williams, R.J., 1986. Learning representations by back-propagating errors. *nature*, *323*(6088), pp.533-536.

4.7 Kingma, D.P. and Welling, M., 2013. Auto-encoding variational bayes. *arXiv preprint arXiv:1312.6114*.

4.8 Mirza, M. and Osindero, S., 2014. Conditional generative adversarial nets. *arXiv preprint arXiv:1411.1784*.

4.9 Chen, X., Duan, Y., Houthooft, R., Schulman, J., Sutskever, I. and Abbeel, P., 2016. Infogan: Interpretable representation learning by information maximizing generative adversarial nets. *Advances in neural information processing systems*, *29*.

4.10 Ronneberger, O., Fischer, P. and Brox, T., 2015, October. U-net: Convolutional networks for biomedical image segmentation. In *International Conference on Medical image computing and computer-assisted intervention* (pp. 234-241). Springer, Cham.

4.11 Jiang, F. and Hirohata, M., 2022. A GAN-Augmented Corrosion Prediction Model for Uncoated Steel Plates. *Applied Sciences*, *12*(9), p.4706.

4.12 Chollet, F., 2017. Xception: Deep learning with depthwise separable convolutions. In *Proceedings of the IEEE conference on computer vision and pattern recognition* (pp. 1251-1258).

4.13 LeCun, Y., Jackel, L.D., Bottou, L., Cortes, C., Denker, J.S., Drucker, H., Guyon, I., Muller, U.A., Sackinger, E., Simard, P. and Vapnik, V., 1995. Learning algorithms for classification: A comparison on handwritten digit recognition. *Neural networks: the statistical mechanics perspective*, *261*(276), p.2.

4.14 Krizhevsky, A., Sutskever, I. and Hinton, G.E., 2017. Imagenet classification with deep convolutional neural networks. *Communications of the ACM*, *60*(6), pp.84-90.

4.15 Simonyan, K. and Zisserman, A., 2014. Very deep convolutional networks for large-scale image recognition. *arXiv preprint arXiv:1409.1556*.

4.16 Szegedy, C., Liu, W., Jia, Y., Sermanet, P., Reed, S., Anguelov, D., Erhan, D., Vanhoucke, V. and Rabinovich, A., 2015. Going deeper with convolutions. In *Proceedings of the IEEE conference on computer vision and pattern recognition* (pp. 1-9).

4.17 Ioffe, S. and Szegedy, C., 2015, June. Batch normalization: Accelerating deep network training by reducing internal covariate shift. In *International conference on machine learning* (pp. 448-456). PMLR.

4.18 Szegedy, C., Vanhoucke, V., Ioffe, S., Shlens, J. and Wojna, Z., 2016. Rethinking the inception architecture for computer vision. In *Proceedings of the IEEE conference on computer vision and pattern recognition* (pp. 2818-2826).

4.19 Szegedy, C., Ioffe, S., Vanhoucke, V. and Alemi, A.A., 2017, February. Inception-v4, inception-resnet and the impact of residual connections on learning. In *Thirty-first AAAI conference on artificial intelligence*.

4.20 Lin, M., Chen, Q. and Yan, S., 2013. Network in network. *arXiv preprint arXiv:1312.4400*.

4.21 Russakovsky, O., Deng, J., Su, H., Krause, J., Satheesh, S., Ma, S., Huang, Z., Karpathy, A., Khosla, A., Bernstein, M. and Berg, A.C., 2015. Imagenet large scale visual recognition challenge. *International journal of computer vision*, *115*(3), pp.211-252.

4.22 Hinton, G., Vinyals, O. and Dean, J., 2015. Distilling the knowledge in a neural network. *arXiv preprint arXiv:1503.02531*, *2*(7).

4.23 Simonyan, K. and Zisserman, A., 2014. Very deep convolutional networks for large-scale image recognition. *arXiv preprint arXiv:1409.1556*.

Chapter 5 Validation of the prediction model combined with the spatial properties of the corroded surface

5.1 Introduction

In Chapter 4, a prediction model for the corroded surface of a steel plate was developed. However, it was impossible to measure the corrosion depth of the same steel plate at different times because measuring the corrosion depth of the steel plate requires rust removal. The steel plates at different stages are different so that there is no continuity in time, and each specimen is independent. Therefore, in this case, it was not enough to use only the RMSE mentioned in Chapter 4 as a method to judge the accuracy of the corrosion prediction model. Because the use of RMSE as the accuracy of the corrosion prediction model judgment criteria, was the current stage of the corrosion depth data of the specimen as input to get the corrosion depth data of the future stage, and the object used to calculate the RMSE was the corrosion depth data of other specimens of the future stage, not the specimen. Therefore, in Chapter 4, RMSE could only be used as a criterion for comparing the performance of each corrosion prediction mode, and the specific prediction capability of the corrosion prediction model needs to be confirmed by other methods. Meanwhile, as one of the disadvantages of deep learning methods, some parameters in the neural network often cannot have practical meaning. Therefore, it is necessary to investigate whether this corrosion prediction model can have excellent performance in simulating the future corroded surface. The spatial statistical analysis method in Chapter 3 can be combined to verify whether the prediction model can accurately predict the spatial properties of the corroded surface. In this chapter, because both accelerated corrosion test ISO16539 Method B and accelerated corrosion test CCT Method A have corrosion depth

data for 3 stages (28 days, 84 days, 168 days), the corrosion prediction model obtained in Chapter 4 was used to predict the corroded surfaces for the second and third stages (84 days, 168 days) of these two accelerated corrosion tests. By comparing the spatial property parameters of the predicted corroded surfaces with those of the actual corroded surfaces, it is possible to confirm whether the corrosion prediction model can perform well in simulating the corroded surfaces of future steel plates.

5.2 Comparative results of predicted and actual values of spatial property parameters

In order to combine the spatial statistical analysis method in Chapter 3 to verify whether the corrosion prediction model in Chapter 4 can accurately predict the spatial properties of the corroded surface, the corrosion prediction model is first needed to obtain the corrosion depth data of the simulated corroded surface of the steel plate. In this section, the corroded surface data of four steels from the first stage (28 days) of accelerated corrosion test ISO16539 Method B and accelerated corrosion test CCT Method A were used as the input to the corrosion prediction model. Then the corrosion depth data of the corroded surface of the steel plates in the second and third stages (84 days, 168 days) were obtained by the prediction model. The spatial property parameters, sill and range, of the corroded surfaces simulated by the corrosion prediction model, were then calculated using the semivariogram. Sill and range were calculated in the same way as mentioned in Chapter 3. The predicted spatial property parameters of the corroded surface of the second and third stages were compared with those of the actual accelerated corrosion test results by ISO16539 Method B and CCT Method A at the second and third stages. Table 5-1 and Table 5-2 show the predicted and actual comparative results of sill and range, respectively.

Because the corrosion depth data from the first stage were used as input to the corrosion prediction model, the predicted results of corroded surface spatial property parameters for the first stage of the two accelerated corrosion tests were not available.

The comparison between the predicted and actual values of the spatial property parameters of corroded surfaces obtained by the prediction model was examined. Figure 5-1 and Figure 5-2 show the comparative results of the sill for normal carbon steel and weathering steel under the accelerated corrosion test ISO16539 Method B corrosion environment, respectively. And Figure 5-3 and Figure 5-4 show the comparative results of the range for normal carbon steel and weathering steel under the accelerated corrosion test ISO16539 Method B corrosion environment, respectively.

Figure 5-5 and Figure 5-6 show the comparative results of the sill for normal carbon steel and weathering steel under the accelerated corrosion test CCT Method A corrosion environment, respectively. And Figure 5-7 and Figure 5-8 show the comparative results of the range for normal carbon steel and weathering steel under the accelerated corrosion test CCT Method A corrosion environment, respectively.

Table 5-1. Comparative results of sill (mm^2).

	ISO16539			CCT Method A		
days	28	84	168	28	84	168
SM400A (prediction)	-	0.00311	0.00953	-	0.01721	0.02288
	-	0.00208	0.01874	-	0.01467	0.02001
	-	0.00296	0.00798	-	0.01332	0.01982
SM490A (prediction)	-	0.00289	0.02418	-	0.00477	0.02112
	-	0.00294	0.02001	-	0.00418	0.01983
	-	0.00221	0.01046	-	0.00521	0.01900
SMA400AW (prediction)	-	0.00453	0.00864	-	0.02433	0.02933
	-	0.00488	0.00901	-	0.02701	0.03199
	-	0.00410	0.01883	-	0.02513	0.02988
SMA490AW (prediction)	-	0.00498	0.01513	-	0.02388	0.02897
	-	0.00471	0.01430	-	0.02181	0.02661
	-	0.00422	0.00832	-	0.01998	0.03142
SM400A (actual)	0.00123	0.00203	0.01000	0.00214	0.01685	0.02468
	0.00094	0.00220	0.01395	0.00197	0.01559	0.02133
	0.00116	0.00261	0.01489	0.00216	0.01346	0.02077
SM490A (actual)	0.00128	0.00267	0.01083	0.00148	0.00538	0.02319
	0.00064	0.00202	0.01462	0.00154	0.00308	0.02011
	0.00058	0.00213	0.01315	0.00140	0.00316	0.01673
SMA400AW (actual)	0.00084	0.00390	0.00681	0.00142	0.02404	0.02843
	0.00098	0.00436	0.01129	0.00231	0.03015	0.03213
	0.00120	0.00415	0.00896	0.00211	0.02712	0.02977
SMA490AW (actual)	0.00096	0.00426	0.00560	0.00290	0.02196	0.02731
	0.00113	0.00369	0.00632	0.00434	0.02543	0.02974
	0.00087	0.00333	0.00460	0.00288	0.02144	0.02916

Table 5-2. Comparative results of range (mm^2).

	ISO16539			CCT Method A		
days	28	84	168	28	84	168
SM400A (prediction)	-	6.045	15.554	-	6.983	24.156
	-	6.104	20.003	-	7.224	20.553
	-	8.986	20.865	-	7.898	21.101
SM490A (prediction)	-	7.360	11.765	-	3.884	20.117
	-	8.901	20.338	-	5.673	19.234
	-	8.602	15.218	-	7.112	17.283
SMA400AW (prediction)	-	7.563	7.695	-	7.321	8.324
	-	4.606	7.310	-	7.110	8.100
	-	3.002	7.369	-	6.121	7.358
SMA490AW (prediction)	-	7.012	6.218	-	8.322	12.565
	-	7.361	4.332	-	7.192	14.198
	-	7.549	4.966	-	10.311	11.106
SM400A (actual)	0.581	6.442	20.495	5.477	7.641	20.144
	0.579	7.986	17.678	5.828	6.096	22.434
	0.552	8.658	10.773	5.976	8.143	19.883
SM490A (actual)	5.515	7.425	10.687	4.382	3.664	17.002
	1.108	7.816	17.393	2.939	4.755	16.838
	1.589	6.651	8.482	3.112	6.881	19.354
SMA400AW (actual)	2.660	5.658	6.692	5.251	7.253	7.899
	2.778	5.687	7.080	6.805	5.179	7.931
	2.237	6.712	7.208	5.112	6.873	8.181
SMA490AW (actual)	1.963	6.085	6.392	6.534	12.159	16.184
	1.682	6.721	6.324	5.768	6.979	7.881
	3.368	5.827	5.854	5.469	7.295	9.322

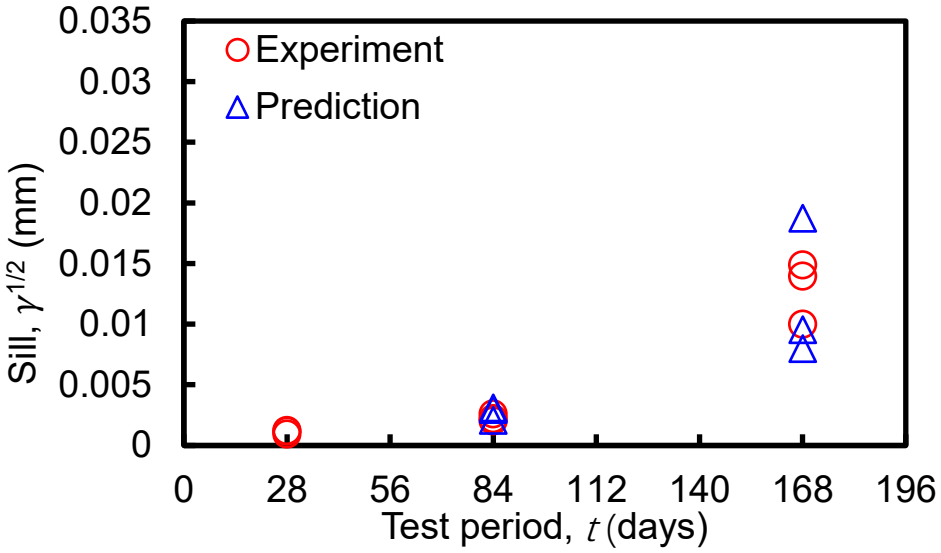

(a) The sill results of SM400A steel plate

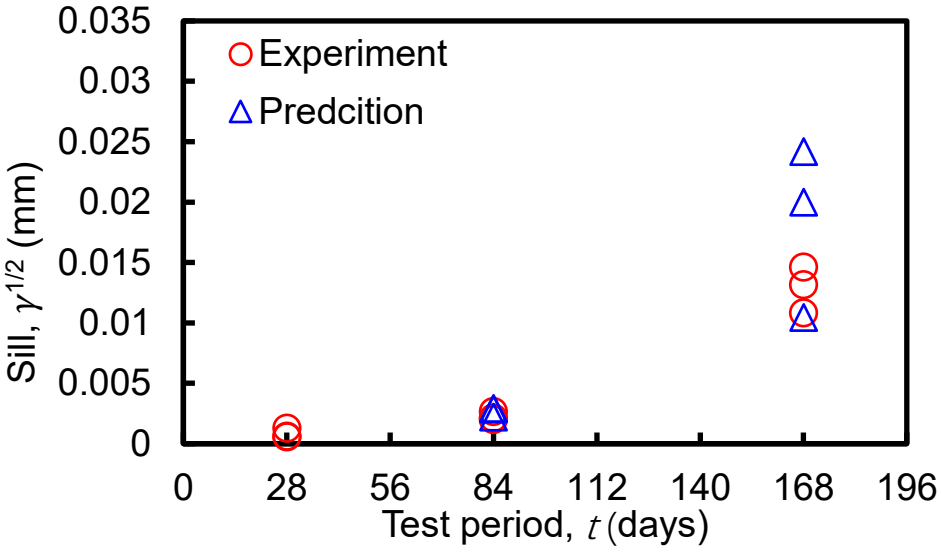

(b) The sill results of SM490A steel plate

Figure 5-1. Comparative results between the predicted and actual sill values for normal carbon steel under ISO16539 Method B.

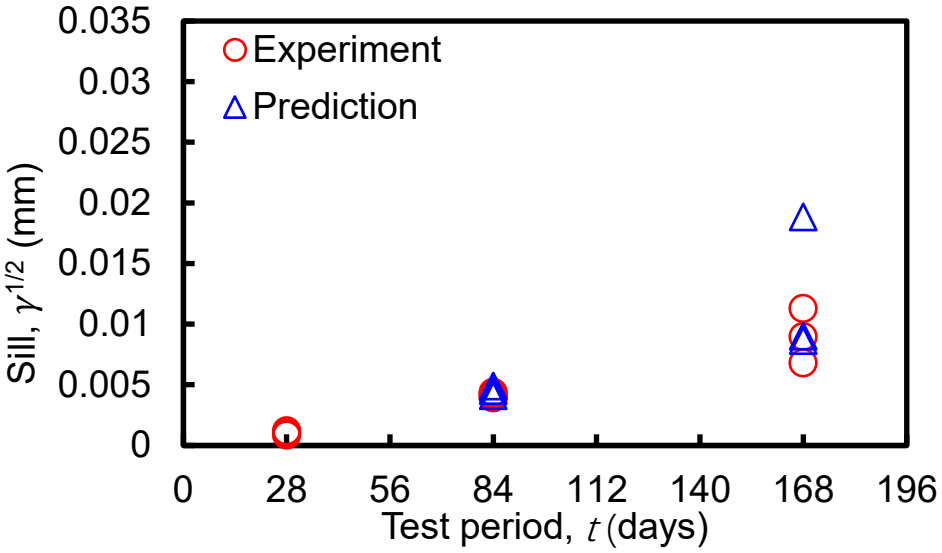

(a) The sill results of SMA400AW steel plate

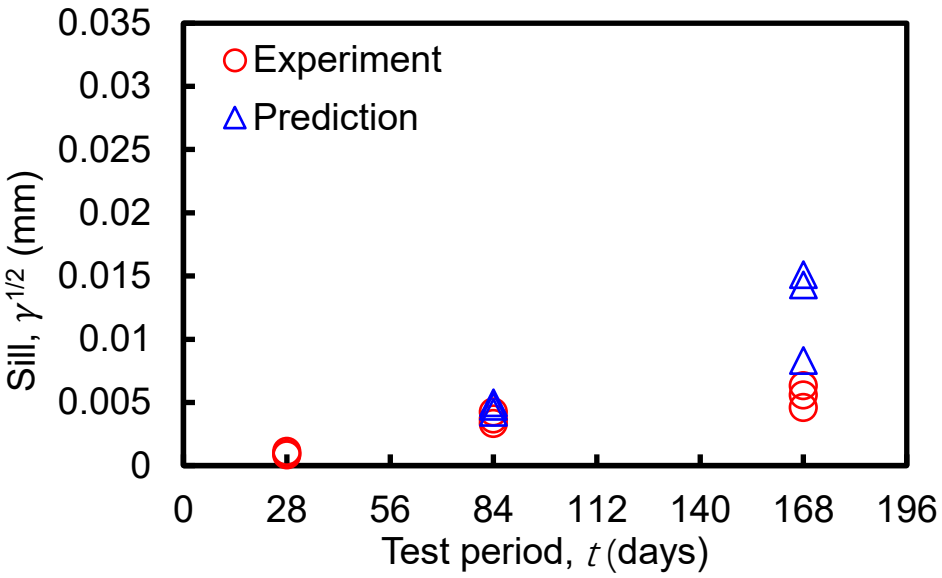

(b) The sill results of SMA490AW steel plate

Figure 5-2. Comparative results between the predicted and actual sill values for weathering steel under ISO16539 Method B.

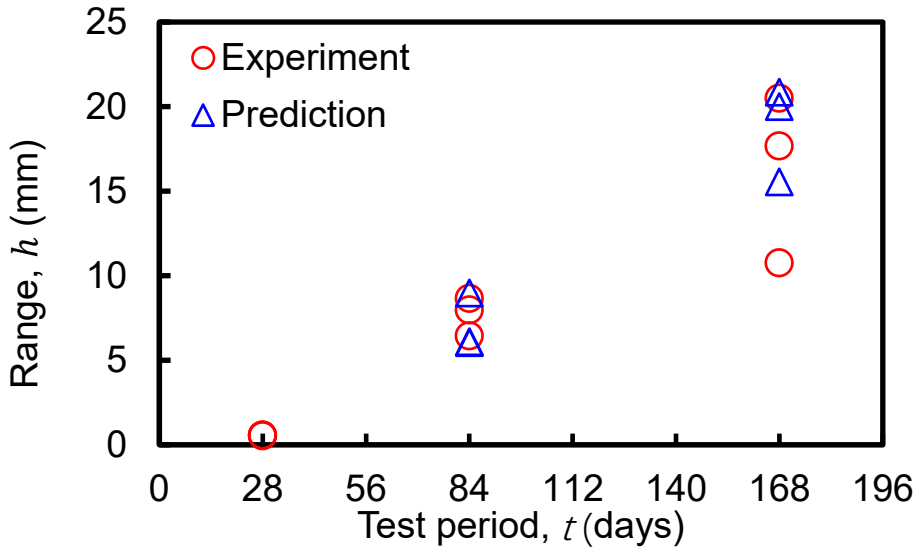

(a) The range results of SM400A steel plate

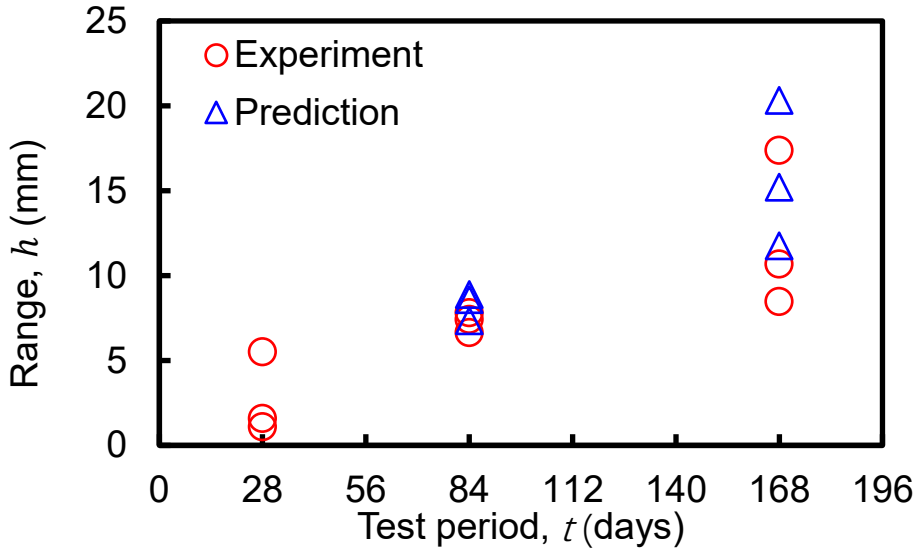

(b) The range results of SM490A steel plate

Figure 5-3. Comparative results between the predicted and actual range values for normal carbon steel under ISO16539 Method B.

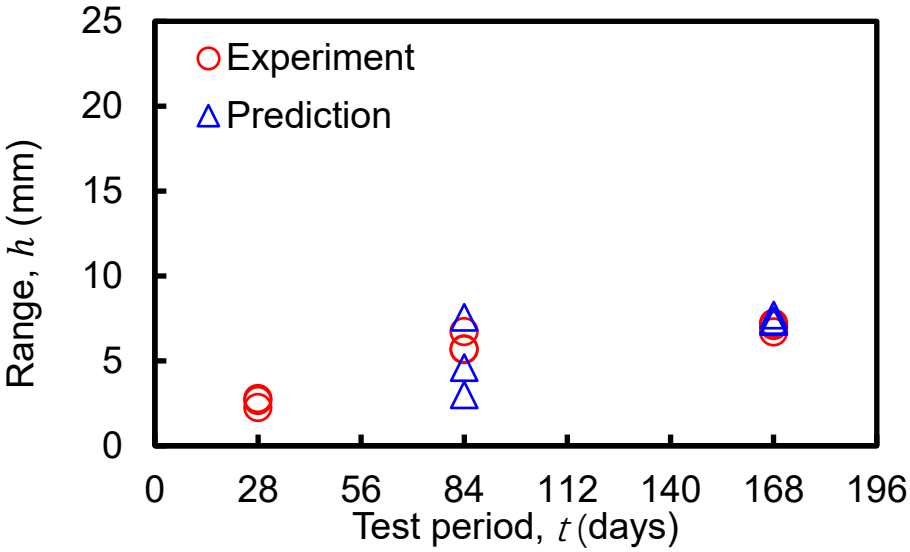

(a) The range results of SMA400AW steel plate

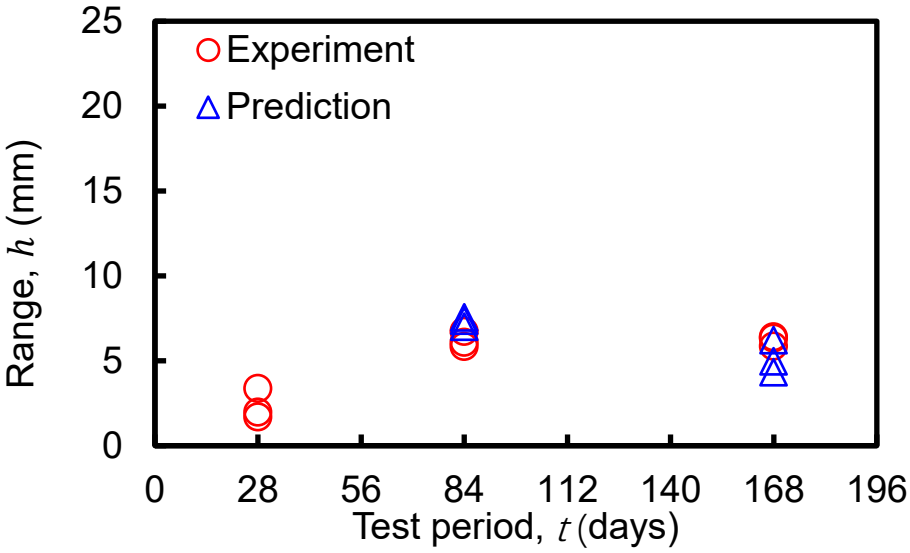

(b) The range results of SMA490AW steel plate

Figure 5-4. Comparative results between the predicted and actual range values for weathering steel under ISO16539 Method B.

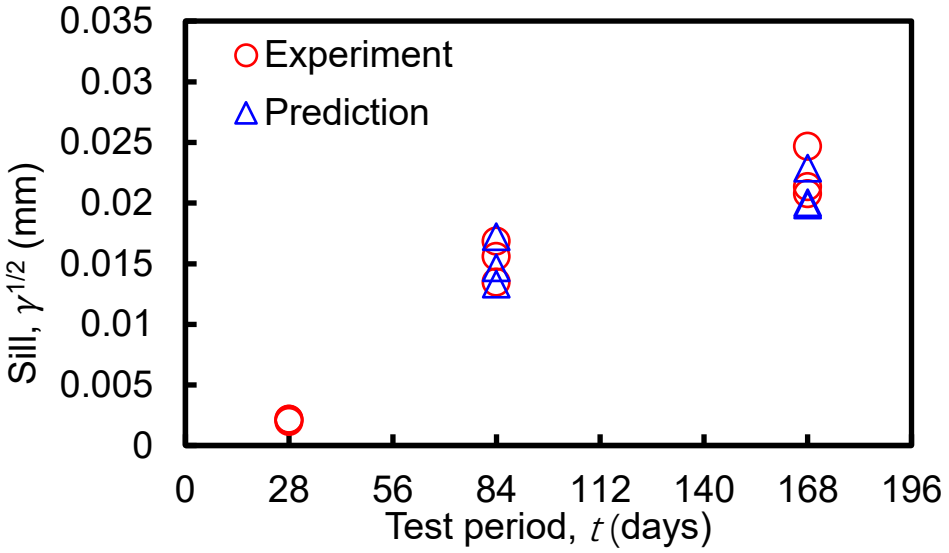

(a) The sill results of SM400A steel plate

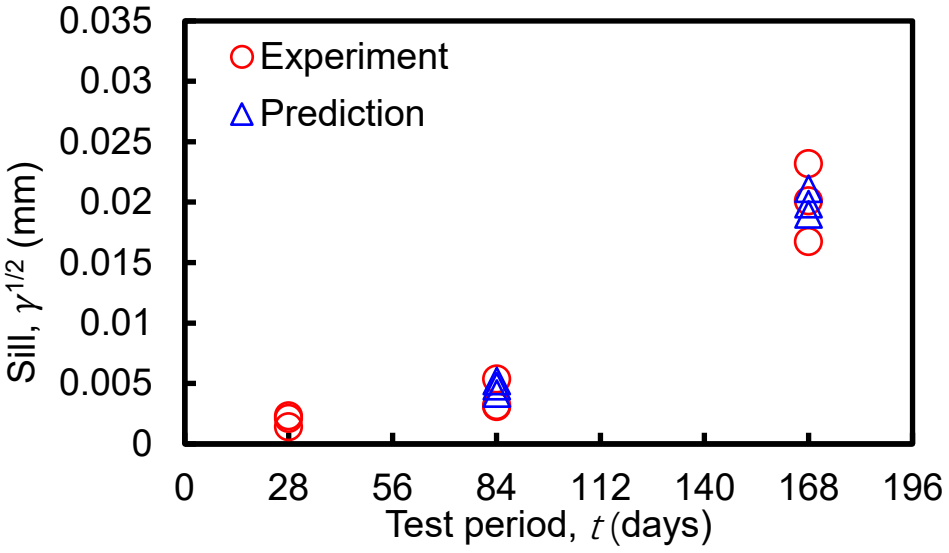

(b) The sill results of SM490A steel plate

Figure 5-5. Comparative results between the predicted and actual sill values for normal carbon steel under CCT Method A.

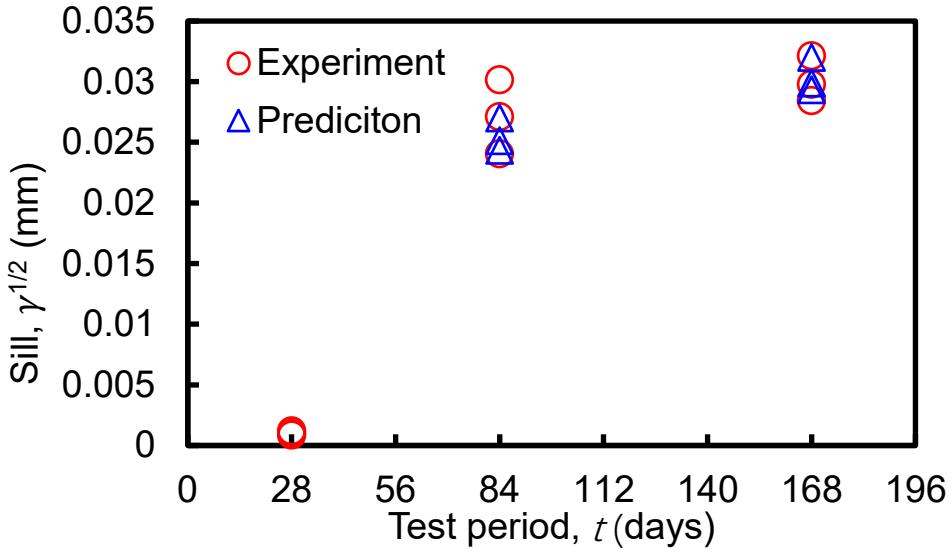

(a) The sill results of SMA400AW steel plate

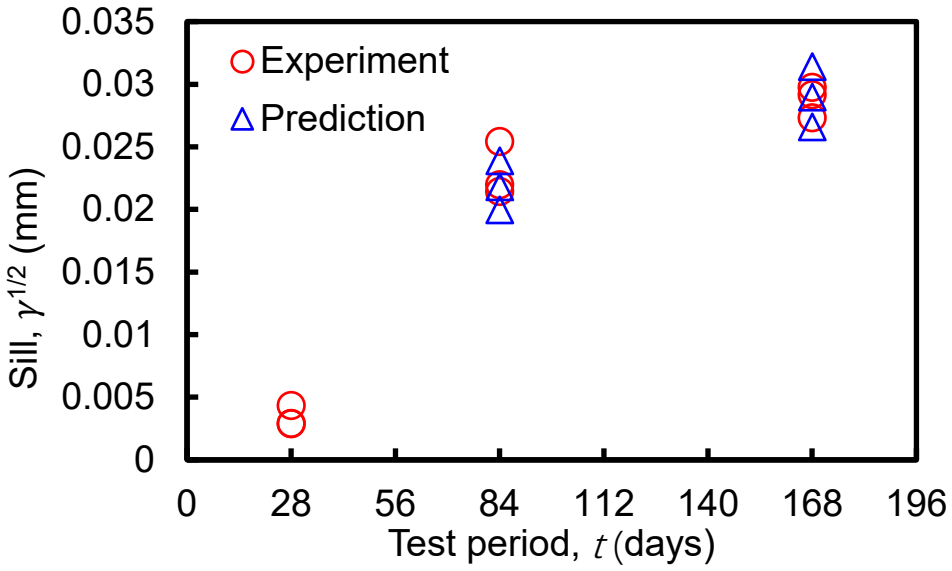

(b) The sill results of SMA490AW steel plate

Figure 5-6. Comparative results between the predicted and actual sill values for weathering steel under CCT Method A.

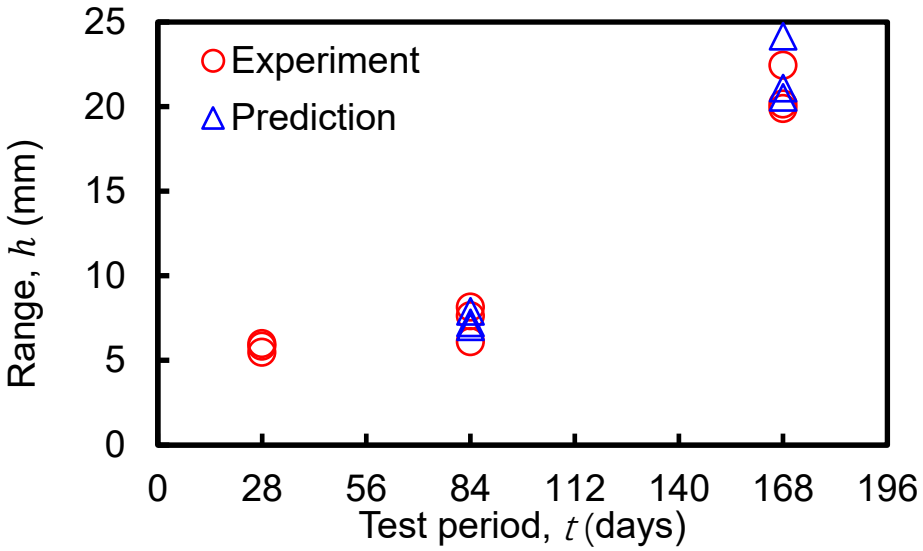

(a) The range results of SM400A steel plate

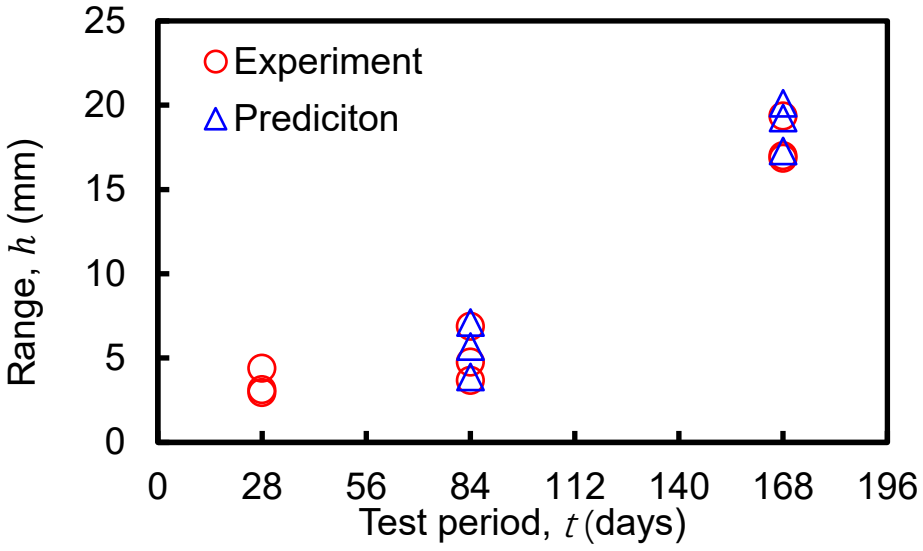

(b) The range results of SM490A steel plate

Figure 5-7. Comparative results between the predicted and actual range values for normal carbon steel under CCT Method A.

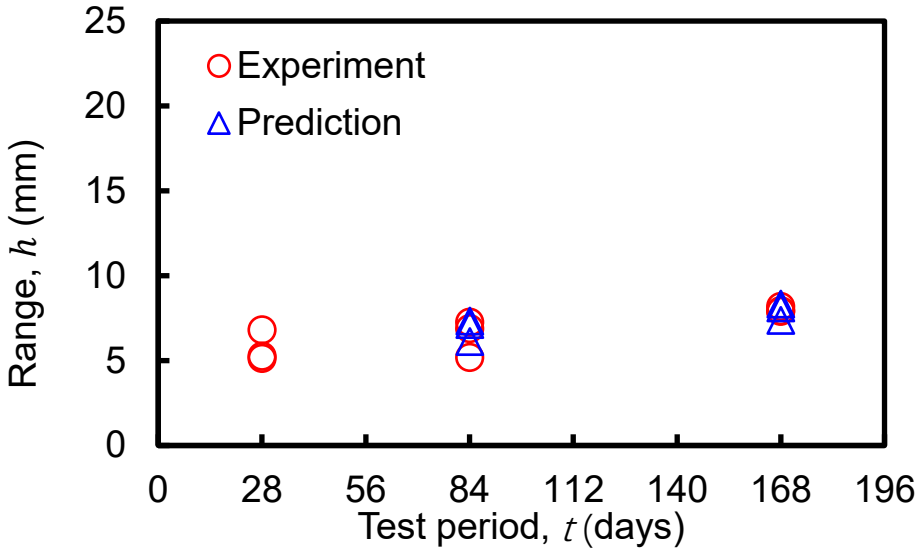

(a) The range results of SMA400AW steel plate

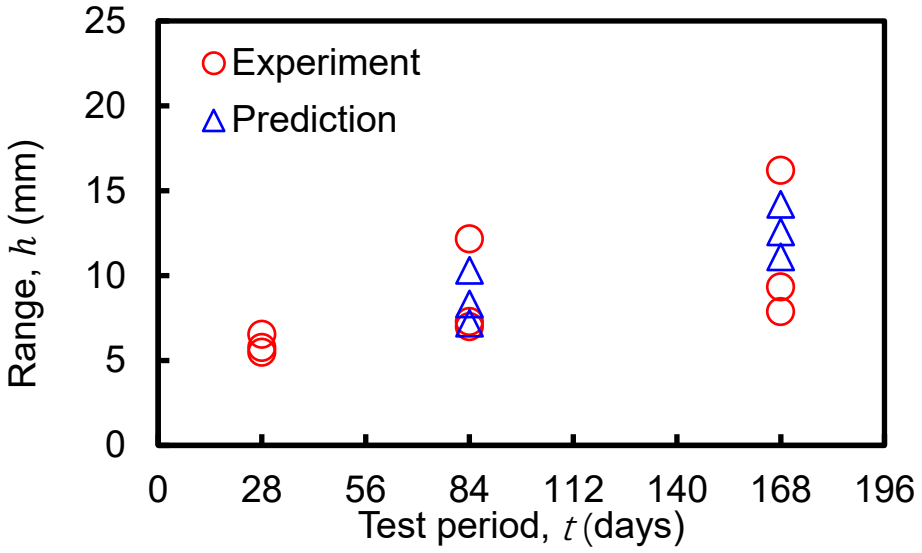

(b) The range results of SMA490AW steel plate

Figure 5-8. Comparative results between the predicted and actual range values for weathering steel under CCT Method A.

From these comparative results, the prediction results of the sill and range obtained by the corrosion prediction model are similar to the actual sill and range values. Because the corrosion prediction model was not available for the corrosion depth data of the first stage (28 days), the comparison time of sill and range was the second stage (84 days) and the third stage (168 days). Among them, the prediction results for the second stage (84 days) were better than those for the third stage (168 days). This is because the input of the prediction model was the data of the first stage (28 days), and the prediction model is more accurate in predicting the near future than the far future.

5.3 Validation of the prediction model

Comparing the predicted values of sill and range with the actual values of sill and range in Table 5-1 and Table 5-2, in this study, the small sample size was obtained, using a student t-test, it is any statistical hypothesis test in which the test statistic follows a student's t-distribution under the null hypothesis [5.1]. It is most commonly applied when the test statistic would follow a normal distribution if the value of a scaling term in the test statistic were known (typically, the scaling term is unknown and therefore a nuisance parameter). When the scaling term is estimated based on the data, the test statistic—under certain conditions—follows a student's t distribution. The t-test's most common application is to test whether the means of two populations are different.

The values marked by "*" are less than 0.05, which means the predicted value is significantly different from the actual value, implying that the prediction model is not accurate. Therefore, the results in Tables 5-3 and 5-4 show that the predicted and actual values of the two spatial property parameters, sill and range, were not significantly different (most P values are greater than 0.05) in all cases except for sill at 168 days and

range at 84 days in the accelerated corrosion test ISO16539 Method B for SMA490AW, indicating that the predictions of spatial properties by this deep learning-based model were consistent with the actual corrosion situation. Based on this accuracy judgment criterion, this corrosion prediction model can predict the spatial properties of the corroded surface of unpainted steel plates with an accuracy of 93.75% (30 / 32).

Table 5-3. t-test results (p-values) of sill and range for prediction model in ISO16539 Method B.

	ISO16539 Method B			
	Sill (mm^2)		Range (mm)	
days	84	168	84	168
SM400A	0.295	0.826	0.609	0.495
SM490A	0.262	0.272	0.165	0.382
SMA400AW	0.238	0.430	0.524	0.076
SMA490AW	0.067	0.032*	0.024*	0.154

Table 5-4. t-test results (p-values) of sill and range for prediction model in CCT Method A.

	CCT Method A			
	Sill (mm^2)		Range (mm)	
days	84	168	84	168
SM400A	0.884	0.437	0.917	0.465
SM490A	0.354	0.989	0.748	0.381
SMA400AW	0.451	0.841	0.603	0.815
SMA490AW	0.567	0.874	0.920	0.611

5.4 Summary

In Chapter 5, the accuracy of the prediction model was validated in conjunction with Chapters 3 and 4. As one of the drawbacks of deep learning methods, some parameters in the neural network are often not practically meaningful. Therefore, the spatial statistical analysis method in Chapter 4 was used to verify whether the prediction model can accurately predict the spatial properties of corroded surfaces. The applicability of the corrosion prediction model was verified by conducting a student t-test on the predicted and actual results, which confirmed that there was no significant difference between the predicted and actual results.

References

5.1 De Winter, J.C., 2013. Using the Student's t-test with extremely small sample sizes. *Practical Assessment, Research, and Evaluation*, *18*(1), p.10.

Chapter 6 Conclusions

In the modern maintenance of steel infrastructure, corrosion has been a matter of great concern. If there is no systematic method to detect and control the corrosion of steel structures, it will not only bring huge economic losses to society, but also threaten people's safety. Therefore, researchers have conducted many studies on the control of corrosion of steel structures. The traditional judgment of the corrosion situation mostly relies on visual inspection and experience, and the judgment of the corrosion progress of different steel in different corrosive environments will be very different. Therefore, the study of corrosion requires a large number of experiments. However, corrosion in the natural environment is usually a long process. The study of corrosion based on the natural environment of corrosion is very difficult, the use of accelerated corrosion tests to simulate the actual corrosion environment can greatly accelerate the progress of corrosion, thereby improving the efficiency of corrosion research under various circumstances.

In recent years, with the development of data science, the use of numerical analysis methods to quantify the progress of corrosion has received more and more attention. The use of numerical analysis to model corrosion can save a lot of labor costs in the maintenance of steel facilities, and is more accurate than traditional corrosion detection and control.

This study starts from the basic corrosion tests, from the analysis of the basic corrosion progress to the analysis of the spatial properties of the corroded surface, and finally to establish an efficient and convenient corrosion prediction model.

In Chapter 2, atmospheric exposure corrosion tests and accelerated corrosion tests were conducted on normal carbon steel (SM400A, SM490A) and weathering steel

(SMA400AW, SMA490AW). Corroded surface observation, corrosion depth measurement, and basic statistical analysis were carried out on the specimens. The average corrosion depths of different steels in different corrosive environments were compared. The average corrosion depths of normal carbon steel and weathering steel specimens were 0.089 mm and 0.044 mm at Miyakojima for 6 months and 0.073 mm and 0.059 mm at Choshi for 12 months. In ISO16539 Method B and CCT Method A, the average corrosion depths for normal carbon steel and weathering steel specimens were 0.218 mm and 0.143 mm, and 0.267 mm and 0.211 mm at 28 days. The accelerated test provided greater corrosion depths than the exposure test. The accelerated test ISO16539 method B provided an average corrosion depth for normal carbon steel at 28 days that is 2.4 to 3.0 times greater than the 6-month Miyakojima and 12-month Choshi exposure tests. In contrast, the average 28-day average corrosion depth of weathering steel by accelerated test ISO16539 Method B was 2.4 to 3.1 times greater than the 6-month and 12-month exposure tests at Miyakojima and Choshi. In the 28-day accelerated test of CCT Method A, the average mean corrosion depth for normal carbon steel was 3.0 to 3.7 times greater than in the 6-month Miyakojima and 12-month Choshi exposure tests. In the 28-day accelerated test CCT Method A, the average mean corrosion depth of weathering steel was 3.6 to 4.6 times that of the 6-month Miyakojima and 12-month Choshi exposure tests. In Chapter 3, a spatial statistical analysis was performed using semivariogram in order to further investigate the spatial statistical properties of the corroded surfaces. This method captured the spatial nature of the corroded surface, allowing a uniform evaluation criterion for the steel subjected to corrosion in different corrosive environments. The spatial properties of corrosion of different steels in different environments were compared to confirm the extent to which the two accelerated corrosion tests simulate the real

corrosive environment. In addition, the applicability of the accelerated corrosion test of ISO16539 Method B for assessing the corrosion characteristics of unpainted steel was confirmed by comparison with the exposure test and the accelerated corrosion test CCT Method A. The corrosion properties of unpainted steel under actual atmospheric conditions could be predicted in a relatively short period of time by accelerated tests ISO16539 Method B and CCT Method A. The semivariogram representing the spatial statical properties of the corroded surface profile showed the same trend for the same type of steel. However, the values of the spatial characteristics of the corroded surface showed differences in different types of steel. Under the accelerated test CCT method A, the spatial properties of the corroded surface of normal carbon steel were closer to the properties of the exposure test. While in the accelerated test ISO16539 method B, weathering steel corroded surface spatial properties were closer to the spatial properties of the exposure test. Therefore, according to the actual situation, different accelerated corrosion tests could be selected to simulate the real corrosion situation.

In Chapter 4, adversarial learning was used to simulate the generation of future corrosion on steel surfaces to build an efficient corrosion model that can be practically applied. The model could predict the next stage of corrosion based on the current corrosion state of the corroded surface. The prediction model could also be used to identify the corrosion stages and the number of days of corrosion. According to the experimental results, the model achieved high accuracy in predicting the corroded surfaces of steel plates. This proposed method could predict corrosion behavior faster and more accurately than traditional methods that usually rely on personal experience.

In Chapter 5, the accuracy of the prediction model was validated in conjunction with Chapters 3 and 4. As one of the drawbacks of deep learning methods, some parameters in

the neural network are often not practically meaningful. Therefore, the spatial statistical analysis method in Chapter 4 was used to verify whether the prediction model can accurately predict the spatial properties of corroded surfaces. The applicability of the corrosion prediction model was verified by conducting a student t-test on the predicted and actual results, which confirmed that there was no significant difference between the predicted and actual results.

In summary, firstly, this study conducted accelerated corrosion tests and atmospheric exposure tests on different types of uncoated steel to verify the simulation degree of accelerated corrosion tests on atmospheric exposure tests. A feasible verification method was provided, and the corrosion effect of a new accelerated corrosion test (ISO16539 Method B) was confirmed. Secondly, by using spatial statistical analysis and deep learning methods, a corrosion prediction model that can be effective for a variety of steels and a variety of corrosion environments was developed. This study contributes positively to reducing the cost and time of corrosion monitoring of steel structures and simplifying the maintenance process.

In future works, more specimens and corrosion time will be added to make the model more accurate. In addition, it will take into account the corrosion of coated steel plates and develop a corrosion prediction model for coated steel structures.

Acknowledgment

Firstly, I would like to give my heartfelt thanks to my supervisor, Associate Professor Hirohata, for his kindness, illuminating guidance, and profound knowledge. In his very busy work schedule, he still read my dissertation carefully and commented on it in detail. Without his keen insights and constant encouragement, my dissertation would not have been completed. Secondly, I am also very grateful to Professor Kamada and Professor Inui for reviewing my dissertation during their busy schedules.

I also express my appreciation to all teachers who have lectured me for their insightful lectures which are of great benefit to me in my research.

I would also like to thank all the members of our laboratory. Thanks to everyone's kindness I have had a great three years here and have a lot of good memories with everyone. Especially this research owes a debt to Liu Jia and Ojima Kazuki. They gave me great support in my research, which enabled me to complete my research successfully.

I would also like to acknowledge the Support for Pioneering Research Initiated by the Next Generation Foundation for their scholarship and SHO-BOND Holdings Co., Ltd for their experiment support.

Finally, my cordial thanks also go to my family member and friends who love and care me and whom I love and care.

December 2022

JIANG FENG

List of publications

Journal publications

[1] Application of Accelerated Cyclic Test with Synthetic Ocean Water Salt-deposition Process to The Evaluation on Corrosion Characteristics of Weathering Steel
Jiang, F., Hirohata, M., Liu, J. and Ojima, K.
Corrosion Engineering, Science and Technology, *57*(3), pp.280-289. **2022.3**

[2] A GAN-Augmented Corrosion Prediction Model for Uncoated Steel Plates
Jiang, F. and Hirohata, M.
Applied Sciences, *12*(9), p.4706. **2022.5**

[3] Geostatistical Analysis and Deep Learning Based Prediction for Corrosion Surfaces of Steel Plates
Jiang, F. and Hirohata, M.
土木学会論文集特集号（応用力学）*No.15, Journal of JSCE.* **2023.2**
Accepted

Conferences

[1] Numerical Simulations for Time-dependent Corrosion Surface of Unpainted Structural Steel Plates Using Spatio-temporal Data
Jiang, F. and Hirohata, M.
IOP Conference Series: Materials Science and Engineering (Vol. 1252, No. 1, p. 012083). **2022.6**
Civil Engineering Conference, The 45th Anniversary of The Establishment of The Faculty of Civil Engineering, 2022.6, Technical University of Košice, Slovakia.

[2] Corrosion Acceleration Test on Weathering Steel and Paintcoated Steel for Bridge Structural Members
Liu, J., Ojima, K., **Jiang, F.**, Hirohata, M., Nakayama, T. and Sakamoto, T.
IOP conference Series, Materials Science and Engineering (Vol. 1252, No.1, p.012042) **2022.6**
Civil Engineering Conference, The 45th Anniversary of The Establishment of The Faculty of Civil Engineering, 2022.6, Technical University of Košice, Slovakia.

[3] Corroded Surface Prediction of Weathering Steel Plates under Different Corrosive Environments Using Generative Adversarial Network
Jiang, F. and Hirohata, M.
第 25 回応用力学シンポジウム，2A01-06-02，2022 年 5 月，鹿児島.

[4] ISO16539-Method B による無塗装鋼板の腐食促進実験
井上颯太，**蒋鋒**，劉佳，廣畑幹人
令和 4 年度土木学会全国大会第 77 回年次学術講演会，I-45，2022 年 9 月，京都.